Modulation of Actin Structure and Dynamics by Actin Binding Proteins

by

Mouna Mohamed Aref Mikati

A dissertation submitted in partial satisfaction of the
requirements for the degree Doctor of Philosophy
in Biochemistry & Molecular Biology

UNIVERSITY OF CALIFORNIA

Los Angeles

2014

ABSTRACT OF THE DISSERTATION

Modulation of Actin Structure and Dynamics by Actin Binding Proteins

by

Mouna Mohamed Aref Mikati

Doctor of Philosophy in Biochemistry & Molecular Biology

University of California, Los Angeles, 2014

Professor Emil Reisler, Chair

Rapid remodeling of the actin cytoskeleton is essential for many cellular processes including cell growth, differentiation, division and motility. The structure and dynamics of the actin cytoskeleton are modulated by various actin-binding proteins. Drebrin, coronin and cofilin are three important players in actin's organization in the cell. This dissertation focuses on characterizing the mechanisms of drebrin, coronin and cofilin interactions with actin and studying their independent and inter-dependent roles in actin structure and dynamics.

First, we investigate DrABD binding interface on actin filaments. Our results reveal polymorphism in DrABD binding to F-actin and suggest the existence of two binding sites. We find that DrABD binding is centered on actin subdomain 2 and that this protein bridges two adjacent actin protomers. We also examine the structural effects of drebrin on F-actin in solution. We use the full length protein and its C-terminal truncated constructs to clarify which domains of drebrin are required for its interactions with actin. We demonstrate that F-actin is

stabilized by drebrin binding. Also, in different cases of longitudinal and lateral interprotomer contact perturbations, we observe the rescue of filament formation by drebrin. Overall, our data suggests that drebrin stabilizes actin filaments through its effect on their interstrand and intrastrand contacts.

Next, we examine coronin and study the effects of its specific CrnΔCC construct (a.a. 1-600) on actin filaments. Using a combination of site-directed mutagenesis, solution biochemistry methods, electron and TIRF microscopy, we analyze the effects of coronin on the structure of actin filaments by studying its effect on inter-protomer contacts in F-actin. We compare coronin's effects on F-actin to the changes in filaments induced by cofilin. We also study how the two proteins act when they are present together, to shed light on the mechanism(s) by which coronin modulates cofilin's effects on actin filaments. Our results provide a plausible mechanism for the synergistic effect CrnΔCC has on the severing activity of cofilin. We find that coronin increases the binding of cofilin to the actin filament and also causes slight structural changes that promote severing by cofilin. Coronin-induced filament rigidity generates a bigger change in stiffness between cofilin free regions and those to which cofilin is bound. This added mechanical asymmetry causes the increase in cofilin's severing of actin filaments.

The dissertation of Mouna Mohamed Aref Mikati is approved.

Frank A. Laski

Margot E. Quinlan

Emil Reisler, Committee Chair

University of California, Los Angeles

2014

I dedicate this thesis to my parents,

for making me who I am,

and to my husband, for supporting me through this journey.

TABLE OF CONTENTS

LIST OF FIGURES

LIST OF TABLES

ACKNOWLEDGEMENTS

I would first like to acknowledge my advisor and committee chair, Dr. Emil Reisler. As a Ph.D. student attending UCLA, I was promised an excellent scientific education, provided by some of the world's most successful and brightest professors. UCLA delivered on that promise, but in Dr. Reisler's lab my schooling extended beyond academics. Under his mentorship, I have grown not only as a researcher and scientist but also as a person. I learned tremendously from the discussions we've had on actin-related topics and I thoroughly enjoyed the ones on music, religion, history and politics. His kindness and selflessness are contagious and his positive outlook on life is inspiring. I am thankful for the wealth of knowledge that he has been willing to share with me and for the support that he has provided me throughout my graduate career, ever so patiently.

I would also like to acknowledge the rest of my committee: Dr. Margot Quinlan, Dr. Greg Payne, Dr. Frank Laski and Dr. James Gober. Dr. Margot Quinlan has been especially helpful and I am very thankful for her support throughout my years as a Ph.D. student.

My lab has also been an excellent support system, both on a professional and personal level. I would like to thank all current and past members for engaging scientific discussions as well as shared life lessons. A huge thank you to Dr. Elena Grintsevich, who agreed to take me under her wings in the Drebrin project, and further provided me with guidance and support throughout the years, along with a sincere friendship. I would also like to thank Pamchal Faroghi, who was a very pleasant person to work with, a confidante, and whose friendship is very dear to me. Many thanks to Daria Cubberly for her help with daily tasks, her taste in upbeat music and the engaging lunch talks. A special thank you to my undergraduate researcher, Danny

O’Brien, who was always ready to tackle new experiments, accommodated my borderline obsessive compulsive tendencies and always had a big smile on his face. I would also like to thank Dr. Christine Chen Kennedy for being such a fun and agreeable lab-mate and a dear friend over the years. A very special thank you to Dr. Courtney White, who was a rotation student in the Reisler lab and the one to originally “hook me up” with a volunteering position with the group; she opened the doors to my Ph.D.

Many thanks to the Quinlab lab members for the scientific discussions during our weekly lab meetings and for being such fun travel companions at conferences.

I would like to thank Dr. Martin Phillips for his help with the many instruments in the Biochemistry facility.

Before joining the Ph.D. program, I completed my undergraduate studies at UCLA. I am truly grateful for the wonderful professors I was blessed to have, both in my science and non-science classes. I have also forged the best friendships during my undergrad and grad years at UCLA, a big shout-out to the amazing friends I have made during the past decade at this university.

Last but not least, I would like to thank my whole family, my life’s greatest cheerleaders and harshest critics, who have molded me into the person I am today. Mom and dad, any attempt to thank you pales in comparison to the gratitude and appreciation I have for the immense support, and the unconditional love you have provided and showered me with throughout the years, and most importantly for blessing me with amazing sisters. Marya and Maha, life would be boring and meaningless without you two, thank you for opening your home to me and offering me a place to crash this past year; this will sound cheesy, but you two are the best siblings anyone can ever ask for ☺. Cyril, there is never a dull moment with you and I thank you

for that, you are my rock, “You are the one for me, for me, Formidable… ” et je t’aime de tout mon cœur. Un très grand merci à ma grand-mère Dodi, ma première maîtresse de français et ma préférée, toujours aussi patiente et généreuse. Chaque été, tu nous retrouvais à l’aéroport, malgré les heures longues passées sur une route assez mal entretenue. « إنت جوهرة » le refrain que tu ne cesses de me répéter dés mon enfance, et bien que je sois plagiaire: «tu es un trésor et je t’adore!». I would also like to thank the newest addition to my family, my brother-in-law Hatem, who is just simply awesome. A big thank you to the Chidiac and Karam families for always being so encouraging and supportive, and for constantly providing me with delicious food.

I would also like to acknowledge the Journal of Molecular Biology for allowing me to reprint my published work in Chapter 2: Grintsevich E.E., Galkin V.E., Orlova A., Ytterberg A.J., Mikati M.M., Kudryashov D.S., Loo J.A., Egelman E.H., Reisler E. “Mapping of Drebrin Binding Site on F-actin”. *J. Mol. Biol.* **2010**, 398(4): 542-24.

I would also like to acknowledge the Journal of Biological Chemistry for allowing me to reprint my published work in Chapter 3: Mikati M.A., Grintsevich E.E., Reisler E. “Drebrin-Induced Stabilization of Actin Filaments”. *J. Biol. Chem.* **2013**, 288(27): 19926-38.

This work was supported by the U.S. Public Health Service grant to Emil Reisler as well as the Whitcome Pre-Doctoral Training Program fellowship and the Azm & Saade Association scholarship awarded to Mouna Mohamed Aref Mikati.

VITA

1997- 2000	Lycée Alphonse de Lamartine, Tripoli, Lebanon
2000- 2002	Granada Hills High School, Los Angeles, CA
2003-2004	Associated Students of OCC- Board of Trustees Orange Coast College
2003-2004	District Wide Student Council Representative Orange Coast College
2007	B.S., Biochemistry Minor, French University of California, Los Angeles
2007-2008	Laboratory Technician Department of Biochemistry University of California, Los Angeles
2008-2014	Tutor Launch Education Los Angeles, CA
2009-2010	Teaching Assistant Department of Biochemistry University of California, Los Angeles
2012-2013	Graduate Student Association Campus Programs Committee University of California, Los Angeles
2011-Present	Chair and Research Advisor Ewing's Sarcoma Research Foundation Los Angeles, CA

PUBLICATIONS AND PRESENTATIONS

- **Mikati M.A.,** Grintsevich E.E., Reisler E. Drebrin-Induced Stabilization of Actin Filaments.(2013). *J Biol Chem*. 288, 19926-19938.

- Grintsevich E.E., Galkin V.E., Orlova A., Ytterberg A.J., **Mikati M.M.**, Kudryashov D.S., Loo J.A., Egelman E.H., Reisler E. (2010). Mapping of Drebrin Binding Sites on F-actin. *J Mol Biol.* 398, 542-554.

Platform Presentations:

- Molecular Biology Institute Retreat, Effects of Coronin on Actin Filaments- UCLA, CA, January 25-26, 2014

Poster Presentations:

- American Society for Cell Biology Meeting, Coronin Effects on Actin Filaments- New Orleans, CA, December 13-18, 2013

- American Society for Cell Biology Meeting, Coronin Effects on Actin Filaments- San Francisco, CA, December 14-19, 2012

- Molecular Biology Institute Retreat, Effects of Coronin on Actin Filaments- Lake Arrowhead, CA, October 19-21, 2012

- American Society for Cell Biology Meeting, Drebrin Affects Lateral and Longitudinal Contacts in F-actin- Denver, CO, December 3-7, 2011

- American Society for Cell Biology Meeting, Binding domain of Drebrin Affects Lateral and Longitudinal Contacts in F-actin- San Diego, CA, December 5-9, 2009

CHAPTER 1

Introduction

Actin is a highly conserved cytoskeletal protein and the most abundant in virtually all eukaryotic cells due to its crucial role and direct involvement in motility based cellular processes. Cell migration and cell shape regulation are central to many biological processes, including wound healing, tissue formation during embryonic morphogenesis, angiogenesis and immune responses. These functions—vital to the development and existence of living organisms— rely primarily on cellular structures, such as stress fibers, dendritic lamellar arrays, cortical networks, filopodial bundles and focal adhesions, the formation of which is modulated by the actin cytoskeleton **(1)**.

The first actin isoform was discovered in muscle cells along with myosin, in 1942. Later, other actin isoforms with a highly conserved sequence were identified in both muscle and non-muscle cells. In fact, sequence conservation among different actin isoforms and across different species is yet another manifestation of the important role this 42-kDa protein has in the cell. Birds and mammals have six genes encoding for six different actin isoforms expressed in a tissue and temporal specific pattern. The six actins are divided into three main groups- alpha, beta, and gamma, with α-actins being the most acidic, γ-actin the most basic and β-actin in-between **(2, 3)**. Four isoforms, $\alpha_{skeletal}$-actin, $\alpha_{cardiac}$-actin, α_{smooth}-actin, and γ_{smooth}-actin, are expressed primarily in skeletal, cardiac, and smooth muscles, respectively. The remaining two isoforms, β_{cyto}-actin and γ_{cyto}-actin are cytoplasmic actins and are found in both muscle and non-muscle cells. All isoforms possess very similar amino acid sequences, with ~ 93% identity among them. β_{cyto}-Actin and γ_{cyto}-actin, which are exactly conserved from birds to mammals, differ only by four biochemically similar amino acids out of the three hundred seventy-five residues **(4, 5)**. More recently, evidence for a bacterial cytoskeleton has also been obtained and although it might not be as intricate and complex as the eukaryotic one, it contains proteins that are similar to

actin. Structural studies have demonstrated that MreB is a prokaryotic homologue of actin that can assemble into helical filamentous structures in a nucleotide-dependent manner **(6, 7, 8)**. ParM, another bacterial protein, has also a high degree of structural similarity to eukaryotic actin. Along with MreB, it is essential for cell viability and is involved in cell morphogenesis, chromosome segregation and cell polarity **(9, 10)**.

The Structure of Monomeric Actin

The first high resolution structure of monomeric actin (G-actin, for globular) was solved in its complex with DNaseI by X-ray crystallography, in 1990 **(11)**. Since then, over 80 structures of actin from different species have been obtained, using a variety of techniques to prevent it from spontaneously polymerizing under high salts conditions. The majority of these structures are of actin in complex with other proteins or small molecules which block its polymerization, while the rest have been obtained by chemically modifying or mutating actin in order to inhibit its polymerization. These structures are compiled in a table format in a recent review **(12)**. Regardless of the ligand bound or the nature of the modification, the conformation of an actin monomer remains nearly unchanged. It follows a clam-shaped structure, flattened in one dimension, formed by two major domains—α and β (referred to as inner and outer domains, respectively, due to their orientation in the filament); the outer and inner domains are further subdivided into two subdomains (SD) each—SD1 and SD2 and SD3 and SD4, respectively (Figure 1.1). Each subdomain contains structural elements important for the stabilization of actin and its interactions with other proteins.

The N- and C-termini reside on opposite faces of the molecule in SD1; these termini are flexible and are often disordered in X-ray structures. SD2 is the smallest sudomain and by far the most flexible one; the outer part— residues 40 to 51— forms a loop that binds DNase I and is

therefore called the DNase I binding loop (D-loop). Due to its high flexibility, the D-loop is disordered in most X-ray structures of actin published to date. It is however predicted to have a β-turn conformation, but has been depicted as an α-helix in one of the crystal structures (Dominguez 2001). However, it is possible that the α-helical D-loop structure is an artifact of crystal packing rather than indeed an intrinsic structure of the protein. The upper cleft found between the α and β domains (the nucleotide binding cleft) binds adenosine nucleotides and its ligated divalent cations (Mg^{2+} under physiological conditions). These cofactors link the two major domains and impart stability to actin and the filaments. The lower cleft, located between SD1 and SD3 is enriched in hydrophobic residues and constitutes the major binding site for most actin binding proteins (ABP) **(13)**. This site, called the hydrophobic cleft, is also important for longitudinal contacts between actin protomers. Its blocking by the insertion of a tetramethylrhodamine (TMR) molecule prevents filament formation **(14)**. The binding affinities of many ABPs depend on the cofactors bound and the structural cross-talk between these two adjacent clefts. The hydrophobic cleft is not to be confused with the hydrophobic loop of actin (H-loop; a.a. residues 262–274), another structural element postulated to swing out from the back of the molecule, between SD3 and 4, and insert into the opposing strand of the filament, establishing important inter-strand contacts in the filament **(15, 16, 17, 18)**. These structurally important regions, along with the WH2-binding loop (W-loop; residues 165–172), are highly dynamic and contribute to inter-and intra-strand contacts along the filament **(19)**. Figure 1.1 shows the structure of ATP- bound monomeric actin with the previously mentioned regions highlighted in different colors.

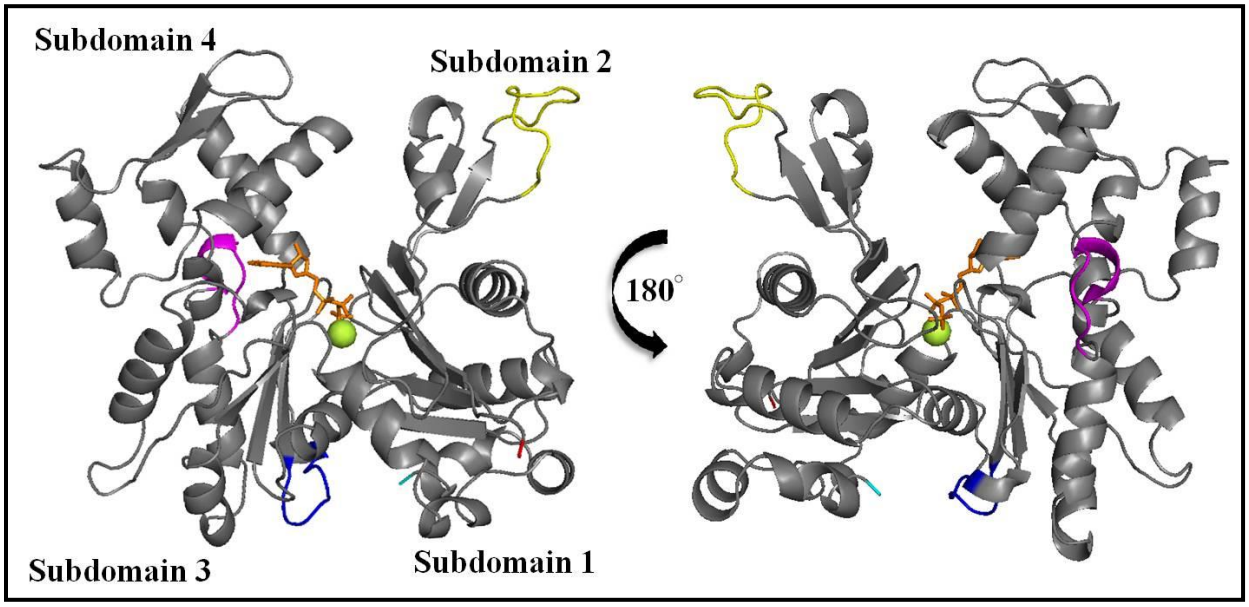

Figure 1.1- Crystal Structure of Monomeric Actin (PDB ID: 1YAG).
The actin monomer is rather flat, fitting into a rectangular prism with dimensions 55 Å× 55 Å ×35 Å. ATP (orange molecule) and Mg^{2+} (lime green sphere) are bound to G-actin. Located in Subdomain 1, the N-terminus is shown in red while the C-terminus is colored cyan. In yellow is the D-loop (residues 40-51), in blue is the W-loop (residues 165-172) and in magenta is the H-plug (residues 264-271). SD1 and SD2 are located in the α domain. SD3 and SD4 are located in the β domain. The original structure is that of yeast actin in complex with human gelsolin segment 1- **(20)**.

Actin Polymerization and the Treadmilling Effect

Under physiological conditions, actin monomers spontaneously polymerize into stable double stranded filaments with a helical arrangement, F-actin (for its filamentous form). Actin filaments are polar and the actin protomers in F-actin all point in the same direction. This polarity can be determined by decorating the filament with myosin heads "S1 fragments", creating a "barbed-end" and a "pointed-end" on the filament. This nomenclature arises from the resemblance of the filaments to arrowheads in electron microscopy images. The barbed end is commonly referred to as the "plus-end", as this ends grows much faster during polymerization than the pointed end, commonly referred to as the "minus-end". Actin has an intrinsic ATPase activity: the terminal phosphate of ATP is hydrolyzed upon incorporation of ATP-G-actin into a filament; the subsequent release of the inorganic phosphate (Pi) turns actin into the adenosine diphosphate bound form (ADP-actin). The ADP+Pi-actin is the intermediate form present between the hydrolysis and Pi release events (Pollard older review). Kinetics studies on α-skeletal actin polymerization report the hydrolysis event at a rate of 0.006 s^{-1} and the release of the inorganic phosphate to be a much slower, with a lag time of ~10 minutes **(21, 22)**. The hydrolysis of ATP is not required for actin polymerization as actin bound to ADP or a non-hydrolyzable ATP analogue can still form filaments **(23)**. The nucleotide state of actin is often used as an age indicator as newly polymerized filaments consist predominately of ATP/ADP+Pi-bound actin protomers, whereas older filaments contain ADP-bound protomers. The hydrolysis and release of the γ-Pi causes conformational changes in actin and results in a destabilization of the pointed-end of the filament, accelerating the dissociation of actin protomers by 5-10 fold at this end of F-actin **(24)**. In the presence of free ATP, the released G-actin subsequently exchanges its bound ADP with ATP, often with the help of other proteins such as profilin. It then

re-incorporates into the barbed-end of the actin filament. This polarized cycling of filaments, called treadmilling, maintains actin filaments in a state of constant flux, or turnover. Figure 1.2 below is a schematic representation of actin treadmilling.

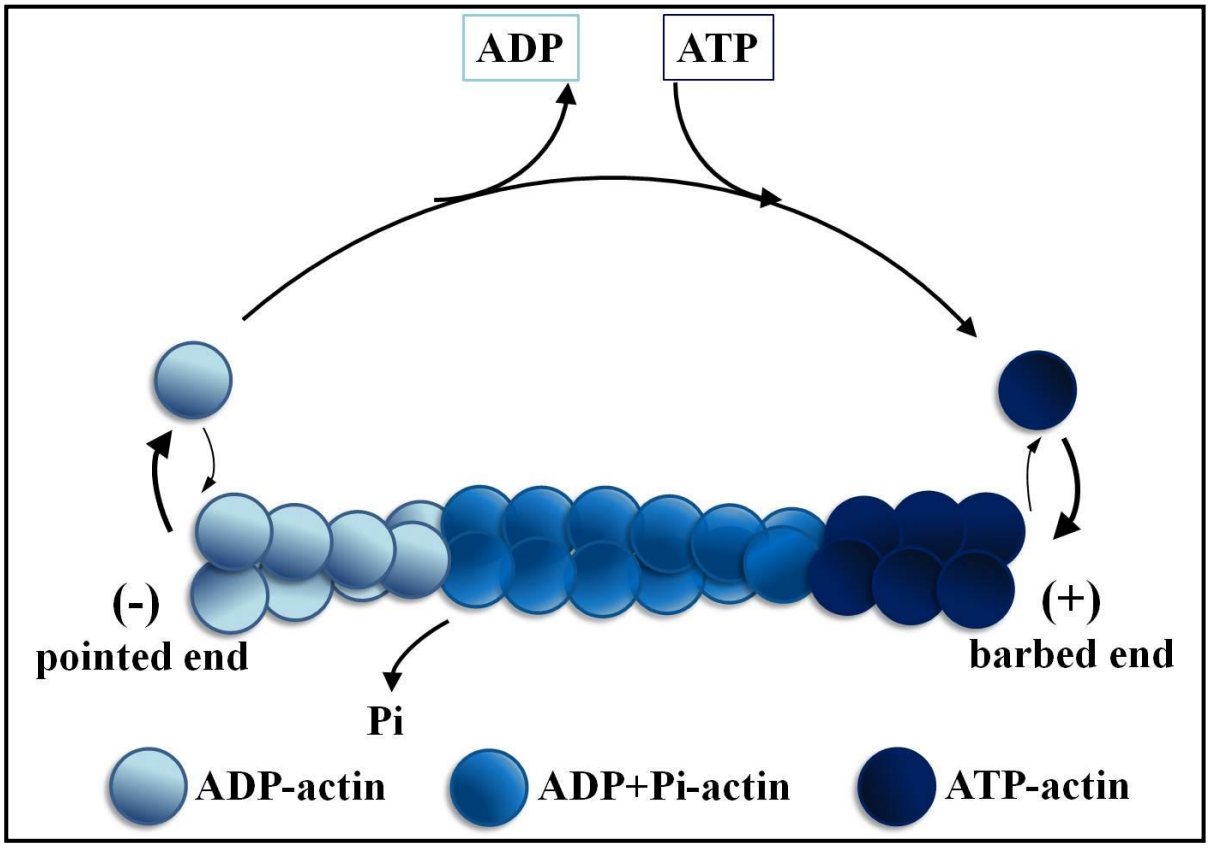

Figure 1.2- Schematic Representation of Actin Treadmilling at Steady-State.
ATP-G-actin binds to the faster growing (+) end and ADP-G-actin dissociates slowly from the (-) end. Actin has an intrinsic ATPase activity that is 40 times faster in the filamentous form; ATP is hydrolyzed as F-actin "ages", creating a polarized filament that contains a mixture of ATP-actin, ADP+Pi actin, and ADP-actin. ADP-bound G-actin exchanges its ADP for ATP and the polymerization cycle is renewed. ABPs have different binding affinities to actin depending on the bound nucleotide.

The dynamic turnover of actin networks is needed as it allows a rapid and precise reconfiguration of actin filaments in response to different spatial and temporal cues in the cell. Diverse physiological processes, such as cell migration, endocytosis, cytokinesis and cell

morphogenesis are actin-based cellular processes that rely on the force and structural organization generated by the dynamic remodeling of the actin cytoskeleton. Eukaryotic cells use a large repertoire of proteins to regulate the assembly and turnover rate of actin filaments, maintain a pool of actin monomers, initiate polymerization and restrict the length of actin filaments **(25)**. These proteins are known as actin binding proteins (ABPs).

Actin Binding Proteins

Actin binding proteins modulate the structure and dynamics of actin filaments and play an important role in actin's organization in the cell. *In vitro,* under physiological solvent conditions, pure actin filaments treadmill very slowly in the absence of regulatory proteins, whereas *in vivo* cells need "faster action" **(26)**. The steady-state treadmilling of pure actin polymers *in vitro* is much slower than of F-actin in living cells due to the rate-limiting step of actin dissociation from the pointed-end **(27, 28)**. Actin binding proteins present *in vivo*, such as ADF/cofilin, accelerate treadmilling rates to close to those observed in motile lamellopodia by increasing the actin dissociation rate from the filaments' pointed-ends. Another example of slow kinetics is the event of nucleation, when actin monomers associate to form dimers and trimers, actin seeds, which are needed for further polymerization. Although the elongation from actin polymers is fast, the spontaneous assembly of pure actin monomers is unfavorable due to the instability of actin dimers and trimers. Without "accessory" proteins to help speed up the process (in this case actin nucleators), actin's *de novo* nucleation will not be fast enough for certain responses to stimuli in the cell. This is why the numerous actin-associated proteins are important in the reconfiguration of actin networks *in vivo*. Each protein has its own activity (or set of activities), timing and location, but they all act in concert to control and regulate the processes and mechanisms by which the actin cytoskeleton is remodeled via nucleation, elongation,

bundling and severing processes. Many of the proteins involved in these key processes are expressed ubiquitously in different types of cells and have been studied extensively, leading to a better understanding of their biochemical and cellular functions. A few categories include—myosins (motor proteins), cofilins (filament destabilizing proteins), tropomyosins/drebrin (filament stabilizing proteins) and Spir/formins/Arp2/3 complex (actin nucleators) **(29)**. Many proteins however remain understudied (or maybe not even discovered yet), the importance of their activity remaining unclear and to a certain extent under-estimated due to insufficient knowledge. In this thesis the main focus has been on three different actin binding proteins, drebrin, coronin and cofilin.

Drebrin

Drebrin, a short for **d**evelopmentally **re**gulated **br**ain prote**in**, is a mammalian neuronal protein enriched at dendritic spines of mature neurons. Dendritic spines are the postsynaptic receptive regions of most excitatory synapses and the shape, size and density of these very dynamic structures have been shown to change during development and adulthood. Dendritic protrusions on immature neurons start out as thin, headless filopodia that eventually mature into spines during later stages of development **(30)**. This maturation is associated with learning, aging, as well as diseases such as mental retardation **(31, 32, 33)**. Indeed, morphological studies of spines in dementia patients show a correlation between brain dysfunction and abnormal spine morphology **(34, 35)**. This has been the driving force behind studying the mechanisms that govern spine maintenance, to further understand higher brain functions, such as memory and learning.

Originally identified in neuronal cells and tissues, drebrins exist in three isoforms – drebrin-A, E1 and E2– generated by the alternative RNA splicing mechanisms of the same gene

(dbn1), and synthesized in patterns depending on the specific developmental stage **(36, 37)**. Drebrin E is the ubiquitous isoform and predominates in the developing brain; drebrin El is abundant at the developmental stage when neurons are migrating, and drebrin E2 is abundant at the stage when neurons are extending their cell processes **(36, 38)**. Drebrin A is the neuron-specific isoform and is predominately expressed in adulthood **(36, 38, 39).** While drebrins have long been considered, by and large, to be specific for the nervous system, a drebrin-E splice variant (drebrin-E2) has been detected in diverse non-neuronal cells **(40, 41, 42)**. Immunoelectron microscopy studies showed actin to be another major cytoskeletal element in dendritic spines **(43, 44)**; it is thought to play a pivotal role in the mechanisms regulating spine plasticity **(43, 45, 46, 47)**. Drebrin binds to and modulates F-actin in dendrites **(48)**.

In addition to organizing the dendritic pool of actin, drebrin also mediates interactions between F-actin and microtubules and acts as a positive regulator of microtubule entry into spines **(49)**. There is increasing evidence that when molecular pathways linked to drebrin malfunction, this results in developmental abnormalities and disease. Indeed, drebrin protein levels were found to be decreased in Alzheimer's disease patients **(50)**. This decrease was also observed in brain samples from patients with Down Syndrome, both from adult and fetal brain samples **(51, 52)**. Furthermore, down-regulation of drebrin-A expression in developing hippocampal neurons suppresses the accumulation of F-actin within dendritic spines **(47)**. A natural intrigue then emerges about the mechanism by which drebrin governs F-actin dynamics and structure in its role in spinal plasticity.

Drebrin is a multidomain protein containing an ADF/cofilin homology (ADF-H) domain in its N-terminal region (residues 8–134) **(53)**. This domain does not bind on its own nor does it depolymerize actin filaments **(54)**. The 85 amino acid sequence in the N-terminal region

(residues 233–317), highly conserved among mammals, is sufficient for the strong binding of drebrin to F-actin, and causes the same rearrangements in the actin cytoskeleton as the full-length drebrin **(55)**. Drebrin can self-assemble and form higher-order oligomers named drebrosomes **(42, 56)**. It was hypothesized that such structures allowed for maintaining a high local concentration of these regulatory proteins in the needed regions in cells.

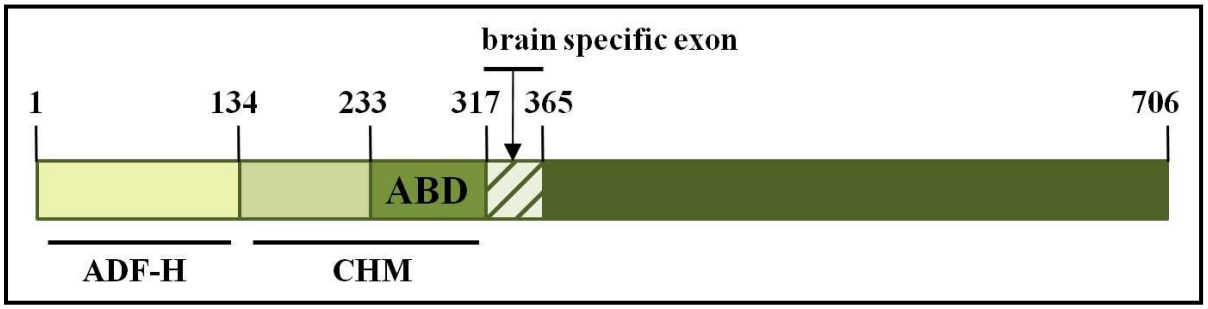

Figure 1.3- Schematic Representation of the Drebrin Molecule.
ADF-H stands for Actin Depolymerization factor-homology domain. **CHM** is the Charged Helical domain. **ABD** stands for Actin Binding Domain. The shaded region is the brain specific exon that is present in Drebrin-A but is absent in Drebrin-E.

Drebrin binds to F-actin with a stoichiometry of one to five protomers (K_d of $\sim$ 0.12 μM) **(54, 57)** and competes and inhibits actin binding activity of several F-actin-binding proteins, such as fascin, tropomyosin and α-actinin **(54, 58)**. Drebrin also inhibits the actin-activated ATPase activity of myosin and reduces the sliding velocity of actin filaments on immobilized myosin. According to the *in vitro* studies, cofilin can displace drebrin from actin filaments **(59)**. This observation is consistent with the finding that drebrin's loss is accompanied by increased levels of cofilin in the brains of Alzheimer's disease patients **(50)**. More recently, it was shown that full length drebrin-A inhibits but does not abolish cofilin-induced severing of actin filaments **(60)**. Taken together, these findings suggest that drebrin modulates the organization of the actin

cytoskeleton within spines, playing a role in the structure-based plasticity of synapses. More recent reports revealed a direct effect of drebrin on the structure of F-actin: Atomic force microscopy (AFM) analysis showed that binding of drebrin-A to actin filaments increases their persistence length and helical pitch (~40 nm *versus* 36 nm for "bare" actin) **(57)**. This stimulated a more detailed probing of drebrin's effects on the structure and dynamics of actin filaments, to help elucidate the mechanism by which these two spine-resident proteins regulate spine plasticity and affect brain functions.

Coronin

Coronin is one of the conserved actin-binding proteins whose influence on actin dynamics in the cell is not well understood yet, but whose involvement in the rearrangement of the actin cytoskeleton is undeniably substantial. Originally identified as a major co-purifying protein in a preparation of contracted actin–myosin from *Dictyostelium discoideum*, it was named coronin due to its localization to crown-like extensions on the surface of these cells **(61)**. Since then, a wide variety of coronins have been identified in many eukaryotic organisms including yeast, nematode, fish and mammals. While *Saccharomyces Cerevisiae* and *schizosaccharomyces Pombe* have a single coronin gene, other organisms like *Drosophila Melanogaster, Dictyoselium discoideium* and *Caenorhabditis elegans* have 2 to 3 coronin genes. Mammals have up to seven different coronin-related genes; they are expressed in most tissues, except for coronin1A which is preferentially expressed in T lymphocytes and other hematopoietic cells **(62, 63)**. Coronins are divided into three subclasses based on their amino acid sequence lengths: Type 1 coronins include coronin-1A, -1B, and -1C; type II coronins include coronin -2A and -2B; finally, type III coronins encompass mammalian coronin -7 and the POD-1 proteins from *Caenorhabtidis elegans* and *Drosophila melanogaster.* Type and I and II

coronins' structure consists of a three- part domain layout. It includes the β-propeller domain which is the N-terminal domain containing 7 WD40 repeats (5 canonical ones flanked by the two non-canonical), followed by a highly variable "unique" region as well as a C-terminal domain that forms a coiled coil (CC) structure (Figure 1.5). Type III coronins differ in their sequence as they are composed of tandem coronin repeats but lack the CC region **(64)**. The crystal structure of the β-propeller domain of murine coronin1 was solved in 2006 (Figure 1.5, **65)**.

In principle, the β-propeller structures often serve as a platform to support protein-protein interactions, but so far only F-actin has been identified as a binding partner of this domain of coronin. The N-terminal extension contains a crucial phosphorylation site (Ser-2) that regulates interactions of coronin with its binding partners **(66, 67)**. The middle linker, or "Unique" region varies in both length and sequence among different coronins.

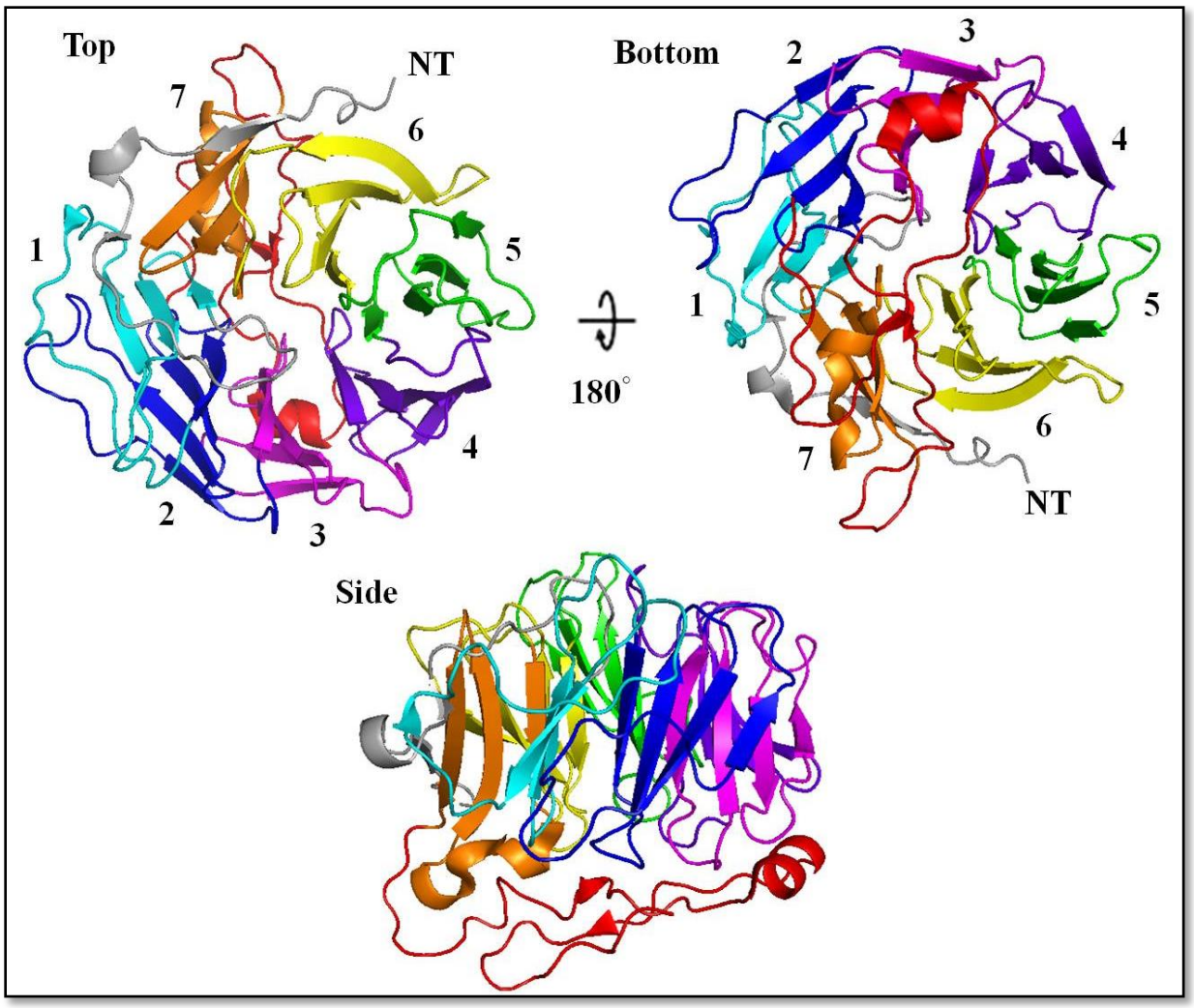

Figure 1.5- The Overall Structure of Murine Coronin1 (PDB ID: 2AQ5).
Ribbon diagrams show the "top" and "bottom" side of the β propeller domain. Individual blades are numbered from one to seven (colored cyan, blue, magenta, purple, green, yellow and orange, respectively). The N-terminus extension (grey) and the C-terminal extension (red) are also shown. The N-terminus is labeled NT. The "side" view highlights the C-terminal extension tightly packing against the "bottom" surface of the propeller **(65).**

S. Cerevisiae Crn1 and *D. Melanogaster* Dpod1 share noted sequence homology with the microtubule binding region of mammalian MAP1B and bind to microtubules, crosslink them and crosslink actin filaments in vitro; this has been confirmed by genetic analyses **(68, 69, 70)**. The coiled coil (CC) region is a classic heptad repeat CC domain that mediates homo-oligomerization. It contains an actin binding site and an Arp2/3 binding site **(71, 72)**.

Functional studies in these organisms have shown coronins to be important regulators of actin based processes such as cytokinesis, cell migration and lamellopodial formation. Dictyostelium cells deficient in coronin move at about half the rate of wild-type controls, have a high frequency of failed cytokinesis and in addition, coronin-null cells also have severe defects in fluid-phase endocytosis. There are no gross defects when coronin is deleted from budding yeast, but when the deletion is coupled with a mutation in actin, cofilin or Apr2/3, synthetic defects in growth and cytoskeletal organization are observed **(68)**. Also overexpression of the *S.Cerevisiae* coronin gene (Crn1) is lethal and disrupts actin organization: it induces the formation of aberrant coronin and Arp2/3 containing F-actin loops **(73)**. In Drosophila, coronin mutations cause disruptions in the actin cytoskeleton of the embryonic imaginal disks and an early pupal lethal phenotype, indicating that this protein is essential for morphogenesis **(74)**. In primary human neutrophils, the inhibition of Coronin1 function by transduction of a dominant-negative form of the protein leads to inhibition of chemotaxis and a reduction in neutrophil spreading and adhesion **(75)**. The list of studies demonstrating the effects of deleting or mutating the different coronin genes is long and emphasizes the importance of the different coronin genes and their role as key players in the proper functioning of eukaryotic cells.

Unraveling the actin-binding interface is an essential step in understanding coronin's role as a key player in the cytoskeleton. It shows the nature of the interactions of the two proteins,

allows further establishing the structural effects they have on each other, and sheds light on the mechanisms used by coronin to regulate other actin binding proteins' activity on actin filaments. A significant effort has been invested in addressing this issue, with different approaches being used for probing coronin's action; however, different modes of binding were proposed by different groups. The first mechanism relied on electron microscopy and three dimensional (3D) reconstruction **(76)** of coronin1-A decorated actin filaments, the second was revealed by systematic mutational analysis of yeast coronin mutant alleles **(77)** and lastly, Ge et al. very recently generated high resolution cryo-EM images of the coronin-actin complex and mapped protein-protein contacts with high precision **(78)**. Galkin et al. EM and 3D reconstruction of coronin-F-actin lead to specific predictions of contact surfaces between these proteins and showed that mammalian Coronin-1A stabilizes F-actin by bridging adjacent actin protomers along the long-pitch strand and stapling opposite protomers on different strands of the actin filament. Gandhi et al. used a systematic mutagenesis approach to identify surfaces on the β-propeller domain of Crn1 required for actin binding. They used a "charge-to-alanine" strategy to design mutations and identified five actin binding coronin surfaces. The models of coronin-F-actin structures (in both ADP- and ADP-BeFx-states) derived from the cryo-EM data in **(78)** are consistent with the interaction surface identified by **(77)**.

All sets of data agree on coronin's interaction with two or more actin subunits in the filament. The EM methods show this directly, while the mutagenesis implicates it since it is difficult to imagine how all of the predicted actin binding surfaces could be interacting with a single actin subunit in the filament. These findings fuel the natural interest to study the structural effects of coronin on actin filaments and to investigate the mechanisms by which it regulates the

functions of cofilin and the Arp2/3 complex. The results of such investigations are presented in Chpater 4.

Cofilin

Cofilin is a member of the Actin Depolymerization Factor- Homology (ADF-H) domain family of proteins and is an essential actin regulatory protein that severs filaments and accelerates actin assembly dynamics by increasing the number of filament ends at which subunits add and dissociate from **(79, 80)**. The involvement of cofilin in controlling the temporal and spatial extent of actin dynamics is seen in processes as diverse as cytokinesis in yeast **(81)**, tumour metastasis in mice **(82)**, neuronal plasticity in rats **(83)**, and Alzheimer's disease **(84)**.

Cofilin is a small 16 kDa protein that is found in all eukaryotic cells and that binds both monomeric and filamentous actin. Unicellular organisms produce only one member of this family, whereas mammals produce three members of the ADF/cofilin family – ADF, non-muscle cofilin (cofilin 1) and muscle cofilin (cofilin 2) **(85).** High resolution 3D crystal structures and NMR solution structures of ADF-H domains from different proteins show that the basic ADF-H fold is composed of four alpha helices (α1–4) surrounded by six beta strands (β1–6) **(86, 87, 88, 89, 90, 91)**. Several groups have mapped the binding sites of cofilin onto both G and F-actin via mutagenesis, fluorescence probing, and chemical cross-linking in an effort to understand cofilin's functions **(92, 93, 94, 95, 96)**. The actin-cofilin interactions are mediated by two separate binding regions of the ADF-H domain, called the G-site and the F-site. The G-site is sufficient to interact with actin monomers (or even the Arp2/3 complex), while both the G- and the F-sites are required for binding to F-actin (**97**). Grintsevich et al. **(92)** showed that cofilin binds to the hydrophobic cleft between subdomains 1 and 3 on G-actin. Further supporting this conclusion, the atomic structure of the C terminal ADF-H domain of mouse twinfilin-1 in

complex with rabbit α-skeletal G-actin revealed that the G-site is incorporated between SD1 and SD3 at the barbed face of the actin monomer and forms contact with its hydrophobic groove and the C-terminus **(98)**. A more recent 3D reconstruction of rabbit α-skeletal F-actin decorated with human cofilin-2 showed that the interaction of ADF-H domains with actin filaments is mediated by two distinct regions, which bind to two adjacent actin subunits within the single-stranded helix of the actin filament **(99)**. One of these resembles the G-site found in the twinfilin-G-actin complex and forms a contact with the barbed face of the upper actin subunit. The other region is composed of two loops, one loop binds to the SD4 and the other to the SD1 region of the lower actin subunit.

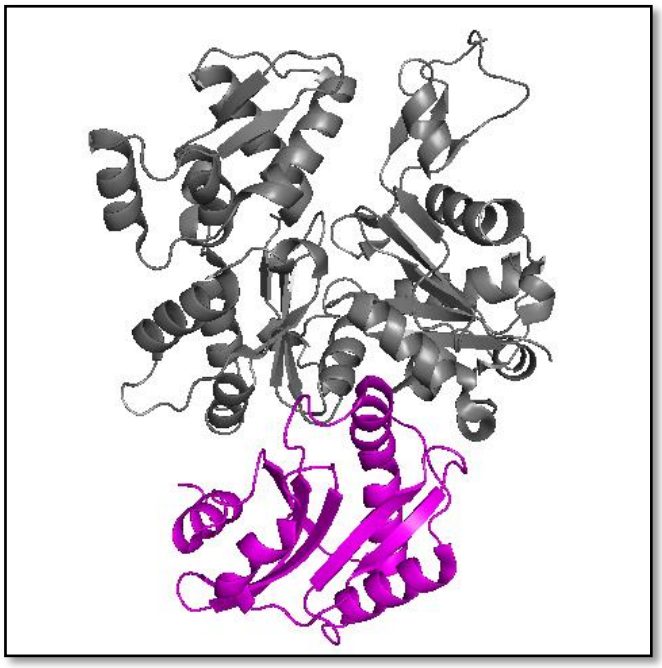

Figure 1.6 Atomic structure of the C-terminal ADF-H domain of twinfilin in complex with rabbit α-skeletal actin monomer.
ADF-H is shown in magenta and actin in gray with its sudomains denoted as SD1, SD2, SD3 and SD4. (The structure is shown from PDB code 3DAW) (Paavilainen et al., 2008).

The ADF/cofilin proteins bind co-operatively to F-actin and display higher affinity for the ADP–actin subunits than for actin subunits bound to ATP or to ADP and inorganic phosphate (P_i) **(100, 101)**. Cofilin is "inactivated" upon phosphorylation of Ser3 at its N-terminus; this modification generates a charge repulsion that inhibits actin binding without altering the protein conformation **(102, 103)**. Cofilin is activated by the Slingshot family of phosphatases **(104)**. Cofilin binds better to older ADP-bound actin filaments and accelerates the release of subunits from the pointed-end through depolymerization and severing, and/or by both processes, while the rate of dissociation from the barbed ends remains unchanged **(101, 106, 107)**. This large increase in the rate-limiting step of the treadmilling cycle at steady state is responsible for the increase in the rate of actin-based motile processes. Because cofilin severs actin filaments, it also acts

indirectly as a nucleator, with severing generating free barbed-ends from which polymerization can occur **(108)**.

The mechanism of depolymerization and severing by cofilin has been studied extensively. Using cryo-electron microscopy and image reconstructions, McGough et al. (30) showed that ADF/cofilin changes the helical twist of F-actin by 5° between protomer *n* and *n* + 1, and reduces torsional rigidity upon binding to F-actin. This change decreases the helical strands crossover distance (from 365 Å in bare actin to ~270 Å when cofilin is bound) and modifies the interprotomer contacts **(108)**. More recently, using cryoelectron microscopy, Galkin et al. generated a 9-Å resolution three-dimensional reconstruction of cofilin-decorated actin filaments showing that human cofilin 2 (Hcof2) substantially displaces subdomain 2 of muscle skeletal actin and causes it to be disordered. Essentially, cofilin disrupts the connection between SD1 and SD2 of adjacent protomers within the same strand and forms a direct contact with them, bridging the two subunits by providing extra contacts and therefore resulting in net stabilization of subunit-subunit contacts **(99)**. This structural effect acts as a double-edged sword. On one edge, cofilin acts as an actin nucleator, able to rescue the polymerization of mutated or chemically modified actin that can no longer polymerize due to weakened inter- and intrastrand contacts (TMR labeled actin, Grimlysin cleaved actin, T203C actin; **109, 110**). Kudryashov et al. proposed that cofilin is able to rescue polymerization by creating a new interface between SD1/ SD3 cleft of the upper protomer to SD2 of the lower protomer, thus reversing the destabilizing effects of actin mutations/modifications **(111)**. On the other hand, the local weakening of the F-actin structure propagates as long-range allosteric effects which result in the destabilization of both inter- and intra-strand filament contacts where cofilin is not bound. This creates mechanical asymmetry along filaments which promotes local

stress accumulation and consequently, causes filaments to sever. Hence, the proposed model of its action is that stabilization occurs under saturating conditions of cofilin, whereas severing occurs more efficiently at the boundaries of changed and unchanged filament segments, under sub-saturating conditions, where regions partially decorated with cofilin accumulate stress that is propagated along the filament in a cooperative manner.

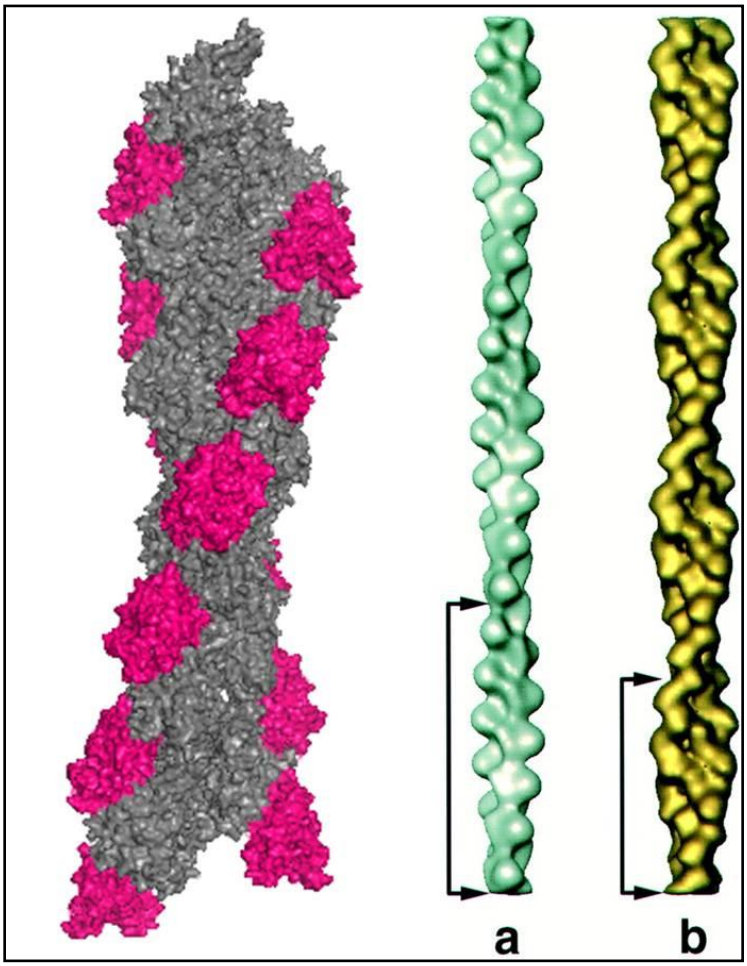

Figure 1.6. Model of cofilin decorated F-actin.
Cofilin (hot pink) binds F-actin (gray) and decreases its twist by 5°, from -167° (a) to -162° (b). Arrows mark the crossover length.
The reconstruction is shown from PDB code 3J0S. The figure showing the change in twist is adapted from McGough et al., **(108)**.

Overview of the Dissertation

This dissertation focuses on the modulation of actin structure and dynamics by three major actin binding proteins, drebrin, coronin and cofilin. Drebrin is a filament-binding protein involved in organizing the dendritic pool of actin. Previous in vivo studies identified the actin-binding domain of drebrin (DrABD), which causes the same rearrangements in the cytoskeleton as the full-length protein.

Chapter 2 investigates the mapping of the DrABD binding interface on actin filaments. Site-directed mutagenesis, electron microscopy images reconstruction, and chemical cross-linking combined with mass spectrometry analysis were employed for this study. Our results showed that DrABD binding bridges two adjacent actin protomers. Site-directed mutagenesis combined with chemical cross-linking and mass spectrometry analysis suggested that the "core" DrABD is centered on actin subdomain 2 and may adopt a folded conformation upon binding to F-actin. The results of electron microscopic reconstruction further revealed polymorphism in DrABD binding to F-actin and suggested the existence of two binding sites. These results provided new structural insight into the previously observed competition between drebrin and several other F-actin-binding proteins.

Chapter 3 of this dissertation examined the structural effects of drebrin on F-actin in solution. Full-length drebrin and its C-terminal truncated constructs were used to clarify the domain requirements for the observed effects. Depolymerization and differential scanning calorimetry assays show that F-actin is stabilized by the binding of drebrin. Also, using solution biochemistry methods and electon microscopy (EM), we observed the rescue of filament formation by drebrin in different cases of longitudinal and lateral interprotomer contact

perturbations. Overall, our data suggested that drebrin stabilizes actin filaments through its effect on their interstrand and intrastrand contacts.

Chapter 4 examines another actin binding protein, coronin, and the effect of its shorter but fully active construct on actin filaments. Using a combination of site-directed mutagenesis, solution biochemistry methods, electron and TIRF microscopy, we looked at the effects of coronin on the structure of actin filaments by studying its effect on inter-protomer contacts in F-actin. We also examined how some of these effects compare to those induced by cofilin, studying how the two proteins behave when they are present together, to shed light on the mechanism(s) by which coronin modulates cofilin's effects on actin filaments. Our results shed light on the small, yet important structural changes that coronin induces in actin filaments, and provide a plausible mechanism by which coronin mediates cofilin-induced disassembly of actin filaments.

REFERENCES

1) Reisler E. & Egelman E.H. (2007). Actin structure and function: what we still do not understand. *J. Biol. Chem.* **282**, 36133-37.

2) Garrels J.I. & Gibson W. (1976). Identification and characterization of multiple forms of actin. *Cell*. **9**, 793-805.

3) Rubenstein P.A. & Spudich J.A. (1977). Actin microheterogeneity in chick embryo fibroblasts. *Proc. Natl. Acad. Sci.* U.S.A. **74**, 120-23.

4) Perrin B.J. & Ervasti J.M. (2010). The actin gene family: function follows isoform. *Cytoskeleton* (Hoboken). **67**, 630-34.

5) Rubenstein P.A. & Wen K.K. (2014). Insights into the effects of disease-causing mutations in human actins. *Cytoskeleton* (Hoboken). **71**, 211-29.

6) van den Ent F., Amos L.A., Löwe J. (2001). Bacterial ancestry of actin and tubulin. *Curr Opin. Microbiol*. **4**, 634-38.

7) van den Ent F. & Amos L.A., Löwe J. (2001). Prokaryotic origin of the actin cytoskeleton. *Nature*. **413**, 39-44.

8) Esue O., Cordero M., Wirtz D., Tseng Y. (2005). The assembly of MreB, a prokaryotic homolog of actin. *J. Biol. Chem*. **280**, 2628-35.

9) Shih Y.L. & Rothfield L. (2006). The bacterial cytoskeleton. *Microbiol. Mol. Biol. Rev*. **70**, 729-54.

10) Møller-Jensen J., Jensen R.B., Löwe J., Gerdes K. (2002). Prokaryotic DNA segregation by an actin-like filament. *EMBO J.* **21**, 3119-27.

11) Kabsch W., Mannherz H.G., Suck D., Pai E.F., Holmes K.C. (1990). Atomic structure of the actin: DNase I complex. *Nature*. **347**, 37-44.

12) Dominguez R. & Holmes K.C. (2011). Actin structure and function. *Annu. rev. biophys*. **40**, 169-86.

13) Dominguez R. (2004). Actin-binding proteins—a unifying hypothesis. *Trends. Biochem. Sci.* **29**, 572–78

14) Dominguez R. & Graceffa P. (2003). Solution properties of TMR-actin: when biochemical and crystal data agree. *Biophys. J*. **85**, 2073-74.

15) Lorenz M., Popp D., Holmes K.C. (1993). Refinement of the F-actin model against X-ray fiber diffraction data by the use of a directed mutation algorithm. *J. Mol. Biol.* **234**, 826-36.

16) Shvetsov A., Musib R., Phillips M., Rubenstein P.A., Reisler E. (2002). Locking the hydrophobic loop 262-274 to G-actin surface by a disulfide bridge prevents filament formation. *Biochemistry*. **35**, 10787-93.

17) Scoville D., Stamm J.D., Toledo-Warshaviak D., Altenbach C., Phillips M., Shvetsov A., Rubenstein P.A., Hubbell W.L., Reisler E. (2006). Hydrophobic loop dynamics and actin filament stability. *Biochemistry*. **45**, 13576-84.

18) Shvetsov A., Galkin V.E., Orlova A., Phillips M., Bergeron S.E., Rubenstein P.A., Egelman E.H., Reisler E. (2008). Actin hydrophobic loop 262-274 and filament nucleation and elongation. *J. Mol. Biol*. **375**, 793-801.

19) Splettstoesser T., Holmes K.C., Noé F., Smith J.C. (2011). Structural modeling and molecular dynamics simulation of the actin filament. *Proteins*. **79**, 2033-43.

20) Vorobiev S., Strokopytov B., Drubin D.G., Frieden C., Ono S., Condeelis J., Rubenstein P.A., Almo S.C. (2003). The structure of nonvertebrate actin: implications for the ATP hydrolytic mechanism. *Proc. Natl. Acad. Sci. U.S.A.* **100**, 5760-65

21) Carlier M.F. & Pantaloni D. (1986). Direct evidence for ADP-Pi-F-actin as the major intermediate in ATP-actin polymerization. Rate of dissociation of Pi from actin filaments. *Biochemistry*. **25**, 7789-92.

22) Carlier M.F. (1987). Measurement of Pi dissociation from actin filaments following ATP hydrolysis using a linked enzyme assay. *Biochem. Biophy.s Res. Commun*. **143**, 1069-75.

23) Carlier M.F., Pantaloni D., Korn E.D. (1984). Evidence for an ATP cap at the ends of actin filaments and its regulation of the F-actin steady state. *J. Biol. Chem*. **259**, 9983-86.

24) Bugyi B. Carlier M.F. (2010). Control of actin filament treadmilling in cell motility. *Annu. Rev. Biophys*. **39**, 449-70.

25) Pollard T.D. & Cooper J.A. (2009). Actin, a central player in cell shape and movement. *Science*. **326**, 1208-12.

26) Pollard T.D., Borisy G.G. (2003). Cellular motility driven by assembly and disassembly of actin filaments. *Cell.* **112**, 453-65.

27) Edelstein-Keshet L. & Ermentrout G.B. (2002). Models for spatial polymerization dynamics of rod-like polymers. *J. Math. Biol*. **40**, 64-96.

28) Pollard T. (1986). Rate constants for the reactions of ATP- and ADP-actin with the ends of actin filaments. *J. Cell Biol.* 103, 2747-54

29) Sheterline P., Clayton J. and Sparrow J.C. (1998) *Protein Profile: Actin*, 4th Ed., Oxford University Press, Inc., New York.

30) Hering H. & Sheng M. (2001). Dendritic spines: structure, dynamics and regulation. *Nat. Rev. Neurosci*. **12**, 880-88.

31) Moser M. B., Trommald M., Andersen P. (1994) An increase in dendritic spine density on hippocampal CA1 pyramidal cells following spatial learning in adult rats suggests the formation of new synapses. *Proc. Natl. Acad. Sci. U.S.A.* **91**, 12673–75

32) Geinisman Y., deToledo-Morrell L., Morrell F., Persina I.S., Rossi M. (1992). Age-related loss of axospinous synapses formed by two afferent systems in the rat dentate gyrus as revealed by the unbiased stereological dissector technique. *Hippocampus.* **4**, 437-44.

33) Purpura D. P. (1974). Dendritic spine "dysgenesis" and mental retardation. *Science.* **186**, 1126–28.

34) Wisniewski K. E., Segan S. M., Miezejeski C. M., Sersen E. A., Rudelli R. D. (1991).The fra(X) syndrome. Neurological, electrophysiological, and neuropathological abnormalities. *Am. J. Med. Genet*. **38**, 476–80.

35) Irwin S. A., Galvez R., Greenough W. T. (2000). Dendritic spine structural anomalies in fragile-x mental retardation syndrome. *Cereb. Cortex*. **10**, 1038–44.

36) Kojima N., Shirao T., Obata K. (1993). Molecular cloning of a developmentally regulated brain protein, chicken drebrin A and its expression by alternative splicing of the drebrin gene. *Brain Res. Mol. Brain Res*. **19**, 101–14.

37) Jin M., Tanaka S., Sekino Y., Ren Y., Yamazaki H., Kawai-Hirai R., Kojima N., Shirao T. (2002). A novel, brain-specific mouse drebrin: cDNA cloning, chromosomal mapping, genomic structure, expression, and functional characterization. *Genomics*. **79**, 686-92.

38) Shirao T. & Obata K. (1986). Immunochemical homology of 3 developmentally regulated brain proteins and their developmental change in neuronal distribution. *Brain Res*. **394**, 233–44.

39) Aoki C., Sekino Y., Hanamura K., Fujisawa S., Mahadomrongkul V., Ren Y., Shirao T. (2005). Drebrin A is a postsynaptic protein that localizes *in vivo* to the submembranous surface of dendritic sites forming excitatory synapses. *J. Comp. Neurol*. **483**, 383–402.

40) Keon B.H., Jedrzejewski P.T., Paul D.L., Goodenough D.A. (2000). Isoform specific expression of the neuronal F-actin binding protein, drebrin, in specialized cells of stomach and kidney epithelia. *J. Cell. Sci.* **113**, 325-36.

41) Peitsch W.K., Grund C., Kuhn C., Schnölzer M., Spring H., Schmelz M., Franke W.W. (1999). Drebrin is a widespread actin-associating protein enriched at junctional plaques, defining a specific microfilament anchorage system in polar epithelial cells. *Eur. J. Cell. Biol*. **78**, 767-78.

42) Peitsch W.K., Hofmann I., Prätzel S., Grund C., Kuhn C., Moll I., Langbein L., Franke W.W. (2001). Drebrin particles: components in the ensemble of proteins regulating actin dynamics of lamellipodia and filopodia. *Eur. J. Cell. Biol*. **80**, 567-79.

43) Matus A., Ackermann M., Pehling G., Byers H. R., Fujiwara K. (1982). High actin concentrations in brain dendritic spines and postsynaptic densities. *Proc. Natl. Acad. Sci. U.S.A.* **79**, 7590–94.

44) Cohen R.S., Chung S.K., Pfaff D.W. (1985). Immunocytochemical localization of actin in dendritic spines of the cerebral cortex using colloidal gold as a probe. *Cell. Mol. Neurobiol.* **3**, 271-84.

45) Fifková E. & Delay R. J. (1982). Cytoplasmic actin in neuronal processes as a possible mediator of synaptic plasticity. *J. Cell Biol.* **95**, 345–50.

46) Matus A. (2000). Actin-based plasticity in dendritic spines. *Science*. **290**, 754–58.

47) Takahashi H., Sekino Y., Tanaka S., Mizui T., Kishi S., Shirao T. (2003). Drebrin-dependent actin clustering in dendritic filopodia governs synaptic targeting of postsynaptic density-95 and dendritic spine morphogenesis. *J. Neurosci.* **23**, 6586–95.

48) Sekino Y., Kojima N., Shirao T. (2007). Role of actin cytoskeleton in dendritic spine morphogenesis. *Neurochem. Int.* **51**, 92–104.

49) Merriam E.B., Millette M., Lumbard D.C., Saengsawang W., Fothergill T., Hu X., Ferhat L., Dent E.W. (2013). Synaptic regulation of microtubule dynamics in dendritic spines by calcium, F-actin, and drebrin. *J. Neurosci.* **33**, 16471-82.

50) Kojima N. & Shirao T. (2007). Synaptic dysfunction and disruption of postsynaptic drebrin-actin complex. A study of neurological disorders accompanied by cognitive deficits. *Neurosci. Res*. **58**, 1–5.

51) Weitzdoerfer R., Dierssen M., Fountoulakis M., Lubec G. (2001). Fetal life in Down syndrome starts with normal neuronal density but impaired dendritic spines and synaptosomal structure. *J. Neural. Transm. Suppl.* **61**, 59–70.

52) Shim K.S. & Lubec G. (2002). Drebrin, a dendritic spine protein, is manifold decreased in brains of patients with Alzheimer's disease and Down syndrome. *Neurosci. Lett*. **324**, 209-12.

53) Lappalainen P., Kessels M.M., Cope M.J., Drubin D.G. (1998). The ADF homology (ADF-H) domain: a highly exploited actin-binding module. *Mol. Biol. Cell*. **9**, 1951-59.

54) Ishikawa R., Hayashi K., Shirao T., Xue Y., Takagi T., Sasaki Y., Kohama K. (1994). Drebrin, a development-associated brain protein from rat embryo, causes the dissociation of tropomyosin from actin filaments. *J. Biol. Chem.* **269**, 29928–33.

55) Hayashi K., Ishikawa R., Kawai-Hirai R., Takagi T., Taketomi A., Shirao T. (1999). Domain analysis of the actin-binding and actin-remodeling activities of drebrin. *Exp. Cell Res*. **253**, 673–80.

56) Peitsch W.K., Hofmann I., Endlich N., Prätzel S., Kuhn C., Spring H., Gröne H.J., Kriz W., Franke W.W. (2003). Cell biological and biochemical characterization of drebrin complexes in mesangial cells and podocytes of renal glomeruli. *J. Am. Soc. Nephrol*. **14**, 1452-63.

57) Sharma S., Grintsevich E. E., Phillips M. L., Reisler E., Gimzewski J. K. (2011). Atomic force microscopy reveals drebrin induced remodeling of F-actin with subnanometer resolution. *Nano Lett*. **11**, 825–827.

58) Sasaki Y., Hayashi K., Shirao T., Ishikawa R., Kohama K. (1996). Inhibition by drebrin of the actin-bundling activity of brain fascin, a protein localized in filopodia of growth cones. *J. Neurochem.* **66**, 980–88.

59) Zhao L., Ma Q.L., Calon F., Harris-White M.E., Yang F., Lim G.P., Morihara T., Ubeda O.J., Ambegaokar S., Hansen J.E., Weisbart R.H., Teter B., Frautschy S.A., Cole G.M. (2006). Role of p21-activated kinase pathway defects in the cognitive deficits of Alzheimer disease. *Nat. Neurosci.* **9**, 234-42.

60) Grintsevich E.E. & Reisler E. (2014). Drebrin inhibits cofilin-induced severing of F-actin. *Cytoskeleton* (Hoboken). **71**, 472-83.

61) de Hostos E.L., Bradtke B., Lottspeich F. Guggenheim R., Gerisch G. (1991). Coronin, an actin binding protein of Dictyostelium discoideum localized to cell surface projections, has sequence similarities to G protein beta subunits. *EMBO J.* **10**, 4097–4104.

62) Suzuki K., Nishihata J., Arai Y., Honma N., Yamamoto K., Irimura T., Toyoshima S. (1995). Molecular cloning of a novel actin-binding protein, p57, with a WD repeat and a leucine zipper motif. *FEBS Lett.* **364**, 283-88.

63) Nal B., Carroll P., Mohr E., Verthuy C., Da Silva M.I., Gayet O., Guo X.J., He H.T., Alcover A., Ferrier P. (2004). Coronin-1 expression in T lymphocytes: insights into protein function during T cell development and activation. *Int. Immunol*. **16**, 231-40.

64) McArdle B. & Hofmann A. (2008). Coronin structure and implications. *Subcell. Biochem.* **48**, 56-71.

65) Appleton B.A., Wu P., Wiesmann C. (2006). The crystal structure of murine coronin-1: a regulator of actin cytoskeletal dynamics in lymphocytes. *Structure*. **14**, 87-96.

66) Cai L., Holoweckyj N., Schaller M.D., Bear J.E. (2005). Phosphorylation of coronin 1B by protein kinase C regulates interaction with Arp2/3 and cell motility. *J. Biol. Chem*. **280**, 31913–23.

67) Cai L., Makhov A.M., Bear J.E. (2007). F-actin binding is essential for coronin 1B function in vivo. *J. Cell. Sci.* **120**, 1779–90.

68) Goode B.L., Wong J.J., Butty A.C., Peter M., McCormack A.L., Yates J.R., Drubin D.G., Barnes G. (1999). Coronin promotes the rapid assembly and cross-linking of actin filaments and may link the actin and microtubule cytoskeleton in yeast. *J. Cell. Biol***. 144**, 83-98.

69) Rothenberg M.E., Rogers S.L., Vale R.D., Jan L.Y., Jan Y.N. (2003). Drosophila pod-1 crosslinks both actin and microtubules and controls the targeting of axons. *Neuron*. **39**, 779–91.

70) Heil-Chapdelaine R.A., Tran N.K., Cooper J.A. (1998). The role of Saccharomyces cerevisiae coronin in the actin and microtubule cytoskeletons. *Curr. Biol*. **8**, 1281–84.

71) Oku T., Itoh S., Okano M., Suzuki A., Suzuki K., Nakajin S., Tsuji T., Nauseef W.M., Toyoshima S. (2003). Two regions responsible for the actin binding of p57, a mammalian coronin family actin-binding protein. *Biol. Pharm. Bull.* **26**, 409–16.

72) Liu C.Z., Chen Y., Sui S.F. (2006). The identification of a new actin-binding region in p57. *Cell. Res*. **16**, 106-122.

73) Humphries C.L., Balcer H.I., D'Agostino J.L., Winsor B., Drubin D.G., Barnes G., Andrews B.J., Goode B.L. (2002). Direct regulation of Arp2/3 complex activity and function by the actin binding protein coronin. *J. Cell. Biol*. **159**, 993-1004.

74) Bharathi V., Pallavi S.K., Bajpai R., Emerald B.S., Shashidhara L.S. (2004). Genetic characterization of the Drosophila homologue of coronin. *J. Cell. Sci*. **117**, 1911-22.

75) Yan M., Di Ciano-Oliveira C., Grinstein S., Trimble W.S. (2007). Coronin function is required for chemotaxis and phagocytosis in human neutrophils. *J. Immunol.* **178**, 5769–78.

76) Galkin V.E., Orlova A., Kudryashov D.S., Solodukhin A., Reisler E., Schröder G.F., Egelman E.H. (2011). Remodeling of actin filaments by ADF/cofilin proteins. *Proc. Natl. Acad. Sci. U S A.* **108**, 20568-72.

77) Gandhi M., Jangi M., Goode B.L. (2009). Functional surfaces on the actin-binding protein coronin revealed by systematic mutagenesis. *J. Biol. Chem.* **285**, 34899-908.

78) Ge P., Durer Z.A., Kudryashov D., Zhou Z.H., Reisler E. (2014). Cryo-EM reveals different coronin binding modes for ADP- and ADP-BeFx actin filaments. *Nat. Struct. Mol. Biol*. **21**, 949-54.

79) Michelot A., Berro J., Guérin C., Boujemaa-Paterski R., Staiger C.J., Martiel J.L., Blanchoin L. (2007). Actin-filament stochastic dynamics mediated by ADF/cofilin. *Curr. Biol.* **17**, 825-33.

80) Roland J., Berro J., Michelot A., Blanchoin L., Martiel J.L. (2008). Stochastic severing of actin filaments by actin depolymerizing factor/cofilin controls the emergence of a steady dynamical regime. *Biophys. J.* **94**, 2082-94.

81) Chen Q. & Pollard T. D. (2011). Actin filament severing by cofilin is more important for assembly than constriction of the cytokinetic contractile ring. J. Cell. Biol. 195, 485–98.

82) Roussos E. T., Condeelis J. S. & Patsialou A. (2011). Chemotaxis in cancer. *Nature Rev. Cancer*. **11**, 573–87.

83) Gu J., Lee C.W., Fan Y., Komlos D., Tang X., Sun C., Yu K., Hartzell H.C., Chen G., Bamburg J.R., Zheng J.Q. (2010). ADF/cofilin-mediated actin dynamics regulate AMPA receptor trafficking during synaptic plasticity. *Nature Neurosci.* **13**, 1208–15.

84) Bamburg J. R. & Wiggan O. P. (2002). ADF/cofilin and actin dynamics in disease. *Trends Cell. Biol.* **12**, 598–605.

85) Vartiainen M.K., Mustonen T., Mattila P.K., Ojala P.J., Thesleff I., Partanen J., Lappalainen P. (2002). The three mouse ADF/cofilins evolved to fulfill cell-specific requirements for actin dynamics. *Mol. Biol. Cell*. **13**, 183–194.

86) Fedorov A.A., Lappalainen P., Fedorov E.V., Drubin D.G., Almo S.C. (1997). Structure determination of yeast cofilin. *Nat. Struct. Biol.* **4**, 366-69.

87) Goroncy A.K., Koshiba S., Tochio N., Tomizawa T., Sato M., Inoue M., Watanabe S., Hayashizaki Y., Tanaka A., Kigawa T., Yokoyama S. (2009). NMR solution structures of actin depolymerizing factor homology domains. *Protein Sci.* **18**, 2384-92.

88) Hellman M., Paavilainen V.O., Naumanen P., Lappalainen P., Annila A., Permi P. (2004). Solution structure of coactosin reveals structural homology to ADF/cofilin family proteins. *FEBS Lett*. **576**, 91-96.

89) Paavilainen V.O., Oksanen E., Goldman A., Lappalainen P. (2008). Structure of the actin-depolymerizing factor homology domain in complex with actin. *J. Cell Biol.* **182**, 51-59.

90) Singh B.K., Sattler J.M., Chatterjee M., Huttu J., Schüler H., Kursula I. (2011). Crystal structures explain functional differences in the two actin depolymerization factors of the malaria parasite. *J. Biol. Chem*. **286**, 28256-64.

91) Strokopytov B.V., Fedorov A., Mahoney N.M., Kessels M., Drubin D.G., Almo S.C. (2005). Phased translation function revisited: structure solution of the cofilin-homology domain from yeast actin-binding protein 1 using six-dimensional searches. *Acta. Crystallogr. D. Biol. Crystallogr*. **61**, 285-93.

92) Grintsevich E.E., Benchaar S.A., Warshaviak D., Boontheung P., Halgand F., Whitelegge J.P., Faull K.F., Loo R.R., Sept D., Loo J.A., Reisler E. (2008). Mapping the cofilin binding site on yeast G-actin by chemical cross-linking. *J. Mol. Biol.* **377**, 395-409.

93) Benchaar S.A., Xie Y., Phillips M., Loo R.R., Galkin V.E., Orlova A., Thevis M., Muhlrad A., Almo S.C., Loo J.A., Egelman E.H., Reisler E. (2007). Mapping the interaction of cofilin with subdomain 2 on actin. *Biochemistry*. **46**, 225-33.

94) Mannherz H.G., Ballweber E., Galla M., Villard S., Granier C., Steegborn C., Schmidtmann A., Jaquet K., Pope B., Weeds A.G. (2007). Mapping the ADF/cofilin binding site on monomeric actin by competitive cross-linking and peptide array: evidence for a second binding site on monomeric actin. *J. Mol. Biol.* **366**, 745-55.

95) Pope B.J., Zierler-Gould K.M., Kühne R., Weeds A.G., Ball L.J. (2004). Solution structure of human cofilin: actin binding, pH sensitivity, and relationship to actin-depolymerizing factor. *J. Biol. Chem.* **279**, 4840-48.

96) Lappalainen P., Fedorov E.V., Fedorov A.A., Almo S.C., Drubin D.G. (1997). Essential functions and actin-binding surfaces of yeast cofilin revealed by systematic mutagenesis. *EMBO J.* **16**, 5520-30.

97) Kardos R., Nevalainen E., Nyitrai M., Hild G. (2013). The effect of ADF/cofilin and profilin on the dynamics of monomeric actin. *Biochim. Biophys. Acta*. **1834**, 2010-9.

98) Paavilainen V.O., Oksanen E., Goldman A., Lappalainen P. (2008). Structure of the actin-depolymerizing factor homology domain in complex with actin. *J. Cell Biol*. **182**, 51-9.

99) Galkin V.E., Orlova A., Kudryashov D.S., Solodukhin A., Reisler E., Schröder G.F., Egelman E.H. (2011). Remodeling of actin filaments by ADF/cofilin proteins. *Proc. Natl. Acad. Sci. U S A*. **108**, 20568-72.

100) Maciver S.K. & Weeds A.G. (1994). Actophorin preferentially binds monomeric ADP–actin over ATP-bound actin: consequences for cell locomotion. *FEBS Lett*., **347**, 251–256.

101) M.F. Carlier, Valérie Laurent, Jérôme Santolini, Ronald Melki,Dominique Didry, Gui-Xian Xia, Yan Hong, Nam-Hai Chua, and Dominique Pantaloni. (1997). Actin depolymerizing factor (ADF/cofilin) enhances the rate of filament turnover: implication in actin-based motility *J. Cell Biol.*, **136**, 1307–1322.

102) Nagaoka R., Abe H., Obinata T. (1996). Site-directed mutagenesis of the phosphorylation site of cofilin: its role in cofilin-actin interaction and cytoplasmic localization. *Cell Motil. Cytoskeleton*. **35**, 200-9.

103) Moriyama K., Iida K., Yahara I. (1996). Phosphorylation of Ser-3 of cofilin regulates its essential function on actin. *Genes Cells*. **1**, 73-86.

104) Niwa R., Nagata-Ohashi K., Takeichi M., Mizuno K., Uemura T. (2002). Control of actin reorganization by Slingshot, a family of phosphatases that dephosphorylate ADF/cofilin. *Cell*. **108**, 233-46.

105) Hawkins M., Pope B., Maciver S. K., Weeds A. G. (1993). Human actin depolymerizing factor mediates a pH-sensitive destruction of actin filaments *Biochemistry*. **32**, 9985–93.

106) Theriot J.A. (1997). Accelerating on a treadmill: ADF/cofilin promotes rapid actin filament turnover in the dynamic cytoskeleton. *J. Cell Biol*. **136**, 1165-8.

107) Condeelis J. (2001). How is actin polymerization nucleated in vivo? *Trends Cell Biol*. **11**, 288-93.

108) McGough A., Pope B., Chiu W., Weeds A. (1997). Cofilin changes the twist of F-actin: implications for actin filament dynamics and cellular function. *J. Cell Biol.* **138**, 771–81.

109) Pelikan Conchaudron A., Didry D., Le K.H., Larquet E., Boisset N., Pantaloni D., Carlier M.F. Analysis of tetramethylrhodamine-labeled actin polymerization and interaction with actin regulatory proteins. *J. Biol. Chem.* **281**, 24036-47.

110) Kudryashov D.S., Phillips M., Reisler E. (2004). Formation and destabilization of actin filaments with tetramethylrhodamine-modified actin. *Biophys. J.* **87**, 1136-45.

111) Kudryashov D.S., Galkin V.E., Orlova A., Phan M., Egelman E.H., Reisler E. (2006). Cofilin cross-bridges adjacent actin protomers and replaces part of the longitudinal F-actin interface. *J. Mol. Biol*. **358**, 785-97.

CHAPTER 2

Mapping of Drebrin Binding Site on F-actin

Reprinted from Journal of Molecular Biology, 398, Elena E. Grintsevich,Vitold E. Galkin, Albina Orlova, A. Jimmy Ytterberg, Mouna M. Mikati, Dmitri S. Kudryashov, Joseph A. Loo, Edward H. Egelman, Emil Reisler, Mapping of Drebrin Binding Sire on F-actin, 542-554, Copyright 2010, with permission from Elsevier Ltd.

Mapping of Drebrin Binding Site on F-Actin

Elena E. Grintsevich[1], Vitold E. Galkin[2]†, Albina Orlova[2]†, A. Jimmy Ytterberg[1]†, Mouna M. Mikati[1], Dmitri S. Kudryashov[1], Joseph A. Loo[1,3,4], Edward H. Egelman[2] and Emil Reisler[1,4]*

[1]*Department of Chemistry and Biochemistry, University of California, Los Angeles, CA 90095, USA*

[2]*Department of Biochemistry and Molecular Genetics, University of Virginia, Charlottesville, VA 22908, USA*

[3]*Molecular Biology Institute, University of California, Los Angeles, CA 90095, USA*

[4]*Department of Biological Chemistry, University of California, Los Angeles, CA 90095, USA*

Received 19 November 2009; received in revised form 18 March 2010; accepted 19 March 2010
Available online
27 March 2010

Drebrin is a filament-binding protein involved in organizing the dendritic pool of actin. Previous *in vivo* studies identified the actin-binding domain of drebrin (DrABD), which causes the same rearrangements in the cytoskeleton as the full-length protein. Site-directed mutagenesis, electron microscopic reconstruction, and chemical cross-linking combined with mass spectrometry analysis were employed here to map the DrABD binding interface on actin filaments. DrABD could be simultaneously attached to two adjacent actin protomers using the combination of 2-iminothiolane (Traut's reagent) and MTS1 [1,1-methanediyl bis(methanethiosulfonate)]. Site-directed mutagenesis combined with chemical cross-linking revealed that residue 238 of DrABD is located within 5.4 Å from C374 of actin protomer 1 and that native cysteine 308 of drebrin is near C374 of actin protomer 2. Mass spectrometry analysis revealed that a zero-length cross-linker, 1-ethyl-3-(3-dimethylaminopropyl) carbodiimide, can link the N-terminal G–S extension of the recombinant DrABD to E99 and/or E100 on actin. Efficient cross-linking of drebrin residues 238, 248, 252, 270, and 271 to actin residue 51 was achieved with reagents of different lengths (5.4–19 Å). These results suggest that the "core" DrABD is centered on actin subdomain 2 and may adopt a folded conformation upon binding to F-actin. The results of electron microscopic reconstruction, which are in a good agreement with the cross-linking data, revealed polymorphism in DrABD binding to F-actin and suggested the existence of two binding sites. These results provide new structural insight into the previously observed competition between drebrin and several other F-actin-binding proteins.

Keywords: actin; drebrin; electron microscopy; mass spectrometry; cross-linking

Edited by R. Craig

**Corresponding author.* E-mail address: reisler@mbi.ucla.edu.

† V.E.G., A.O., and A.J.Y. contributed equally to this work.

Current address: A. J. Ytterberg, Department of Biochemistry and Molecular Biology, University of Southern Denmark, 5230 Odense, Denmark.

Abbreviations used: ABP, actin-binding protein; mAbp1, mammalian actin-binding protein 1; DrABD, actin-binding domain of drebrin (sequence 233–317); $DrABD_{300}$, sequence 233–300 of drebrin; drADF, ADF-homology domain of drebrin (sequence 1–134); EDC, 1-ethyl-3-(3-dimethylaminopropyl) carbodiimide; EM, electron microscopic; GST, glutathione *S*-transferase; MS, mass spectrometry; MS/MS, tandem mass spectrometry; MTS, bis(methanethiosulfonate); MTS1, 1,1-methanediyl bis(methanethiosulfonate); MTS8, 3,6-dioxaoctane-1,8-diyl bis(methanethiosulfonate); MTS17, 3,6,9,12,15-pentaoxaheptadecane-1,17-diyl bis(methanethiosulfonate); SD1–SD4, subdomains 1–4; WT, wild type.

Introduction

Dendritic spines are known to be very motile and change their shape during neuronal development and in adult brain in response to various stimuli.[1] The actin cytoskeleton is a primary modulator of spine morphology. Drebrin is a filament-binding protein that is involved in organizing the dendritic pool of actin.[1] It was shown that synaptic deterioration in the brains of Alzheimer's disease patients is accompanied by dramatically decreased levels of drebrin. Reduced drebrin levels are also observed in Down syndrome.[2] Biochemical analysis of various tissues revealed that depending on specific growth state and cell density, drebrin can form higher-order oligomers named "drebrosomes," which consist of drebrin and actin alone.[3,4] It was hypothesized that such complexes allow for high local concentrations of drebrin and may play a role in the local regulation of actin assembly, as was previously shown for some tropomyosins.[5]

Drebrin binds to F-actin with a stoichiometry of one to five protomers (K_d of ~0.12 μM) and shows no actin severing, nucleating, or bundling activity *in vitro*.[6] It was previously reported that drebrins compete with F-actin-binding proteins, such as α-actinin, tropomyosin, and fascin.[6–8] Drebrin inhibits the actin-activated ATPase activity of myosin, but its effect on actomyosin sliding velocity remains unclear. A 3-fold decrease in actin sliding velocity was previously reported, but it was not confirmed in recent studies.[9,10] According to *in vitro* studies, drebrin can be displaced from actin filaments by cofilin.[11] This observation is consistent with the finding that drebrin loss is accompanied by increased levels of cofilin in the brains of Alzheimer's disease patients.[2]

Drebrin shares homology with mammalian actin-binding protein 1 (mAbp1) through an N-terminal ADF-homology domain and helical/charged motif (HCm), which is specific only to these two proteins.[12,13] However, the helical/charged motif is more extended in drebrins than in mAbp1 and contains a unique sequence (residues 233–300/317) that was identified in previous *in vivo* studies as the actin-binding domain of drebrin (DrABD) (Scheme 1).[14,15] Interestingly, this 85-amino-acid DrABD causes the same rearrangements in the actin cytoskeleton as the full-length drebrin and is highly conserved among mammals.[8,14] Both drebrin and the homologous mAbp1 are present in neuronal cells and contain an ABD within their helical/charged motif.[1,16] Nevertheless, overexpression of DrABD and the helical/charged domain of mAbp1 has different effects on the morphology and density of dendritic spines. Similar to full-length drebrin, overexpression of DrABD in rat hippocampal neurons transforms mature dendritic spine into immature dendritic filopodia (without changing the overall density of the spines) and causes the loss of synaptic contacts. This destabilizing effect of drebrin on spine morphology appears to be mediated entirely through its ABD.[8] Thus, DrABD structurally and functionally represents a unique motif among the known actin-binding modules.

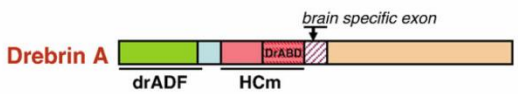

Scheme 1. Domain organization of drebrin A.

The important role of drebrin in actin regulation calls for structural understanding of the actin–drebrin complex. To date, no structural information on drebrin–actin interaction has been reported. In this study, we probed the binding interface of DrABD on actin filaments using site-directed mutagenesis, electron microscopic (EM) reconstruction, and chemical cross-linking combined with mass spectrometry (MS) analysis. Our results revealed that DrABD makes extensive contacts with subdomain 1 (SD1) and SD2 on actin and shows polymorphism in F-actin binding. Our data provide structural insight into the previously observed competition between drebrin and some of the actin side-binding proteins, such as α-actinin, cofilin, and tropomyosin.

Results

Characterization of the drebrin constructs

It was previously documented that only the N-terminal part of the drebrin molecule and DrABD in particular show actin binding and remodeling activity *in vivo*. We compared the actin binding properties of the isolated drebrin ADF-homology domain (drADF; residues 1–134), DrABD, and drebrin construct 1–300 containing both ADF and DrABD domains. Since it was previously shown that overexpression of both the 233–317 drebrin fragment (DrABD) and the 233–300 drebrin fragment ($DrABD_{300}$) causes *in vivo* effects similar to those of the full-length drebrin,[14,15] the actin binding properties of these constructs were tested under identical experimental conditions and compared with each other.

Drebrin 1–300 binds to F-actin with high affinity, K_d of ~0.2 μM (similar to that of full-sized drebrin),[6] and a binding stoichiometry of ~1:3 (Fig. 1a). Under the conditions of our experiments, the isolated drADF did not show any binding to F-actin (Fig. 1c and d).

Pelleting experiments have shown that N-GST (glutathione *S*-transferase)-fused DrABD binds to F-actin with relatively low affinity compared with the construct 1–300 (K_d = 6.6 ± 0.4 μM) (Fig. 1b). The C-terminal truncation of DrABD, to produce $DrABD_{300}$, does not affect its binding to F-actin significantly (K_d = 7.6 ± 0.6 μM). For both constructs, the DrABD/F-actin binding stoichiometry was close to 1:2 DrABD/actin protomers; the actual mole ratio (1:1.6) may reflect DrABD oligomerization, partial

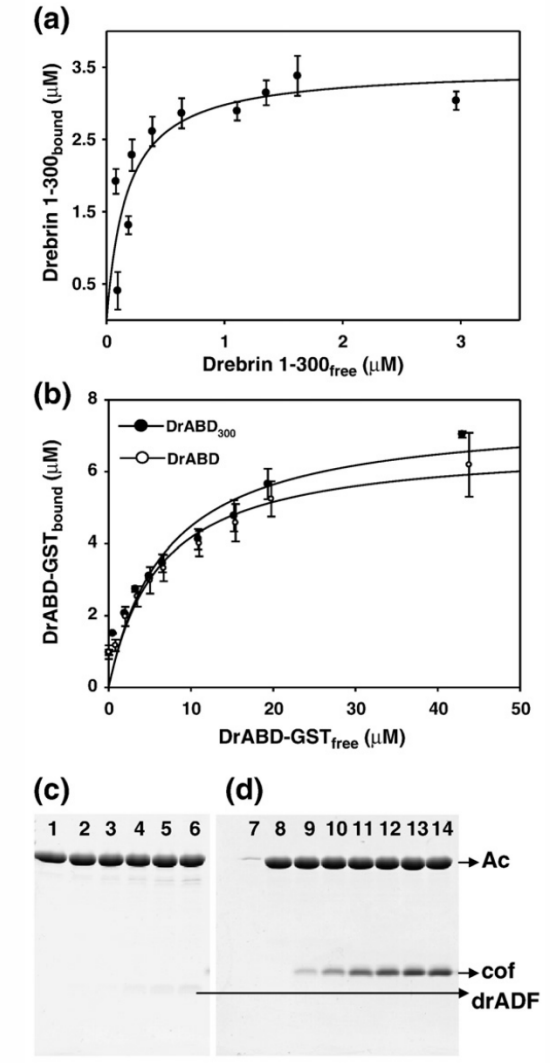

Fig. 1. Binding of the drebrin constructs to actin filaments. Binding affinity of drebrin constructs for F-actin was estimated by pelleting assays (see Materials and Methods). (a) Binding of the 1–300 drebrin construct to actin filaments (10 μM). The continuous line corresponds to the best data fit. A K_d of the 1–300 drebrin construct for F-actin (0.17±0.005 μM) was calculated based on two independent experiments. (b) Binding affinities of N-GST-fused DrABD constructs for F-actin (10 μM). Continuous lines correspond to the best data fit with K_d values of 6.6±0.4 and 7.6±0.6 μM for DrABD and $DrABD_{300}$, respectively. K_d is an average value obtained in two independent experiments, as described in Materials and Methods. (c) Co-sedimentation of drADF with F-actin (*Ac*) (10 μM). (d) Control co-sedimentation of yeast cofilin (*cof*) with F-actin (10 μM) under the same conditions as in (c). Buffer composition: 5 mM Mops, pH 7.2, 0.2 mM $CaCl_2$, 0.4 mM ethylene glycol bis(β-aminoethyl ether)*N*,*N*′-tetraacetic acid, 0.2 mM ATP, 1 mM DTT, 50 mM KCl, and 2 mM $MgCl_2$. Lanes 1–6, 10 μM F-actin co-sedimented with 1.25, 2.5, 5, 10, 15, and 25 μM concentrations of drADF; lanes 9–14, 10 μM F-actin co-sedimented with 1.25, 2.5, 5, 10, 15, and 25 μM concentrations of yeast cofilin; lanes 7 and 8, F-actin, supernatant and pellet, respectively.

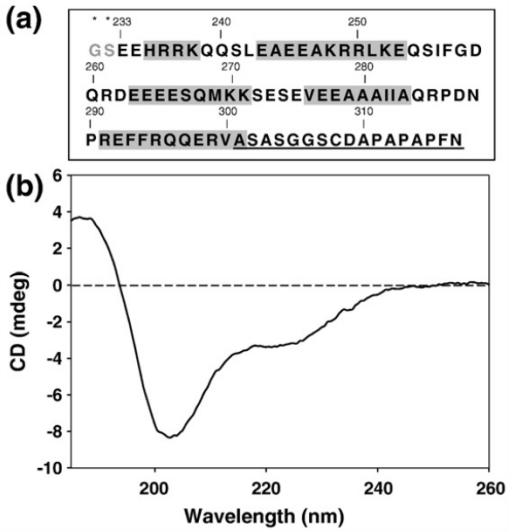

Fig. 2. Structure of DrABD. (a) Sequence of DrABD. Residues predicted to form helical structures are shown in gray (Jpred 3). The C-terminal extension that is truncated in $DrABD_{300}$ construct is underlined. Two extra amino acids at the N-terminus of the recombinant DrABD constructs are marked with asterisks. (b) CD spectrum (average of eight runs) of DrABD. Based on the results of two independent experiments, the secondary structure composition of DrABD is estimated to contain 28% helix, 15% β-sheets, and 57% turns and random coil.

occupancy of actin filament by DrABD, or its multiple binding modes (see Discussion).

DrABD has no homology among known proteins, and its sequence is abundant in glutamic acid (~19%) and arginine (~11%) (Fig. 2a). The secondary structure of this actin-binding module, as revealed by circular dichroism (CD) spectroscopy, contains 28% helix, 15% β-sheet, 21% turns, and 36% random coil (a total of 57% unstructured) (Fig. 2b). The secondary structure of DrABD is invariable over the pH range 5.0–8.6 (data not shown).

EM reconstruction of F-actin decorated with the drebrin constructs

EM images of F-actin alone and actin decorated with DrABD and 1–300 constructs are shown in Fig. 3a, b, and b*, respectively. Despite affinity differences, the same modes of F-actin binding and binding polymorphism were documented for both DrABD (Fig. 3d–h) and drebrin 1–300 constructs (Fig. 3d*–h*).

Extensive decoration of actin filaments was observed in the presence of DrABD (Fig. 3b), as well as with the shorter construct $DrABD_{300}$ and N-GST-fused DrABD (data not shown). We collected 9749 segments from images of actin filaments decorated with the drebrin fragment. During the first step of sorting, segments were separated by the occupancy (see Materials and Methods and Appendix A) and

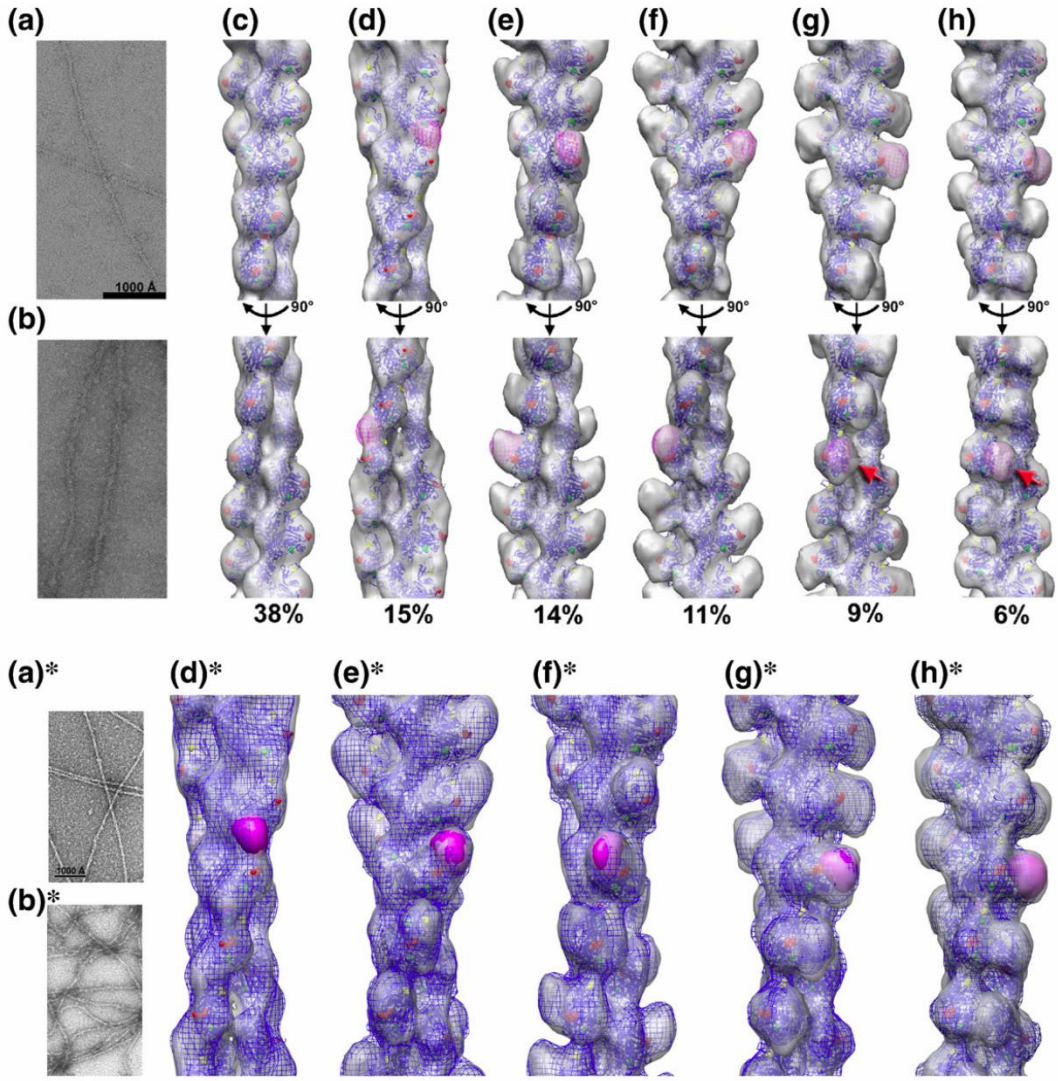

Fig. 3. EM and three-dimensional reconstruction of the drebrin–F-actin complex. (a, a*, b, b*) Electron micrographs of F-actin alone (a and a*), filaments decorated with the DrABD construct (b), and those decorated with the drebrin 1–300 construct (b*). (c–h) Three-dimensional reconstructions of pure F-actin (c) and five modes of binding of drebrin to F-actin (d–h). Atomic model of actin filament docked into each map is shown as blue ribbons (c–h). F-actin residues 99 and 100 (red), 51 (yellow), and 374 (green) are shown as spheres (c–h). (d–h) An electron density envelope that corresponds to a globular protein containing 84 amino acid residues is shown as magenta meshwork. (d∗–h∗) Comparison of the binding modes of DrABD and drebrin 1–300 construct to F-actin. Reconstructions of F-actin decorated with DrABD are shown as transparent surfaces, while volumes that resulted from filaments complexed with the 1–300 construct containing both DrABD and AFD-homology domain are shown as blue meshwork. Atomic model of actin filament docked into each map is shown as blue ribbons (d*–h*). F-actin residues 99 and 100 (red), 51 (yellow), and 374 (green) are shown as spheres (a–e). An electron density envelope that corresponds to a globular protein composed of 84 amino acid residues is shown as magenta solid surface. The modes of binding obtained for drebrin 1–300 construct are similar to the ones observed for isolated DrABD.

"naked" F-actin segments were reconstructed separately from occupied ones. Reconstruction of the naked F-actin (Fig. 3c) was similar to the reconstruction of pure F-actin from our previous studies.[17] Five modes of DrABD binding to actin filaments are shown in Fig. 3d–h. To estimate whether the observed additional mass in the reconstructions was consistent with the molecular weight of the drebrin construct, we used a portion of the globular CH domain of α-actinin (Protein Data Bank ID 1wku) that consists of 84 residues (~9 kDa). This model protein fragment was filtered to ~24-Å resolution, and its expected molecular volume was docked into the drebrin density in each map (Fig. 3d–h, magenta mesh). In the first mode (Fig. 3d), drebrin bridges to two adjacent actin

protomers and makes an extensive contact with SD1 and SD2. In the mode shown in Fig. 3e, drebrin is located in front of actin SD1. We also observed drebrin in a mode similar to the one shown in Fig. 3d, but in this mode, DrABD interacts with one protomer at a time (Fig. 3f). We suggest that all three modes shown in Fig. 3d, e, and f are variations of a major DrABD binding site (~40% of segments), which involves SD1 and SD2 of actin.

We found that ~15% of the segments decorated with DrABD reflect a different type of attachment (Fig. 3g and h). In the binding mode shown in Fig. 3g, DrABD is attached to the sides of SD1 and SD2. In this case, the observed mass was larger than the mass corresponding to a globular protein fragment of 84 amino acids, which suggests that, in this mode, DrABD binds to filaments as an oligomer. Interestingly, in this mode, DrABD makes contact with SD4 of an actin protomer on the opposite strand (Fig. 3g, red arrow). This contact is more prominent in the mode shown in Fig. 3h.

The same modes of binding as documented for DrABD were also observed for the 1–300 construct, despite its much higher affinity for F-actin (~0.2 μM) (Figs. 1a and 3d*–h*). It should be noted that the 1–300 construct may contain weak actin-interacting sites other than DrABD, which would explain its higher affinity for the actin filaments. However, the results of EM reconstruction suggest that DrABD contains the strongest binding site within the 1–300 drebrin fragment and probably competes with weaker bound structural elements for interaction with actin when the 1–300 fragment is added in excess. Based on our EM results and previous *in vivo* studies, the DrABD construct was chosen for mapping the drebrin binding site on F-actin.

DrABD bridges two actin protomers

To probe the DrABD/F-actin binding interface via cross-linking reactions, we employed the modification of DrABD with 2-iminothiolane (Traut's reagent). This reagent was used to introduce sulfhydryl (-SH) groups on the surface of the fragment. Potentially, all five lysines (K238, K248, K252, K270, and K271) and the N-terminal amino group can be modified with 2-iminothiolane. Additionally, DrABD contains native cysteine 308 within its C-terminal unstructured extension (residues 301–317). Considering the relatively low affinity of DrABD to actin, we attached first the cross-linking reagents to F-actin, as was done earlier for the mapping of the actin–thymosin β4 complex.[18] Cross-linking experiments revealed that DrABD modified with Traut's reagent can be covalently attached to MTS1 [1,1-methanediyl bis (methanethiosulfonate)]-pre-modified F-actin, yielding two protein populations: actin–DrABD heterodimer and species that, according to their molecular weight, correspond to a complex of two actin protomers and one DrABD molecule (Fig. 4a). A control experiment was carried out using MTS1-pre-modified F-actin and intact DrABD construct with no modifications. A significant amount of actin–DrABD heterodimer was detected by SDS-PAGE under nonreducing conditions, indicating that native C308 on DrABD is involved in the cross-linking (Fig. 4b).

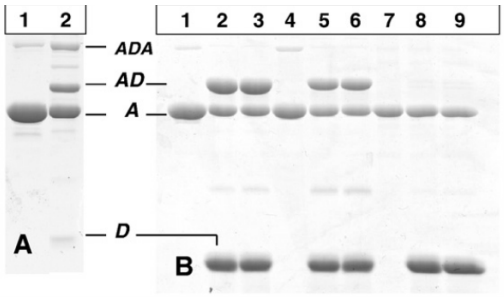

Fig. 4. DrABD is near the C-terminal regions of two adjacent actin protomers. (a) DrABD treated with 2-iminothiolane (Traut's reagent) can be covalently attached to MTS1-pre-modified skeletal F-actin: lane 1, MTS1-modified F-actin (10 μM) (*A*); lane 2, 2-iminothiolane-treated DrABD (20 μM) incubated for 5 min with MTS1-modified actin. Two main cross-linking products were detected: actin–DrABD heterodimer (*AD*) and the species that, according to molecular weight and MS analysis, corresponds to two actin protomers and one DrABD (*ADA*). (b) Native C308 of DrABD is within 5.4 Å from C374 on actin: lanes 1–3, skeletal F-actin; lanes 4–6, WT yeast actin; lanes 7–9, yeast actin mutant C374A. Lanes 1, 4, 7, MTS1-modified actins; lanes 2, 5, and 8, MTS1-modified actins in the presence of DrABD (5-min reaction time); lanes 3, 6, and 9, same as lanes 2, 5, and 8 but with 17-min reaction time. The final concentrations of actin and DrABD were 9.5 and 28.5 μM, respectively.

C-terminal region of DrABD (residues 301–317) cross-links to C374 on actin

Our experiments revealed that DrABD can be efficiently cross-linked to both skeletal muscle (α-) and yeast wild-type (WT) (cytoplasmic) F-actin pre-modified with MTS1. The similar cross-linking yield (~60%) obtained for both actins may indicate that the DrABD–actin interaction is not isoform specific. C-terminal cysteine 374 is the most reactive cysteine on actin and is expected to be efficiently modified with MTS1 reagents.[19] However, to confirm that the cross-linking on actin indeed involves C374, we used a yeast actin mutant with this residue substituted to alanine (C374A). No cross-linking was detected in the case of C374A actin mutant, which indicates that native C308 of drebrin locates within 5.4 Å from C-terminal cysteine 374 on actin (Fig. 4b).

MS analysis of the purified complex of 2-iminothiolane-modified DrABD attached simultaneously to two actin protomers revealed that disulfide (MTS1) cross-linking between native C308 on DrABD and C10 on actin may also occur (Appendix B). However, the fact that unmodified DrABD can be efficiently cross-linked to WT yeast actin, which lacks C10, suggests that this type of attachment reflects a minor mode of DrABD–actin binding.

The N-terminal part (233–271) of DrABD can be cross-linked to SD1 and SD2 of two adjacent actin protomers

Site-directed mutagenesis was employed to locate the N-terminal part of DrABD (sequence 233–271) on actin filaments. Based on the results obtained with 2-iminothiolane-modified DrABD (Fig. 5a), all five lysines (K238, K248, K252, K270, and K271) and the N-terminal glycine were potential candidates for cross-linking to the second actin protomer. To identify the residues on DrABD that are in close proximity actin, we created five mutants with single lysine-to-cysteine replacements in the construct $DrABD_{300}$. These mutants did not impair the complex formation of $DrABD_{300}$ with F-actin (see Materials and Methods). The fact that DrABD bridges two actin protomers, making contacts with their C-terminal segments, called for probing the DrABD interaction with actin SD2. Actin mutants D51C/C374S and S60C/C374A were employed for such mapping. Mutant A144C/C374A was chosen to test for the binding of DrABD to the hydrophobic cleft between SD1 and SD3 of actin, which is known to interact with several actin-binding proteins (ABPs). All yeast actin mutants employed in this study show normal polymerization properties.[20,21]

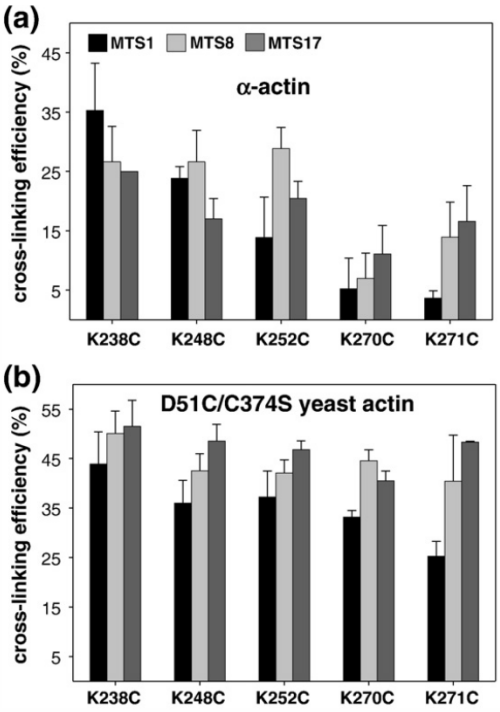

Fig. 5. Mapping DrABD binding interface on F-actin. (a and b) Thiol-specific cross-linking of five DrABD mutants to skeletal F-actin (a) or to yeast actin mutant D51C/C374S (b) modified with MTS reagents of different lengths. Residue 238 of drebrin is within 5.4 Å from the Cys374 of actin (C-terminus). Residues 238, 248, 252, 270, and 271 of drebrin are within ~12.1 Å from residue 51 on actin (D-loop, SD2). F-actin was pre-modified with MTS immediately prior to the cross-linking. The final concentrations of actin and DrABD were 10 and 30 μM, respectively. The reactions were stopped with *N*-ethyl maleimide after 5 min, and the resulting mixtures were analyzed by SDS-PAGE. Relative intensities of protein bands were determined by densitometric analysis. Cross-linking efficiencies were estimated as follows: [Actin Total (Before the Reaction) − Uncross-Linked Actin Monomer Left After 5 Min]/Total Actin, (%). Black, MTS1 (5.4 Å); light gray, MTS8 (12.1 Å); dark gray, MTS17 (19 Å).

We used a series of bis(methanethiosulfonate) (MTS) reagents as molecular rulers to estimate the distances between single reactive cysteines on actin and on DrABD mutants.[21] Experiments with skeletal F-actin pre-modified with MTS1 (5.4 Å) revealed that K238C is the one cross-linked most efficiently to C374 on actin among the five $DrABD_{300}$ mutants (Fig. 5a). The cross-linking yields for three DrABD mutants, K238C, K248C, and K252C, and the MTS8 [3,6-dioxaoctane-1,8-diyl bis(methanethiosulfonate)]-pre-modified F-actin were very similar (27%–29%). These results suggest that lysines 238, 248, and 252 are in close enough proximity to C374 of actin (~12 Å) to be involved in the formation of a trimer consisting of 2-iminothiolane-modified DrABD attached simultaneously to two actin protomers (Fig. 4a). The low cross-linking efficiency documented for mutants K270C and K271C and actin pre-modified with the MTS reagents of different lengths precludes their proximity to C374 on actin (Fig. 5a).

The experiments with MTS-modified yeast actin D51C/C374S revealed that all five $DrABD_{300}$ mutants could be linked very efficiently to actin with reagents of length ranging from ~12.1 Å (MTS8) to 19 Å [MTS17; 3,6,9,12,15-pentaoxaheptadecane-1,17-diyl bis(methanethiosulfonate)] (Fig. 5b). These data indicate that the N-terminal part of DrABD is centered on SD2 of actin. However, in the case of MTS1-modified D51C/C374S actin, the cross-linking efficiency of the introduced cysteine residues decreases with increasing distance from the N-terminus of the DrABD construct (Fig. 5b). The fact that all five $DrABD_{300}$ mutants can be cross-linked efficiently to residue 51 on actin may indicate that the construct can adopt a folded conformation upon binding to F-actin.

No cross-linking was detected with all five $DrABD_{300}$ mutants and yeast actin S60C/C374S, with the reactive cysteine in SD2 facing the nucleotide binding cleft, and yeast actin A144C/C374A, containing a reactive cysteine in the hydrophobic cleft (SD3) of actin (data not shown).

Zero-length cross-linking of DrABD to SD1 of actin

Our experiments showed that DrABD can be efficiently cross-linked to F-actin using the zero-length cross-linker 1-ethyl-3-(3-dimethylaminopropyl) carbodiimide (EDC) (Fig. 6a; Appendix C). Bands corresponding to actin, DrABD, and actin–DrABD heterodimer were excised from the SDS-PAGE gel and subjected to in-gel trypsin digest to

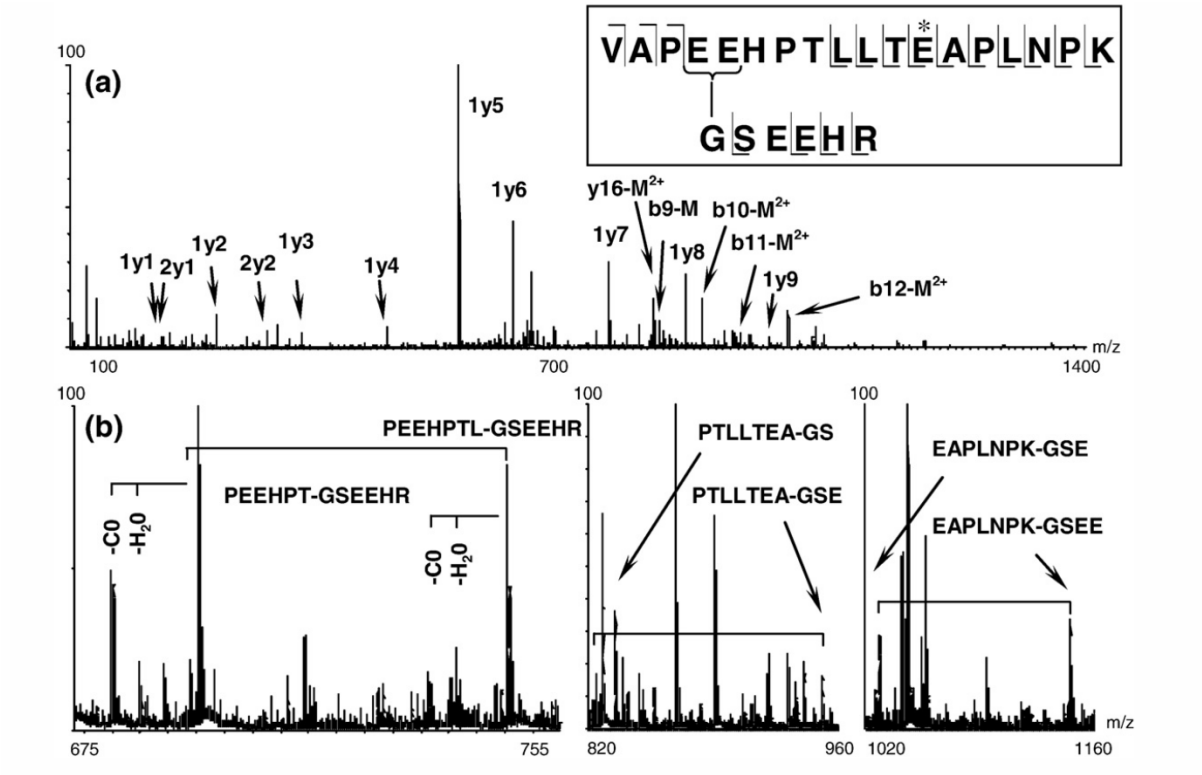

Fig. 6. N-terminus of DrABD constructs can be attached to SD1 of actin with the zero-length cross-linking reagent EDC. (a) Tryptic peptides of DrABD–actin heterodimer were analyzed by MS/MS. The 663.61 $(M+4H)^{4+}$ peak in MS spectra, corresponding to cross-linked peptides, was fragmented using electrospray ionization MS/MS (Waters Synapt QTOF mass spectrometer). Some of the identified fragments are indicated in the figure. The first digit indicates the peptide from which the fragment originates (1 = actin, 2 = drebrin), the letter refers to the ion series, and the last digit represents the ion number. Hyphenated labels indicate cross-linked fragments, with the left fragment originating from actin and the right one from drebrin. "M" represents intact drebrin peptide. The inset shows a schematic representation of the cross-linked peptides. In the scheme, the cross-linked residues are connected with a continuous line (major site); a minor cross-linking site on actin peptide is marked by the asterisk. (b) Internal ions of the cross-linked peptides support the attachment of N-terminal Gly of DrABD to E99/E100 (major population) and E107 (minor cross-link) on actin.

map the cross-linked sites. Cleavage products were analyzed by electrospray ionization tandem MS (MS/MS). A peptide ion ($[M+4H]^{4+} = m/z$ 663.61) unique to the cross-linked heterodimer was fragmented by MS/MS and matched to the two cross-linked peptides: actin 96–113 and drebrin 233–236, containing extra G–S extension at the N-terminus. The fragments were deconvoluted to a zero-charge spectrum and matched with theoretical masses predicted for the three cross-linking sites on the actin peptide (E99, E100, and E107) and the single cross-linking site on drebrin (the N-terminus) to fully assign the spectrum. The data were first filtered using a maximum error of ±100 ppm to ensure high quality of the matches. In a second filtering step, the average and standard deviation of the errors were calculated and one standard deviation from the average (27±37 ppm) was used as a filter. The identified fragments were then matched with the raw spectrum to increase the confidence by using the multiple charge states of each fragment. Fifty-seven fragments were found with unique interpretations (24 had two or more charge states), 11 fragments matched to sequences occurring more than once in the peptide sequence, and 16 ions could be matched to more than one fragment (within experimental error). To assign the latter to single fragments, we evaluated the number of fragmentations necessary to form the fragment and the presence of supporting ions from related fragments. The mass-to-charge ratio (m/z) and the charge of each fragment were manually verified from the raw spectrum. The interpretation of the data fits with a cleavage of 24 bonds, out of 26. Twenty-one fragments support a cross-link at E99 or E100 located in SD1 (major population) of actin, while 6 fragments (i.e., a minor population) support a cross-link at E107 (Fig. 6b; Appendix C).

Discussion

In order to identify contact sites between actin and drebrin, we employed site-directed mutagenesis, EM reconstruction, chemical cross-linking, and MS analysis. Using a set of thiol-specific reagents of different lengths as molecular rulers, we were able to assign the distances between selected residues on

actin and DrABD in the range of 0 to ~19 Å. The results of EM reconstruction revealed polymorphism in DrABD binding to actin filaments and suggested the existence of at least two binding sites for DrABD.

The contents of helical and β-structures estimated for DrABD using CD spectroscopy were 28% and 15%, respectively. However, secondary structure prediction algorithms did not predict any β-structures in DrABD (Fig. 2). Our current crystallization attempts, if successful, would resolve this contradiction. The level of random coil and turns estimated by CD (57%) was in good agreement with the predictions made by Jpred 3 (~50%), which suggests proper folding.[22] The affinity of DrABD for F-actin determined by pelleting experiments (K_d of ~6.6–7.6 μM) was relatively low compared with the affinity reported for the full-length drebrin (0.12 μM).[6] Our observation that drebrin construct 1–300 has a significantly higher affinity for F-actin compared with DrABD (~0.2 μM; Fig. 1) raises the possibility that regions other than DrABD may also contribute to the actin binding. We hypothesize that either the ADF-homology domain or the linker region (residues 143–232) contributes to the stronger binding of drebrin 1–300 to F-actin than that of DrABD. Our EM reconstruction results (see below) suggest that DrABD is the strongest actin binding region within the 1–300 drebrin fragment, and identification of weaker binding sites is a subject for a separate study.

The fact that the shorter construct of $DrABD_{300}$ (with deletion of 17 C-terminal amino acids) has approximately the same affinity to F-actin as the longer construct (sequence 233–317) indicates that the unstructured region 301–317 does not contribute significantly to the DrABD/F-actin interaction (Fig. 1b).

Chemical cross-linking for mapping the protein binding interface

Several DrABD and actin mutants containing single reactive cysteines were reacted with a series of thiol-specific bifunctional MTS reagents to probe the actin–DrABD binding interface. In general, the cross-linking efficiency depends on the reactivity and accessibility of the targeted residues, stability of the cross-linking reagents in solution, and experimental conditions (pH, temperature, reaction time).

The results of our cross-linking and pelleting experiments suggest that DrABD bridges two adjacent actin protomers. However, these data are insufficient to determine the orientation of DrABD on actin filaments. Based on our results summarized in Fig. 7, we discuss the interaction of DrABD with protomers 1 and 2 in the actin filament.[23]

Cross-linking of DrABD to actin SD1 (protomer 1)

After thrombin cleavage, the recombinant DrABD constructs contain a G–S N-terminal extension. MS analysis identified the N-terminal glycine on DrABD as a residue cross-linked to F-actin with a zero-length cross-linking reagent (EDC) (Appendix C). On actin, three residues in SD1 were shown to be involved in EDC cross-linking with DrABD: E99 and/or E100 (major population) and E107 (minor population) (Fig. 6). Although a distinction between cross-linking to E99 and E100 is not possible from the fragmentation pattern of the cross-linked peptides, we conclude based on the abundance of the internal fragments of the cross-linked peptides that DrABD cross-linking to E107 of actin represents a minor population. The analysis performed using GETAREA 1.0 software showed a significant decrease in solvent accessibility for actin residue E107 compared with E99 and 100. Based on that, we cannot rule out the possibility that the N-terminus of DrABD is flexible and locates in close proximity to all three residues (E100, E99, and E107) but its coupling to E107 is restricted by the accessibility of that residue. It is also conceivable that minor cross-linking to E107 of actin may reflect an alternative mode of DrABD binding or result from local damage to actin over the course of the reaction. Despite the high level of flexibility of DrABD in solution (our unpublished NMR data) and the predicted disordered state of its N-terminal region, only one cross-linked peptide was identified in the sample containing the DrABD–actin

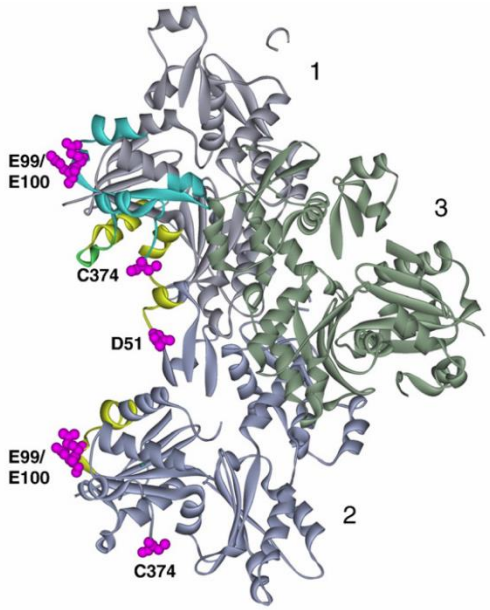

Fig. 7. Summary of the cross-linking results. Holmes model of actin filament structure.[23] Actin protomers are marked as 1, 2, and 3. Actin residues involved in cross-linking with DrABD are shown in magenta. Actin peptides involved in interactions with cofilin[17] and α-actinin[24] are shown in yellow and blue (protomer 1), respectively. The overlap between cofilin and α-actinin binding sites is shown in green (protomer 1).

heterodimer, which indicates a specific DrABD interaction with the 99–107 actin region.

Cross-linking experiments employing skeletal α-actin pre-modified with MTS reagents and DrABD mutants containing single cysteine substitutions revealed that the N-terminal part of DrABD makes contact with the C-terminus of actin. Based on the highest cross-linking efficiency of the K238C mutant to MTS1-modified actin, we conclude that residue 238 of DrABD locates within ~5.4 Å from C374 of actin (Fig. 5a). The fact that longer-spanning reagents [MTS8 (12.1 Å) and MTS17 (19 Å)] cross-link the same K238C mutant to actin at lower efficiency may indicate that, in the extended conformation, these reagents do not fit well into the space between the two cysteine residues in the DrABD–actin complex, while the "*gauche*" conformations of the reagents may not have the appropriate geometry for bridging residues 374 and 238. Similar amounts of actin–DrABD heterodimer were obtained in the presence of mutants K238C, K248C, and K252C with MTS8, which indicates that these three residues are within ~12 Å from the C-terminus of actin. Low cross-linking efficiency between C374 of actin and DrABD mutants C270 and C271 observed with the MTS reagents of different lengths indicates that those residues are distant from the C-terminus of actin (Fig. 5a).

Cross-linking of DrABD to actin SD1 and SD2 (protomer 2)

Experiments with yeast actin mutant D51C/C374S containing a single reactive cysteine in SD2 revealed that DrABD is close to this actin region. Residues 238, 248, 252, 270, and 271 on DrABD can all be efficiently attached to residue 51 on actin with MTS reagents of various lengths (5.4–19 Å) (Fig. 5b). The efficiency of these reactions with MTS1 and MTS8 is slightly higher (by ~8%) for the DrABD mutant K238C (Fig. 5b). According to secondary structure predictions, lysines 248 and 252 of DrABD are located on a helix, and lower cross-linking efficiency for these mutants, compared with K238C, may indicate decreased solvent accessibility of these two residues. Our results indicate that all five lysines on DrABD are located within ~12 Å or even closer (5.4 Å in the case of K238) residue 51 on actin.

Our cross-linking experiments also revealed that the C-terminal region of DrABD interacts with actin SD1 and that native cysteine 308 of drebrin locates within 5.4 Å from C374 on actin (Fig. 4b). Minor cross-linking between C10 on actin and C308 on DrABD may reflect the flexibility of the C-terminal region of the DrABD construct, but it could also indicate an alternative binding mode (Appendix B).

EM reconstruction of F-actin decorated with DrABD is consistent with cross-linking results

We used a single-particle approach for the EM reconstruction of F-actin decorated with DrABD.[25] This method allows for sorting relatively short filament segments (~400 Å long) by occupancy and the mode of drebrin binding to F-actin.

In four modes of binding (Fig. 3d–f and h), the mass attributed to DrABD is consistent with a globular protein of ~9 kDa attached to F-actin. The results of EM reconstruction together with the mapped location of residues 238, 248, 252, 270, and 271 on DrABD within ~12 Å from residue 51 on actin lead to the conclusion that DrABD may adopt a globular conformation upon binding to actin. Our data suggest that in the modes presented in Fig. 3d–f and h, DrABD binds to F-actin predominantly as a monomer. However, we cannot exclude the possibility that in these four modes actin filaments are decorated by drebrin dimers/oligomers, which are not observed due to low occupancy or disorder.

According to the EM reconstruction and in good agreement with our cross-linking results, DrABD makes extensive contacts with SD1 and SD2 of actin (Fig. 3). In the modes presented in Fig. 3d and f, DrABD interacts with SD1 and SD2 that involves residues 51 and 99–100. In the mode shown in Fig. 3e, DrABD is located in front of SD1 of actin and the interface involves residues 99 and 100. In the minor binding mode presented in Fig. 3g, residues 51, 99, 100, and 374 are in proximity to DrABD density. Also, in the mode presented in Fig. 3h, residues 51 and 374 are likely to be involved in the interaction with drebrin. Taken together, the EM data support the existence of two binding sites for DrABD on actin: a major site (modes shown in Fig. 3d–f, ~40% segments) and a minor site (modes shown in Fig. 3g and h, ~15% segments) where DrABD is shifted to the sides of SD1 and SD2 of actin and makes cross-strand contact with another actin protomer.

Our cross-linking experiments revealed that DrABD can be simultaneously attached to two adjacent actin protomers within one helical strand. According to our mapping, C374 residues on two adjacent protomers are involved in such double cross-linking, which appears to be inconsistent with the results of EM reconstruction (Figs. 4 and 5a). However, it should be noted that the C-terminal extension of DrABD that cross-links to C374 of actin with MTS1 (Fig. 4b) is predicted to be unstructured. Computational analysis performed using Insight II software revealed that the length of this C-terminal extension (amino acids 301–317, C^{α} to C^{α}) spans between 4.7 and 26.7 Å. If this region is disordered, it would not be observed in the EM reconstructions. According to our MS analysis, a short N-terminal extension of DrABD makes contact with actin residues 99–100. We may speculate that DrABD consists of a helical core with the unstructured extensions docked to the SD1 regions of two adjacent actin protomers. An atomic-resolution structure of the DrABD–actin complex will be required to confirm this hypothesis.

Polymorphism of DrABD binding to actin: implications for competition with other ABPs

Along with drebrins, many other ABPs are involved in the regulation of the actin cytoskeleton in neuronal cells. At the molecular level, the interplay between ABPs in this system is poorly understood. Our results provide new structural insight into the reciprocal relationship between drebrin and other ABPs in the cell. Multiple binding modes to F-actin documented here for DrABD were reported earlier for other proteins, such as cofilin,[17] utrophin,[26] and tropomyosin.[27–30] Thus, binding polymorphism is not an exception among actin-interacting proteins and may play an important role in actin cytoskeletal regulation. Because construct 1–300 of drebrin binds to F-actin significantly tighter than DrABD yet shows the same modes of attachment to actin filaments (Figs. 1a and 3d*–h*), the *in vivo* competition of DrABD with other ABPs would be functionally important.

This study revealed that the main DrABD binding site overlaps with the cofilin binding site on actin filaments, which would explain the competition between these two proteins.[11] Cofilin interacts with two actin protomers within the same helical strand: with an upper protomer at the hydrophobic cleft between SD1 and SD3 and with a lower protomer at the interface formed by SD1 and SD2. On the lower protomer, peptides 44–50, 28–29, and 88–101 appear to be involved in cofilin binding (F-binding site).[17,31] On the upper protomer, the C-terminus of actin was shown to interact with cofilin.[21,32] Thus, our mapping of DrABD sites on actin to regions proximal to residues D51, E99, E100 and the C-terminus indicates their overlap with the cofilin binding site.

It has been shown that drebrin overexpression causes displacement of α-actinin from dendritic spines, which is consistent with earlier *in vitro* observations.[8] An α-actinin was documented previously to interact with residues 86–117 and 350–375 on actin.[24] We have shown here that actin residues 99–107 and its C-terminus are near DrABD, explaining the previously observed competition between these two proteins. According to the *in vitro* studies, α-actinin can interact with both F-actin (through tandem CH domains) and NMDA receptors (through its central "rod" domain), anchoring actin filaments to the membrane.[33,34] It is likely that the competition between drebrin and α-actinin affects the anchoring of actin filaments to the membrane and leads to the formation of the long protrusions observed upon drebrin overexpression. We may hypothesize that the observed polymorphism of DrABD binding to F-actin plays a role in the competition with spectrin family proteins, such as utrophin, which have multiple actin-binding modes.[26]

Based on *in vitro* studies, it was suggested that drebrin and tropomyosin compete for the same actin binding site. In the absence of atomic-resolution structures, the detailed mechanism of such competition remains unclear. Also, we cannot exclude that observed inhibition of drebrin binding occurs due to tropomyosin-induced conformational changes in F-actin. Our data suggest that the primary binding site of drebrin (Fig. 3d–f) is inconsistent with simultaneous interaction of drebrin and myosin with F-actin because myosin binds to a similar interface on F-actin.[35] It is possible that the attachment of F-actin decorated by drebrin A to a glass surface coated with myosin-V occurs because of the shift of DrABD from its primary binding site to the minor one located on the side of the filament.[10]

Materials and Methods

Materials

MTS cross-linking reagents, MTS1, MTS8, and MTS17, were purchased from Toronto Research Chemicals (North York, Ontario, Canada). Millipore-filtered water and analytical-grade reagents were used in all experiments.

Molecular cloning and mutagenesis

Mouse (*Mus musculus*) brain RNA was purified using TRIzol reagent (Invitrogen). Reverse transcriptase-PCR was performed using SuperScript II (Invitrogen) to generate cDNA. Full-length drebrin A cDNA was cloned into pCR2.1-TOPO vector (Invitrogen) and used as a template for all drebrin constructs. DrABD was cloned into BamH1 and EcoR1 sites of pGEX-4T1 expression vector. $DrABD_{300}$ construct was created by introducing a stop codon after amino acid 300 (Val) in DrABD with a QuikChange kit (Stratagene). DrABD mutants K238C, K248C, K252C, K270C, and K271C that contain single lysine-to-cysteine replacements were created using the same kit. Drebrin construct 1–300 was obtained by introducing a stop codon after residue 300 in full-length drebrin A DNA subcloned into pGEX-4T1 expression vector. The primers for cloning and mutagenesis are given in Appendix D.

Protein expression and purification

Rabbit skeletal actin was purified from rabbit back muscle as described by Spudich and Watt.[36] Yeast actin was purified as described previously.[21] All drebrin ABD constructs were expressed in Rosetta cells. Cells were grown at 37 °C until $OD_{600} = 0.6–0.8$, following the induction with 0.2 mM IPTG and 2 h of expression. Proteins were purified on glutathione-agarose according to the manufacturer's instructions and as detailed in Appendix A. The single cysteine mutations introduced into $DrABD_{300}$ construct did not impair its complex formation with F-actin (Fig. 8). Consequently, we employed these mutants for mapping the drebrin interface on actin.

Actin polymerization and DrABD binding assays

Actin polymerization was monitored via light scattering with the PTI fluorometer set at 350 nm for the excitation and emission wavelengths. For pelleting experiments,

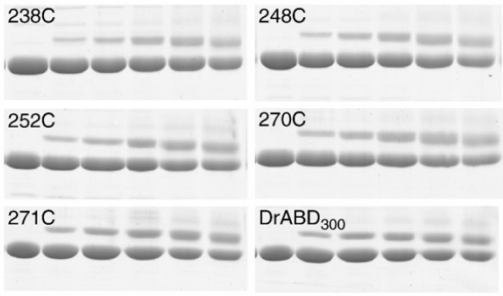

Fig. 8. Single cysteine substitutions introduced into DrABD do not impair its ability to bind F-actin. Time course of cross-linking reactions (0, 5, 10, 20, 40, and 75 min) between skeletal F-actin (10 μM) and $DrABD_{300}$ mutants (30 μM) in the presence of EDC (30 μM). The higher mobility bands correspond to actin, whereas the lower mobility bands represent the cross-linked actin–DrABD complex. Reaction conditions: 5 mM Mops, pH 7.2, 0.2 mM $CaCl_2$, 0.2 mM ATP, 0.11 mM TCEP, 100 mM KCl, and 2 mM $MgCl_2$.

polymerization of skeletal actin was induced by addition of 2.0 mM $MgCl_2$ and 100 mM KCl to the actin solution in 5 mM Tris, pH 8.0, 0.2 mM $CaCl_2$, 0.2 mM ATP, and 5 mM β-mercaptoethanol. The samples were centrifuged at 312,500*g* for 30 min, at 4 °C, in a Beckman TLA-100 rotor. Resulting pellets were solubilized in gel sample buffer and analyzed by SDS-PAGE. To quantify the amount of N-GST-fused DrABD co-sedimented with F-actin, we loaded 0.4–3.6 μg of purified constructs on each gel as the standards. Gels were stained with Coomassie Blue. The intensities of the bands were estimated using Scion Image Software. Binding parameters (K_d and B_{max}) were obtained by fitting the average data points in SigmaPlot 9.0. The resulting curves (Fig. 1) represent the best fit.

Actin modification and cross-linking

Immediately prior to the reaction, DTT was removed from G-actin samples over a Sephadex G-50 spin column equilibrated with thiol-free buffer containing 5 mM Mops, pH 7.2, 0.2 $CaCl_2$, and 0.2 mM ATP. Drebrin ABD constructs were passed through a Zeba Desalt Spin Column (Pierce) equilibrated with the same buffer. Actin was polymerized in the presence of 2.0–3.0 mM $MgCl_2$ and 100 mM KCl. The reactions of F-actin modification with MTS were carried out at room temperature (1–10 min), at molar ratios of 0.95:1 of MTS/actin. Cross-linking reaction was started by mixing DrABD constructs with MTS-pre-modified F-actin. Aliquots were withdrawn from the reaction mixtures at selected time points, and free cysteine residues were blocked with *N*-ethyl maleimide. Cross-linking progress was monitored by SDS-PAGE under nonreducing conditions.

Circular dichroism

CD spectra of DrABD (0.5 mg/ml) in 5 mM Tris, pH 7.8, at 25 °C were measured using a J-700 polarimeter (Jasco). Eight replicates of each spectrum were recorded using scanning speed of 20 nm/min, a data pitch of 0.5 nm, and a 4-s dwell time. Samples were measured in a quartz cuvette with a path length of 0.01 cm. CD spectra were deconvoluted using the Selcon3 algorithm. Secondary structure obtained from the CD spectra was compared with that calculated from the secondary structure prediction algorithm Jpred 3.

MS and data analysis

Actin, DrABD, and EDC cross-linked heterodimers were separated using PAGE. The gel bands were digested as described previously.[37] Actin, DrABD, and the trimer, consisting of 2-iminothiolane-modified DrABD attached to two adjacent protomers through MTS1, were separated using size-exclusion chromatography and digested in-solution as described earlier[38] and detailed in the Appendix A. The peptides were first analyzed by matrix-assisted laser desorption/ionization time-of-flight MS (Voyager DE-STR, Applied Biosystems, Framingham, MA), using the dried droplet method with dihydroxybenzoic acid as matrix, and then by MS/MS. The digests were desalted using microcolumns[39] packed with POROS R2 beads (Applied Biosystems) and eluted directly into glass capillaries (Proxeon Biosystems, Odense, Denmark) to be analyzed manually by MS/MS (Synapt HDMS, Manchester, UK).

Spectra for the unmodified samples were acquired first and then used as controls during the analysis of the cross-linked sample to determine unique peptide ions. In each analysis, a few relevant peptides were analyzed, each up to 25 min to ensure high spectrum quality. A small portion of the sample, cross-linked using MTS1, was incubated with 10 mM DTT for 1 h and analyzed by MS/MS to verify the disulfide nature of the cross-link. The cross-linked peptides were identified through manual interpretation of the raw spectra. To unambiguously assign the cross-linking site, we exhaustively assigned the spectra using in-house written Perl scripts. First, theoretical masses were calculated from the cross-linked peptides, allowing for multiple cross-linking sites and modifications, and then the theoretical masses were matched with mass lists generated by processing the raw spectra with Mascot Distiller 2.0 using an error of 0.1 Da or 100 ppm. Assignments were verified in the raw spectra using isotope patterns and charge states. In some cases, more than one peptide assignment was possible within the experimental error, and then the number of cleavages and supporting ions (e.g., water loss or ammonium loss) was used to select the most likely candidate.

EM reconstruction

G-actin was purified using Superdex-200 column and frozen in liquid nitrogen. Before each experiment, an aliquot of actin was thawed at 4 °C and clarified by centrifugation (100,000*g*, 1 h). Actin (5 μM) was polymerized in 10 mM Tris–HCl buffer, pH 7.8, containing 50 mM KCl, 1 mM $MgCl_2$, 1 mM DTT, and 0.2 mM ATP, for 1.5–2 h. To obtain the filaments decorated with DrABD, we incubated 1–2 μM concentration of F-actin with 10–15 μM concentration of DrABD for 12–15 min at room temperature. An identical procedure was used for decorating actin with the 1–300 drebrin construct. Samples were applied to glow-discharged carbon-coated grids and stained with 2% uranyl acetate. The grids were examined in a Tecnai-12 electron microscope (FEI) under minimal-dose conditions at an accelerating voltage of 80 keV and a nominal magnification of 30,000×.

The SPIDER software package[40] was used for most image processing, but the EMAN package[41] was used to extract filament images from micrographs. A Nikon COOLPIX 8000 scanner was used to digitize micrographs at a raster of 4.16 Å per pixel. The IHRSR method[25] was used to generate an overall reconstruction from 9749 segments (each 416 Å long) of actin filaments decorated with DrABD (Fig. 3b). Comparison of the overall reconstruction with the reconstruction of pure F-actin[17] revealed an additional mass attached to the front and side parts of SD1 and SD2 of actin protomers (see Appendix A for details). To evaluate whether that density was arising from a single drebrin molecule or was rather a superposition of multiple states of binding, we designed a set of models to decompose the additional density into several classes based on the possible location of drebrin on F-actin. The size of the additional mass, along with the quality of the actin portion of the map, was used as a guideline in the sorting process. The position of drebrin in its five modes of binding to F-actin relative to the additional density in the overall reconstruction is shown in Supplemental Fig. 1. A detailed description of the sorting procedures has been published earlier.[26,42]

UCSF Chimera software[43] was used to fit the crystal structure of actin[44] into the experimental maps. Atomic coordinates from crystal structures were converted to density maps, and these were filtered to the resolution of the experimental map and docked manually.

Acknowledgements

This work was supported by the US Public Health Service through grants GM 077190 (to E.R.) and RR 20004 (to J.A.L.), the National Institutes of Health through grant GM081303 (to E.H.E.), and the National Science Foundation through grant MCB 0316269 (to E.R.). We thank Courtney White for helping with isolating drebrin-encoding DNA. We are grateful to Dora Warshaviak for assisting with computational analysis.

Supplementary Data

Supplementary data associated with this article can be found, in the online version, at doi:10.1016/j.jmb.2010.03.039

References

1. Sekino, Y., Kojima, N. & Shirao, T. (2007). Role of actin cytoskeleton in dendritic spine morphogenesis. *Neurochem. Int.* **51**, 92–104.
2. Kojima, N. & Shirao, T. (2007). Synaptic dysfunction and disruption of postsynaptic drebrin–actin complex: a study of neurological disorders accompanied by cognitive deficits. *Neurosci. Res.* **58**, 1–5.
3. Peitsch, W. K., Hofmann, I., Pratzel, S., Grund, C., Kuhn, C., Moll, I *et al.* (2001). Drebrin particles: components in the ensemble of proteins regulating actin dynamics of lamellipodia and filopodia. *Eur. J. Cell Biol.* **80**, 567–579.
4. Peitsch, W. K., Hofmann, I., Endlich, N., Pratzel, S., Kuhn, C., Spring, H. *et al.* (2003). Cell biological and biochemical characterization of drebrin complexes in mesangial cells and podocytes of renal glomeruli. *J. Am. Soc. Nephrol.* **14**, 1452–1463.
5. Grenklo, S., Hillberg, L., Zhao Rathje, L. S., Pinaev, G., Schutt, C. & Lindberg, U. (2008). Tropomyosin assembly intermediates in the control of microfilament system turnover. *Eur. J. Cell Biol.* **87**, 905–920.
6. Ishikawa, R., Hayashi, K., Shirao, T., Xue, Y., Takagi, T., Sasaki, Y. & Kohama, K. (1994). Drebrin, a development-associated brain protein from rat embryo, causes the dissociation of tropomyosin from actin filaments. *J. Biol. Chem.* **269**, 29928–29933.
7. Sasaki, Y., Hayashi, K., Shirao, T., Ishikawa, R. & Kohama, K. (1996). Inhibition by drebrin of the actin-bundling activity of brain fascin, a protein localized in filopodia of growth cones. *J. Neurochem.* **66**, 980–988.
8. Biou, V., Brinkhaus, H., Malenka, R. C. & Matus, A. (2008). Interactions between drebrin and Ras regulate dendritic spine plasticity. *Eur. J. Neurosci.* **27**, 2847–2859.
9. Hayashi, K., Ishikawa, R., Ye, L. H., He, X. L., Takata, K., Kohama, K. & Shirao, T. (1996). Modulatory role of drebrin on the cytoskeleton within dendritic spines in the rat cerebral cortex. *J. Neurosci.* **16**, 7161–7170.
10. Ishikawa, R., Katoh, K., Takahashi, A., Xie, C., Oseki, K., Watanabe, M. *et al.* (2007). Drebrin attenuates the interaction between actin and myosin-V. *Biochem. Biophys. Res. Commun.* **359**, 398–401.
11. Zhao, L., Ma, Q. L., Calon, F., Harris-White, M. E., Yang, F., Lim, G. P. *et al.* (2006). Role of p21-activated kinase pathway defects in the cognitive deficits of Alzheimer disease. *Nat. Neurosci.* **9**, 234–242.
12. Kessels, M. M., Engqvist-Goldstein, A. E. Y. & Drubin, D. G. (2000). Association of mouse actin-binding protein 1 (mAbp1/SH3P7), an Src kinase target, with dynamic regions of the cortical actin cytoskeleton in response to Rac1 activation. *Mol. Biol. Cell*, **11**, 393–412.
13. Xu, W. & Stamnes, M. (2006). The actin-depolymerizing factor homology and charged/helical domains of drebrin and mAbp1 direct membrane binding and localization via distinct interactions with actin. *J. Biol. Chem.* **281**, 11826–11833.
14. Hayashi, K., Ishikawa, R., Kawai-Hirai, R., Takagi, T., Taketomi, A. & Shirao, T. (1999). Domain analysis of the actin-binding and actin-remodeling activities of drebrin. *Exp. Cell Res.* **253**, 673–680.
15. Hayashi, K. & Shirao, T. (1999). Change in the shape of dendritic spines caused by overexpression of drebrin in cultured cortical neurons. *J. Neurosci.* **19**, 3918–3925.
16. Haeckel, A., Ahuja, R., Gundelfinger, E. D., Qualmann, B. & Kessels, M. M. (2008). The actin-binding protein Abp1 controls dendritic spine morphology and is important for spine head and synapse formation. *J. Neurosci.* **28**, 10031–10044.
17. Galkin, V. E., Orlova, A., Lukoyanova, N., Wriggers, W. & Egelman, E. H. (2001). Actin depolymerizing factor stabilizes an existing state of F-actin and can change the tilt of F-actin subunits. *J. Cell Biol.* **153**, 75–86.
18. Reichert, A., Heintz, D., Echner, H., Voelter, W. & Faulstich, H. (1996). Identification of contact sites in the actin–thymosin beta4 complex by distance-dependent thiol cross-linking. *J. Biol. Chem.* **271**, 1301–1308.
19. Kim, E., Miller, C. & Reisler, E. (1996). Polymerization and *in vitro* motility properties of yeast actin: a comparison with rabbit skeletal α-actin. *Biochemistry*, **35**, 16566–16572.

20. Gerson, J. H., Kim, E., Muhlrad, A. & Reisler, E. (2001). Tropomyosin–troponin regulation of actin does not involve subdomain 2 motions. *J. Biol. Chem.* **276**, 18442–18449.
21. Grintsevich, E. E., Benchaar, S. A., Warshaviak, D., Boontheung, P., Halgand, F., Whitelegge, J. P. *et al.* (2008). Mapping the cofilin binding site on yeast G-actin by chemical cross-linking. *J. Mol. Biol.* **377**, 395–409.
22. Cole, C., Barber, J. D. & Barton, G. J. (2008). The Jpred 3 secondary structure prediction server. *Nucleic Acids Res.* **36**, W197–W201.
23. Holmes, K. C., Popp, D., Gebhard, W. & Kabsch, W. (1990). Atomic model of the actin filament. *Nature*, **347**, 44–49.
24. McGough, A., Way, M. & DeRosier, D. (1994). Determination of the alpha-actinin-binding site on actin filaments by cryoelectron microscopy and image analysis. *J. Cell Biol.* **126**, 433–443.
25. Egelman, E. H. (2000). A robust algorithm for the reconstruction of helical filaments using single-particle methods. *Ultramicroscopy*, **85**, 225–234.
26. Galkin, V. E., Orlova, A., VanLoock, M. S., Rybakova, I. N., Ervasti, J. M. & Egelman, E. H. (2002). The utrophin actin-binding domain binds F-actin in two different modes: implications for the spectrin superfamily of proteins. *J. Cell Biol.* **157**, 243–251.
27. Lehman, W., Galinska-Rakoczy, A., Hatch, V., Tobacman, L. S. & Craig, R. (2009). Structural basis for the activation of muscle contraction by troponin and tropomyosin. *J. Mol. Biol.* **388**, 673–681.
28. Bacchiocchi, C., Graceffa, P. & Lehrer, S. S. (2004). Myosin-induced movement of [alpha][alpha], [alpha][beta], and [beta][beta] smooth muscle tropomyosin on actin observed by multisite FRET. *Biophys. J.* **86**, 2295–2307.
29. Lehman, W., Craig, R. & Vibert, P. (1994). Ca^{2+}-induced tropomyosin movement in Limulus thin filaments revealed by three-dimensional reconstruction. *Nature*, **368**, 65–67.
30. Xu, C., Craig, R., Tobacman, L., Horowitz, R. & Lehman, W. (1999). Tropomyosin positions in regulated thin filaments revealed by cryoelectron microscopy. *Biophys. J.* **77**, 985–992.
31. McGough, A., Pope, B., Chiu, W. & Weeds, A. (1997). Cofilin changes the twist of F-actin: implications for actin filament dynamics and cellular function. *J. Cell Biol.* **138**, 771–781.
32. Paavilainen, V. O., Oksanen, E., Goldman, A. & Lappalainen, P. (2008). Structure of the actin-depolymerizing factor homology domain in complex with actin. *J. Cell Biol.* **182**, 51–59.
33. Wyszynski, M., Lin, J., Rao, A., Nigh, E., Beggs, A. H., Craig, A. M. & Sheng, M. (1997). Competitive binding of [alpha]-actinin and calmodulin to the NMDA receptor. *Nature*, **385**, 439–442.
34. Shirao, T. & Sekino, Y. (2001). Clustering and anchoring mechanisms of molecular constituents of postsynaptic scaffolds in dendritic spines. *Neurosci. Res.* **40**, 1–7.
35. Holmes, K. C., Angert, I., Jon Kull, F., Jahn, W. & Schroder, R. R. (2003). Electron cryo-microscopy shows how strong binding of myosin to actin releases nucleotide. *Nature*, **425**, 423–427.
36. Spudich, J. A. & Watt, S. (1971). The regulation of rabbit skeletal muscle contraction: I. Biochemical studies of the interaction of the tropomyosin–troponin complex with actin and the proteolytic fragments of myosin. *J. Biol. Chem.* **246**, 4866–4871.
37. Shevchenko, A., Wilm, M., Vorm, O. & Mann, M. (1996). Mass spectrometric sequencing of proteins from silver-stained polyacrylamide gels. *Anal. Chem.* **68**, 850–858.
38. Ytterberg, A. J., Peltier, J. B. & van Wijk, K. J. (2006). Protein profiling of plastoglobules in chloroplasts and chromoplasts. A surprising site for differential accumulation of metabolic enzymes. *Plant Physiol.* **140**, 984–997.
39. Gobom, J., Nordhoff, E., Mirgorodskaya, E., Ekman, R. & Roepstorff, P. (1999). Sample purification and preparation technique based on nano-scale reversed-phase columns for the sensitive analysis of complex peptide mixtures by matrix-assisted laser desorption/ionization mass spectrometry. *J. Mass Spectrom.* **34**, 105–116.
40. Frank, J., Shimkin, B. & Dowse, H. (1981). Spider—a modular software system for electron image processing. *Ultramicroscopy*, **6**, 343–357.
41. Ludtke, S. J., Baldwin, P. R. & Chiu, W. (1999). EMAN: semiautomated software for high-resolution single-particle reconstructions. *J. Struct. Biol.* **128**, 82–97.
42. Galkin, V. E., Orlova, A., Lukoyanova, N., VanLoock, M. S., Haag, P., Bullard, B. & Egelman, E. H. (2003). The location of ubiquitin in *Lethocerus* arthrin. *J. Mol. Biol.* **325**, 623–628.
43. Pettersen, E. E., Goddard, T. D., Huang, C. C., Couch, G. S., Greenblatt, D. M., Meng, E. C. & Ferrin, T. E. (2004). UCSF Chimera—visualization system for exploratory research and analysis. *J. Comput. Chem.* **25**, 1605–1612.
44. Schutt, C. E., Myslik, J. C., Rozycki, M. D., Goonesekere, N. C. W. & Lindberg, U. (1993). The structure of crystalline profilin–[beta]-actin. *Nature*, **365**, 810–816.

Supplementary Information

APPENDIX A

Drebrin constructs purification -- The collected *E. coli* cells were frozen in liquid nitrogen and stored at -80 °C. All glutathione S-transferase (GST)-tagged drebrin constructs were recovered from the soluble fractions. Lysis buffer (Buffer A: 10 mM Na_2HPO_4, 1.8 mM KH_2PO_4, 140 mM NaCl) was supplemented with 0.2 mM PMSF and protease inhibitors cocktail (Roche). Additional wash step was introduced for all the constructs (Buffer A containing 0.64 M NaCl). For pelleting experiments, N-GST fused constructs were eluted with 10 mM glutathione buffer and further purified on Superdex-75 gel-filtration column. Alternatively, on-column thrombin cleavage was performed overnight at 4 °C. For CD experiments, DrABD constructs were additionally purified on Superdex-75 column.

Samples preparation for mass spectrometry analysis -- 50 µg of each sample were precipitated with 100% acetone overnight at -20˚C. The aggregates were collected by centrifugation and the pellets were washed by incubation in 80% acetone, 10% methanol, 0.2% acetic acid and 9.8% water for 30 minutes at -20˚C. The supernatant were removed after centrifugation, and the pellet were incubated in 20 µl DMSO for 30 min at room temperature on a shaker. The proteins were then digested overnight with trypsin (1:20 protease to protein ratio) in 50 mM ammonium bicarbonate and 30% DMSO. The resulting peptides were extracted, lyophilized and resuspended in 5% formic acid.

Electron microscopic reconstruction of DrABD-decorated F-actin -- Five model volumes with additional density attached to each of these sites, along with the naked F-actin volume, were projected and cross-correlated with the 9,749 raw segments. Each class was reconstructed

separately, starting from a featureless solid cylinder. A substantial number of segments (n = 3,668) were found to be naked filaments and resulted in the reconstruction shown in Fig. 3(c) with helical symmetry of -166.3°/27.6Å. The three largest occupied classes of segments yielded reconstructions having the drebrin molecule attached in between Subdomain 1 (SD1) and Subdomain 2 (SD2) (n = 1,413, Fig. 3(d)), to the front of SD1 (n = 1,336, Fig. 3(e)), or side of SD1/SD2 (n = 1,047, Fig. 3(f)). The corresponding symmetries for each class were found as being 165.8°/27.1 Å, 165.8°/27.6 Å, and 166.2°/27.1 Å, respectively. The two small classes revealed drebrin attached to the side (n = 925, Fig. 3(g)) or back (n = 613, Fig. 3(h)) of SD1 of actin. These classes converged to the symmetries of 166°/27.5 Å and 166.1°/27.2 Å, respectively.

APPENDIX B

(A)

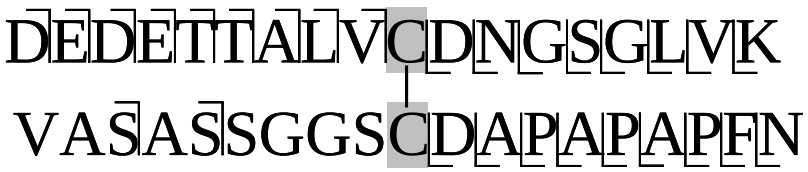

(B)

F-actin		Drebrin	$[M+2H]^{2+}$	Error (ppm)	$[M+3H]^{3+}$	Error (ppm)
DEDETTALVCDNGSGLVK		VASASGGSCDAPAPAPFN	1762.18	-56	1175.26	61

(C)

F-actin		Drebrin	ion types	$[M+H]^{+}$
CDNGSGLVK		VASASGGSCDAPAPAPFN	y9-M	2508.25
VCDNGSGLVK		VASASGGSCDAPAPAPFN	y10-M	2607.31
LVCDNGSGLVK		VASASGGSCDAPAPAPFN	y11-M	2720.39
ALVCDNGSGLVK		VASASGGSCDAPAPAPFN	y12-M	2791.37
TALVCDNGSGLVK		VASASGGSCDAPAPAPFN	y13-M	2892.41
TTALVCDNGSGLVK		VASASGGSCDAPAPAPFN	y14-M	2993.42
DEDETTALVCDNGSGLVK		VASASGGSCD	M-b10	2740.30

DEDETTALVCDNGSGLVK		VASASGGSCDA	M-b11	2811.31
DEDETTALVCDNGSGLVK		VASASGGSCDAPA	M-b13	2979.34
DEDETTALVCDNGSGLVK		VASASGGSCDAPAPA	M-b15	3147.38
DEDETTALVCDNGSGLVK		VASASGGSCDAPAPAPF	M-b17	3391.35

APPENDIX 2. **C308 on DrABD cross-links to C10 of actin (minor population).** DrABD cross-linked to two adjacent actin protomers were isolated by size exclusion chromatography, digested with trypsin and analyzed by nanoESI-MS/MS. Two peaks were unique to the cross-linked sample compared to controls (skeletal actin and DrABD) and the peptides were matched to actin and drebrin. (a) Schematic representation of actin peptide 1 – 18 cross-linked to the drebrin peptide 300 - 317 (*y*-ions are indicated by left-facing bars, *b*-ions are indicated by right-facing bars). Actin peptide 1 – 18 is acetylated on the N-terminus, and the actin and drebrin peptides are linked through a disulfide bond. The formation of the disulfide bond was verified by reducing the sample with DTT and reanalyzing the digest. As expected, the two peaks corresponded to the cross-linked peptide disappeared after reduction. (b) Indicates the mass and error of the two detected charge states and (c) lists some of the cross-linked fragments with deconvoluted masses. ‘M’ indicates intact peptide.

APPENDIX C

Summary of the observed ions resulting from the fragmentation of the actin-drebrin EDC cross-linked peptide at *m/z* $[M+4H]^{4+}$ = 663.61 (error 30.8 ppm)

[#] Cross-link (-); alternative fit (/); M – intact peptide; wl – loss of water; al – ammonia loss

**isobar fit* – two or more matches with identical composition/masses

***best fit* – more than one match with different masses, all within experimental error. The best alternative is reported.

*** fit within experimental error and supported by additional fragments

$[M+H]^+$	Error	$[M+2H]^{2+}$	Error	$[M+3H]^{3+}$	Error	Type of Ion #	Peptide Sequence		Site	Comment
							Actin	Drebrin		
86.10	39.8					im L	L			Isobar fit*
974.52	24.3					1b9	VAPEEHPTL			
1087.61	28.1					1b10	VAPEEHPTLL			
147.12	52.3					1y1	K			
244.18	40.2					1y2	PK			
341.19	37.0					1y3al	NPK			
358.22	39.8					1y3	NPK			
471.31	38.8					1y4	LNPK			
551.32	10.8					1y5al	PLNPK			
568.37	36.5	284.69	35.4			1y5	PLNPK			
639.41	36.6					1y6	APLNPK			
768.45	36.4					1y7	EAPLNPK			
851.47	13.4					1y8wl	TEAPLNPK			
869.50	34.4	435.25	28.7			1y8	TEAPLNPK			
982.59	31.1					1y9	LTEAPLNPK			
1095.67	30.7					1y10	LLTEAPLNPK			
1293.78	32.6	647.39	17.8			1y12	PTLLTEAPLNPK			
		715.91	7.5			1y13	HPTLLTEAPLNPK			
1218.64	34.1					[1b2:12]/ [1b3:13]/ [1b4:14]	APEEHPTLLTE/ PEEHPTLLTEA/ EEHPTLLTEAP			Isobar fit
493.23	54.6					[1b3:6]/ [1b4:7]	PEEH/EEHP			Isobar fit
		459.25	22.3			1b3:10	PEEHPTLL			
235.13	47.8					1b6:7	HP			
203.11	36.0					1a11:12	TE			
231.11	42.1					1b11:12	TE			Best fit**
302.15	39.1					1b11:13	TEA			
396.24	31.8					1b13:16	APLN			
183.16	34.8					1a14:15	PL			
211.15	38.4					1b14:15	PL			

325.20	38.5					[1b14:16]/[1b15:17]	PLN/LNP			Isobar fit
215.15	50.4					[1b8:9]/[1b10:11]	TL/LT			Isobar fit
175.13	37.7					2y1		R		
312.19	44.1					2y2		HR		Best fit
441.24	36.1					2y3		EHR		
1221.60	40.6	611.42	228.2			b5-M	VAPEE	GSEEHR	99/100	
1358.65	32.7	679.83	27.9			b6-M	VAPEEH	GSEEHR	99/100	Best fit
		835.43	30.0	557.29	40.8	b9-M	VAPEEHPTL	GSEEHR	99/100	
		877.81	-148.7	585.64	21.7	a10-M	VAPEEHPTLL	GSEEHR	99/100	Best fit
				589.29	1.5	b10-Mal	VAPEEHPTLL	GSEEHR	99/100	
		891.97	28.3			b10-M	VAPEEHPTLL	GSEEHR	99/100	Best fit
		933.49	27.8	622.66	23.1	b11-Mwl	VAPEEHPTLLT	GSEEHR	99/100	Best fit
		942.49	27.0	628.66	21.6	b11-M	VAPEEHPTLLT	GSEEHR	99/100	Best fit
		993.00	13.4			a12-M	VAPEEHPTLLTE	GSEEHR	99/100/107	Best fit
		998.01	28.5			b12-Mwl	VAPEEHPTLLTE	GSEEHR	99/100/107	
		1007.02	28.2	671.68	24.0	b12-M	VAPEEHPTLLTE	GSEEHR	99/100/107	
		1033.53	24.9	689.36	30.5	b13-Mwl	VAPEEHPTLLTEA	GSEEHR	99/100/107	
		1042.53	26.0	695.36	24.6	b13-M	VAPEEHPTLLTEA	GSEEHR	99/100/107	
		1147.61	28.8			b15-M	VAPEEHPTLLTEAPL	GSEEHR	99/100/107	
						M-M	VAPEEHPTLLTEAPLNPK	GSEEHR	99/100/107	
1023.52	10.9					y7-b3	EAPLNPK	GSE	107	
1134.60	46.4					y7-b4wl	EAPLNPK	GSEE	107	Best fit
1152.60	41.6	576.80	36.8			y7-b4	EAPLNPK	GSEE	107	Best fit
				827.77	25.4	y16-M	PEEHPTLLTEAPLNPK	GSEEHR	99/100/107	
		785.89	35.0			b2:9-M	APEEHPTL	GSEEHR	99/100	Best fit
		842.43	31.5			b2:10-M	APEEHPTLL	GSEEHR	99/100	Best fit
		948.47	26.7	632.66	33.9	[b2:12-Mwl]/[b3:13-Mwl]/[b4:14-Mwl]	APEEHPTLLTE/PEEHPTLLTEA/EEHPTLLTEAP	GSEEHR	99/100/107	Isobar fit
		957.48	28.2	638.59	-67.2	[b2:12-M]/[b3:13-M]/[b4:14-M]	APEEHPTLLTE/PEEHPTLLTEA/EEHPTLLTEAP	GSEEHR	99/100/107	Isobar fit
1051.48	37.4	526.27	79.5			b3:5-M	PEE	GSEEHR	99/100	
1160.56	45.6	580.86	168.9			[a3:6-M]/[a4:7-M]	PEEH/EEHP	GSEEHR	99/100	Isobar fit
1188.55	42.8					[b3:6-M]/[b4:7-M]	PEEH/EEHP	GSEEHR	99/100	Isobar fit
1358.62	8.5	679.83	32.6			a3:8-M	PEEHPT	GSEEHR	99/100	***
		684.83	42.9	456.88	23.0	b3:8-Mwl	PEEHPT	GSEEHR	99/100	
1386.66	40.8	693.83	35.6	462.88	15.9	b3:8-M	PEEHPT	GSEEHR	99/10	

									0	
		736.37	33.9	491.27	68.7	a3:9-M	PEEHPTL	GSEEHR	99/100	Best fit
		741.36	30.8	494.58	27.1	b3:9-Mwl	PEEHPTL	GSEEHR	99/100	Best fit
		750.38	45.3	500.58	31.5	b3:9-M	PEEHPTL	GSEEHR	99/100	
		792.90	15.6			a3:10-M	PEEHPTLL	GSEEHR	99/100	
		806.91	27.6	538.26	0.5	b3:10-M	PEEHPTLL	GSEEHR	99/100	
		848.43	27.6			b3:11-Mwl	PEEHPTLLT	GSEEHR	99/100	
		857.45	38.6	571.98	68.6	b3:11-M	PEEHPTLLT	GSEEHR	99/100	
		921.96	31.6	614.97	21.1	b3:12-M	PEEHPTLLTE	GSEEHR	99/100/107	Best fit
		1119.57	20.9			[b3:16M]/[b4:17-M]	PEEHPTLLTEAPLN/EEHPTLLTEAPLNP	GSEEHR	99/100/107	Isobar fit
		758.39	35.8			b4:10-M	EEHPTLL	GSEEHR	99/100	
953.40	98.0					[a7:13-b3]/[a8:14-b3]	PTLLTEA/TLLTEAP	GSE	107	
		491.27	43.5			[b7:13-b3]/[b8:14-b3]	PTLLTEA/TLLTEAP	GSE	107	Isobar fit
824.45	-0.9	412.72	13.6			[a7:13-b2]/[a8:14-b2]	PTLLTEA/TLLTEAP	GS	107	
971.49	-8.5					b6:13-b2wl	HPTLLTEA	GS	107	
989.53	23.5					b6:13-b2	HPTLLTEA	GS	107	

APPENDIX D. **Primers used for cloning and site-directed mutagenesis**

Drebrin construct	Forward primer	Reverse primer
Drebrin full length (pCR2.1-TOPO)	CATGGCCGGCGTCAGCTTCAGC	CTAATCACCACCCTCGAAGCCCTCTTCC
Drebrin full length (pGEX-4T1)[#]	GATCGGATCCGCCGGCGTCAGCTTCAGC	CCGCTCGAGTTACTAATCACCACCCTCGAAGCCCTC
DrABD, seq 233-317*	GATCGGATCCGAGGAGCACAGGAGGAAACAGCAG	CCGGAATTCCTAGTTGAAGGGTGCAGGCGCAGG
DrABD$_{300}$; Drebrin 1-300	CAGCAGGAACGAGTGTAATCGGCCTCTGGTGGC	GCCACCAGAGGCCGATTACACTCGTTCCTGCTG
K238C	GAGGAGCACAGGAGGTGCCAGCAGAGTCTGGAAGC	GCTTCCAGACTCTGCTGGCACCTCCTGTGCTCCTC
K248C	GAAGCTGAAGAAGCCTGCAGGAGGTTAAAGGAG	CTCCTTTAACCTCCTGCAGGCTTCTTCAGCTTC
K252C	GCCAAGAGGAGGTTATGCGAGCAGTCTATC	GATAGACTGCTCGCATAACCTCCTCTTGGC
K270C	GAAGAGTCCCAGATGTGCAAGTCGGAGTCAGAG	CTCTGACTCCGACTTGCACATCTGGGACTCTTC
K271C	GAGTCCCAGATGAAGTGCTCGGAGTCAGAGGTG	CACCTCTGACTCCGAGCACTTCATCTGGGACTC

The PCR product was subcloned into the BamH1 and XhoI sites of pGEX-4T1 expression vector

*The PCR product was subcloned into the BamH1 and EcoR1 sites of pGEX-4T1 expression vector

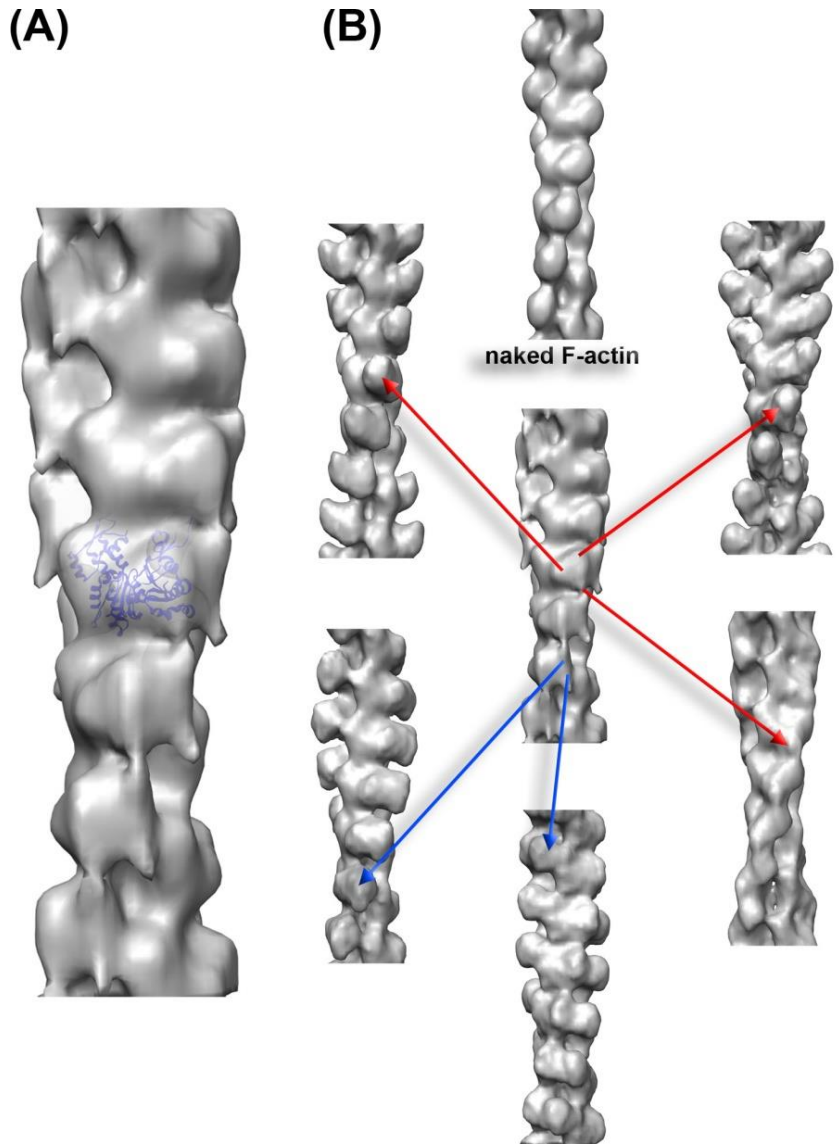

Supplemental Figure 1. The position of DrABD in its five modes of binding to F-actin relative to the additional density in the overall reconstruction. The overall reconstruction of F-actin segments decorated with a derbrin construct revealed traces of the bound drebrin all over SD1, SD2, and the top of SD4. Actin crystal structure is shown as blue ribbons (pdb entry 1HLU). To evaluate whether that density was a superposition of multiple states of binding rather than being arising from a single drebrin molecule a set of models were designed to decompose the additional density into several classes based on a possible location of drebrin on F-actin. The size of the additional mass along with the quality of the actin portion of the map was used as a guideline in the sorting process. All the five modes of binding of drebrin to F-actin that are shown in Figure 6 are related to the additional density in the overall reconstruction, and this is marked with red (major mode) and blue (minor mode) arrows.

CHAPTER 3

Drebrin-Induced Stabilization of Actin Filaments

This research was originally published in Journal of Biological Chemistry. Mouna A. Mikati, Elena E. Grintsevich, Emil Reisler. Drebrin-Induced Stabilization of Actin Filaments. *J. Biol. Chem*. 2013; 288:19926-19938.

Drebrin-induced Stabilization of Actin Filaments*

Received for publication, March 27, 2013, and in revised form, May 15, 2013 Published, JBC Papers in Press, May 21, 2013, DOI 10.1074/jbc.M113.472647

Mouna A. Mikati[‡1], **Elena E. Grintsevich**[‡1], **and Emil Reisler**[‡§2]

From the [‡]*Department of Chemistry and Biochemistry and the* [§]*Molecular Biology Institute, University of California Los Angeles, Los Angeles, California 90095*

Background: Drebrin is a mammalian neuronal protein that binds to and organizes filamentous actin (F-actin) in dendritic spines.
Results: Drebrin protects actin filaments from depolymerization and rescues their formation in different cases of longitudinal and lateral contact perturbation.
Conclusion: Drebrin stabilizes actin filaments through its effect on their interstrand and intrastrand contacts.
Significance: We elucidate the mechanism by which drebrin governs F-actin dynamics in dendritic spines.

Drebrin is a mammalian neuronal protein that binds to and organizes filamentous actin (F-actin) in dendritic spines, the receptive regions of most excitatory synapses that play a crucial role in higher brain functions. Here, the structural effects of drebrin on F-actin were examined in solution. Depolymerization and differential scanning calorimetry assays show that F-actin is stabilized by the binding of drebrin. Drebrin inhibits depolymerization mainly at the barbed end of F-actin. Full-length drebrin and its C-terminal truncated constructs were used to clarify the domain requirements for these effects. The actin binding domain of drebrin decreases the intrastrand disulfide cross-linking of Cys-41 (in the DNase I binding loop) to Cys-374 (C-terminal) but increases the interstrand disulfide cross-linking of Cys-265 (hydrophobic loop) to Cys-374 in the yeast mutants Q41C and S265C, respectively. We also demonstrate, using solution biochemistry methods and EM, the rescue of filament formation by drebrin in different cases of longitudinal interprotomer contact perturbation: the T203C/C374S yeast actin mutant and grimelysin-cleaved skeletal actin (between Gly-42 and Val-43). Additionally, we show that drebrin rescues the polymerization of V266G/L267G, a hydrophobic loop yeast actin mutant with an impaired lateral interface formation between the two filament strands. Overall, our data suggest that drebrin stabilizes actin filaments through its effect on their interstrand and intrastrand contacts.

The function of cells depends on the maintenance of their morphology, their motility, and the ability to adapt their shape in response to external stimuli. Dendritic spines are dynamic structures, and their shape, size and density have been shown to change during development and adulthood (1). During development, dendritic protrusions initiate out as filipodia, which mature into spines (2). These changes are associated with learning, aging, and diseases such as mental retardation (3, 4). Indeed, morphological studies of spines in dementia patients show a correlation between brain dysfunction and abnormal spine morphology (5, 6). This highlights the crucial need for studying the mechanisms of spine maintenance to understand higher brain functions such as memory and learning. F-actin is one of the major cytoskeletal components of spines (7–9) and is believed to play a pivotal role in the mechanisms regulating spine plasticity (10, 11). Drebrin is an F-actin binding protein enriched in dendritic spines of neurons (12, 13) and is involved in organizing the dendritic pool of actin (1). Drebrin protein levels were found to be decreased in Alzheimer's disease (14) and Down syndrome patients (15, 16). Furthermore, down-regulation of drebrin A expression in developing hippocampal neurons suppresses the accumulation of F-actin within dendritic spines (11). A natural interest then arises in the mechanism by which drebrin governs F-actin dynamics and structure in its role in spinal plasticity.

Drebrin binds to F-actin with a stoichiometry of 5:1 (actin: drebrin protomers, K_d of ~ 0.12 μM) (17, 18) and competes with and inhibits the activity of F-actin-binding proteins such as α-actinin, tropomyosin, fascin, and myosin (17, 19, 20). In this study we employed drebrin A, a neuron-specific isoform that is expressed predominantly in the adult brain (12, 21, 22), and its shorter fragments, DrbABD[3] (amino acids 233–300/317 containing the actin binding domain (ABD) (23)), Drb1–300 (amino acids 1–300 containing the ADF homology domain (ADF-H), ABD, and the helical charged motif), and Drb2–252 (amino acids 2–252 containing the ADF-H and helical charged motif and truncated after a predicted coiled-coil region). A schematic of the drebrin molecule is shown in Fig. 7.

Recent atomic force microscopy analysis showed that binding of drebrin A to actin filaments increases their persistence length and helical pitch (~40 nm *versus* 36 nm for "bare" actin) (18), revealing its effect on the structure of F-actin. This stimulated a more detailed probing of the structural effects of drebrin on actin filaments to elucidate the mechanism by which

* This work was supported by United States Public Health Service Grant GM 077190 (to E. R.). This work was also supported by the UCLA Molecular Biology Institute Whitcome Pre-doctoral Training Program (to M. A. M.).

[1] Both authors contributed equally to this work.

[2] To whom correspondence should be addressed: Department of Chemistry and Biochemistry, 407 Charles E. Young Dr. East, University of California Los Angeles, Los Angeles, CA 90095. Tel.: 310-825-2668; E-mail: reisler@mbi.ucla.edu.

[3] The abbreviations used are: Drb, drebrin; ABD, actin-binding domain; ADF-H, actin depolymerization factor homology; CP, capping protein; Lat-A, latrunculin; DSC, differential scanning calorimetry; B-end, barbed-end; P-end, pointed end; GC, gelsolin-capped; TM, tropomyosin.

these two spine-resident proteins regulate spine plasticity and affect brain functions. Here we examine the overall effect of drebrin on F-actin stability and the intrastrand and interstrand contacts in the lateral and longitudinal interfaces of F-actin.

EXPERIMENTAL PROCEDURES

Proteins—Actin from rabbit back muscle was prepared as described by Spudich and Watt (24). Actin was kept on ice in G buffer (5.0 mM Tris, (pH 8.0), 0.2 mM $CaCl_2$, 0.2 mM ATP, 5 mM β-mercaptoethanol) and used within 2 weeks from its purification. Skeletal actin was labeled with pyrene-maleimide as described before (25). Pyrene-maleimide was obtained from Molecular Probes (Eugene, OR).

Grimelysin-cleaved G-actin was obtained as described previously (26). Ca-G-actin (2.0 mg/ml) was digested at an enzyme: protein mass ratio of 1:50 overnight on ice. Because actin cleaved with *Escherichia coli* protease (ECP) (between Gly-42 and Val-43) is resistant to further proteolysis by this protease, protease inhibitor was not added.

Yeast actin mutants were purified in the Ca-G-actin form by DNase I affinity chromatography (25). 25% sucrose was added to the DNase I column elution buffer for protein stability. DNase I was purchased from Bio-World. Yeast actin was stored in a Ca^{2+}G-buffer (5 mM Tris-HCl (pH 8.0) containing 0.2 mM $CaCl_2$, 0.2 mM ATP, and 1 mM DTT). Actin was further purified by passage over Sephacryl S-200 equilibrated in Ca-G buffer to eliminate residual actin oligomers. Full-length drebrin A, Drb-FL, was purified according to Sharma *et al.* (18), and the shorter drebrin constructs were purified according to Grintsevich *et al.* (23).

Depolymerization Assays—Actin depolymerization assays using Lat-A or by dilution were performed at 25 °C by adding 20 μM Lat-A to 2 μM actin labeled with pyrene maleimide (25% or 5% labeled) or by diluting actin to below its barbed-end Cc ([actin] = 0.08 μM) in 50 mM KCl, 2 mM $MgCl_2$, 5 mM β-mercaptoethanol, 0.2 mM ATP, 5 mM Tris (pH 8.0) in the presence or absence of saturating amounts of drebrin. Actin was first polymerized using KMH buffer (50 mM KCl, 2 mM $MgCl_2$, 1 mM DTT, 0.2 mM ATP, 10 mM Hepes (pH 7.4)) for 1 h at 25 °C and then incubated at 2 μM with 10 nM heterodimeric capping protein (CP) for 10 min at 25 °C before initiating depolymerization. Gelsolin was purified using methods published previously (27). Gelsolin-actin seeds were formed by incubating 10 μM skeletal actin with 5 μM gelsolin overnight on ice. Latrunculin (Lat-A) was purchased from Sigma. Actin depolymerization was followed by a decrease in pyrene fluorescence, with the excitation wavelength set at 365 nm and the emission set at 407 nm, using an Alphascan fluorimeter (Photon Technology International). Rates were calculated by measuring the slope of the decay in fluorescence over the first 60 s of the reaction (ΔFluo/sec). Samples were then incubated overnight at 4 °C. The next day, their fluorescence intensity was recorded, they were spun at high speed (TLA100, 95,000 rpm, 4 °C, 20 min), and both the supernatants and pellets were loaded on an SDS-PAGE gel. The total change in fluorescence ($Fmax_{day\ 1}$-$Fmin_{day\ 2}$) was measured, and it corresponded to the amount of actin in the supernatant (quantified from the SDS gel using ScionImage software). Subsequently, initial rates of depolymerization were converted to micromolar/second. Binding densities for Drb-FL in Fig. 1*A* were calculated on the basis of K_d = 0.12 μM and a binding stoichiometry of 1:5 (DrbFL:actin). For Drb1–300, in Fig. 2*C*, binding densities report the amount of drebrin pelleted along with the remaining F-actin (Drb density = $[Drb]_{pellet}/([FA]_{pellet}/3)\times100\%$. The control experiments testing the efficiency of capping (for both CP and gelsolin) were performed as follows. 2 μM actin labeled with pyrene maleimide actin was polymerized by addition of 2 mM $MgCl_2$ and 50 mM KCl, and the change in fluorescence was followed. When a plateau was reached, 1 μM profilin-bound G-actin labeled with 5% pyrene maleimide (1:10 actin:profilin ratio) was added to detect any additional increase in fluorescence (indicating elongation from uncapped barbed ends because profilin actin is not incorporated into filaments from the pointed ends). No elongation was detected. The positive control was performed with uncapped filaments as follows. 2 μM actin labeled with 5% pyrene maleimide actin was polymerized by addition of 2 mM $MgCl_2$ and 50 mM KCl, and the change in fluorescence was followed. Once a plateau was reached, 1 μM profilin-bound G-actin labeled with 5% pyrene maleimide (1:5 actin:profilin ratio) was added to the mixture, and an increase in fluorescence was detected because of elongation at the barbed ends.

Differential Scanning Calorimetry—Differential scanning calorimetry (DSC) experiments were carried out in an N-DSC II calorimeter (CSC). Mg-ATP-G-actin in G buffer (2 mM Tris, 0.2 mM $CaCl_2$, 0.2 mM ATP, 0.1 mM tris(2-carboxyethyl)phosphine (TCEP), 0.4 mM EGTA, 0.1 mM $MgCl_2$ (pH 8)) was polymerized with 2 mM $MgCl_2$ and 100 mM KCl. Final protein mixtures contained 10 mM Pipes, 1 mM Tris, 0.2 mM $CaCl_2$, 0.2 mM ATP, 0.1 mM tris(2-carboxyethyl)phosphine, 2.0 mM $MgCl_2$, and 100 mM KCl (pH 7.5).

Disulfide Cross-linking—Prior to the cross-linking reactions, DTT (or βME) was removed from actin by passing it over a Sephadex G-50 column equilibrated with 5 mM HEPES, (pH 7.5), 0.2 mM $CaCl_2$, and 0.2 mM ATP. The eluted G-actin was polymerized for 30 min with 3.0 mM $MgCl_2$ at room temperature. $DrbABD_{233-300}$ was passed through a Zeba-spin desalting column to exchange the buffer into 5 mM HEPES (pH 7.5), 0.2 mM $CaCl_2$, 0.2 mM ATP, and 3 mM $MgCl_2$. Disulfide cross-linking was catalyzed by addition of 4 μM $CuSO_4$ to actin at room temperature. Samples of the reaction were taken at different time points (0–60 min), at which reactions were stopped with 10 mM *N*-ethylmaleimide. 10 μM BSA was added to the samples after the reaction was stopped with *N*-ethylmaleimide and before mixing the different aliquots with sample loading buffer and loading them on SDS electrophoresis gels. All samples were analyzed by SDS electrophoresis gels to determine the extent of cross-linking. Scion Image was used to quantify band intensities (I), which were normalized to the monomer band at time 0′ (I_0) to generate decay plots (I/I_0) using Sigma Plot software.

Actin Polymerization—Actin polymerization was assessed by following the increase in light scattering as a function of time with a PTI fluorometer set at 350 nm for the excitation and emission wavelengths. Polymerization of actin was induced by addition of 2 mM $MgCl_2$ and 50 mM KCl, except for the T203C/C374S mutant, which was polymerized by the addition of 3 mM

$MgCl_2$ alone because of its sensitivity to KCl. Actin polymerization data are offset to time zero. For experiments at 25 °C, the desired drebrin construct was mixed with Mg-G-actin in Mg-G buffer (10 mM Hepes (pH 7.5), 0.2 mM ATP, 4 mM EGTA, 0.1 mM $MgCl_2$, and 1 mM dithiothreitol). Temperature was regulated with a thermostated water bath and set at 25 °C unless stated otherwise.

Electron Microscopy—The undiluted samples from each experiment were applied to carbon-coated grids and stained with 1% uranyl acetate. The grids were examined in a JEM1200-EX electron microscope (JEOL) at an accelerating voltage of 80 keV and a nominal magnification of 80,000.

RESULTS

Drebrin Stabilizes Actin Filaments—Prior studies revealed a structural effect of drebrin on actin filaments. Here, full-length neuron-specific Drebrin-A (Drb-FL) and its N-terminal construct (sequence 1–300, Drb1–300) were employed to test their effect on actin depolymerization. On the basis of previous reports (23, 18), Drb1–300 binds to skeletal F-actin with an affinity close to that Drb-FL but with a lower binding stoichiometry (each Drb1–300 molecule binds at a ratio of 1:3 drebrin: actin protomer, whereas Drb-FL binds at a mole ratio of 1:5 drebrin:actin). This indicates that Drb1–300 represents the "actin-binding core" of drebrin, making it an important tool to study F-actin-drebrin interactions.

To probe for the stabilization of F-actin by drebrin, we examined filament depolymerization in pyrene assays in the presence of a G-actin-sequestering agent, Lat-A (Fig. 1). We tested the effect of increasing concentrations of Drb-FL on the depolymerization of uncapped actin filaments and filaments capped at the barbed end with heterodimeric CP. In uncapped filaments, barbed-end (B-end) depolymerization predominates because it is significantly faster than the pointed-end (P-end) one (28, 29). Drb-FL significantly decreased the depolymerization rates of uncapped filaments, reaching 88% inhibition at full saturation. Best fit of the data shows that 50% inhibition of depolymerization of uncapped F-actin is achieved at a low binding density of drebrin (~18%) (Fig. 1*A*).

In addition, high-speed cosedimentation revealed that, in the presence of both Lat-A and Drb-FL, actin filaments do not depolymerize fully (in contrast to the no-drebrin control), even after 18 h of incubation at 4 °C (Fig. 1*B*). The nature of this effect is not yet clear. To rule out Drb-FL-induced nucleation of Lat-A-bound G-actin, we performed control experiments in which 2 μM G-actin mixed with a 10-fold excess of Lat-A was left overnight in polymerizing conditions at 4 °C in the presence and absence of Drb-FL. Neither sample showed any pelleted actin when spun at high speeds the next day (data not shown), suggesting that Drb-FL did not allow nucleation of Lat-A bound G-actin.

Depolymerization at the P-end of filaments capped with CP was slow (compared with uncapped ones), and any further decrease in rate because of the protection by Drb-FL could have been too small to detect (Fig. 1*A*). The simplest way to assess more accurately the effect of drebrin on P-end depolymerization was to increase the observed rates of depolymerization by increasing the number of free P-ends. To this end, we employed another B-end capper, gelsolin. For this assay we polymerized actin filaments from gelsolin seeds (see "Experimental Procedures"). This allows controlling the number of P-ends because filaments will polymerize preferably from preformed gelsolin-actin seeds. As expected, at an actin:gelsolin ratio of 130:1, the observed depolymerization from P-ends was faster than in CP-capped filaments. Using this assay, we detected the inhibition of P-end depolymerization by Drb-FL. The degree of inhibition was smaller than for uncapped filaments. Fig. 1*C* shows representative plots of total (from both barbed and pointed ends) pyrene-F-actin disassembly and gelsolin-capped (GC) F-actin (from P-ends) disassembly in the presence of Drb-FL. Drb-FL causes ~88% inhibition (Fig. 1*C*, *upper panel, bar plot*) of total depolymerization *versus* 48% inhibition of P-end depolymerization at the same binding density (90%) (Fig. 1*C*, *lower panel, bar plot*). As revealed by high-speed cosedimentation analysis, the binding of Drb-FL to F-actin at equilibrium was not affected by gelsolin capping (data not shown). Also, it is worth mentioning that elongation of CP- or gelsolin-capped F-actin from the profilin-G-actin complex was not detected in control experiments, confirming that drebrin does not displace either capping protein from the barbed end (data not shown). An additional indication of actin stabilization by drebrin was provided by DSC assays. The T_m of F-actin was increased by 0.5 °C in the presence of saturating amounts of Drb-FL (Fig. 1*D*).

Lat-A assisted F-actin depolymerization experiments were repeated with the shorter drebrin construct, Drb1–300, and depolymerization was again observed from uncapped filaments and GC-filaments. Based on the determined depolymerization rates the inhibition of F-actin depolymerization by Drb1–300 was ~40%, and it was similar for the gelsolin-capped (GC) and non-capped filaments at the same Drb1–300 binding density (~90%) (Figs. 2 A&B). In addition, complete depolymerization of filaments was also inhibited in the presence of Drb1–300, as there was less actin found in the supernatant of F-actin solutions pelleted after overnight incubation with Lat-A at 4 °C (Fig. 2*C*).

We also performed depolymerization experiments in the presence of Drb-FL and Drb1–300 (5 and 11-fold excess over their K_d, respectively) using the standard dilution-induced method where F-actin is diluted below its Cc (80 nM). Both types of depolymerization assays (dilution-based and Lat-A assisted) yielded very similar results (data not shown). Overall, full-length drebrin showed a stronger F-actin stabilizing effect on uncapped filaments than the Drb1–300 construct at 90% binding density. The differences in the inhibition of depolymerization between Drb-FL and Drb1–300 were rather unexpected considering similar affinities of both constructs for F-actin (see "Discussion" for details).

In addition, equimolar amounts of Drb1–300 also increased the T_m of F-actin by 0.5 °C in DSC assays (Fig. 2*D*), which is consistent with the overall F-actin stabilization. The relatively small, but reproducible effect of drebrin on the melting temperature of F-actin can be attributed to the fact that Drb1–300 itself undergoes a thermal unfolding with a peak maximum at 59.7 °C, *i.e.* 10 °C below that of F-actin (data not shown). Considering the fact that there would be a small overlap between the Drb1–300 and F-actin melting peaks, it is possible that only

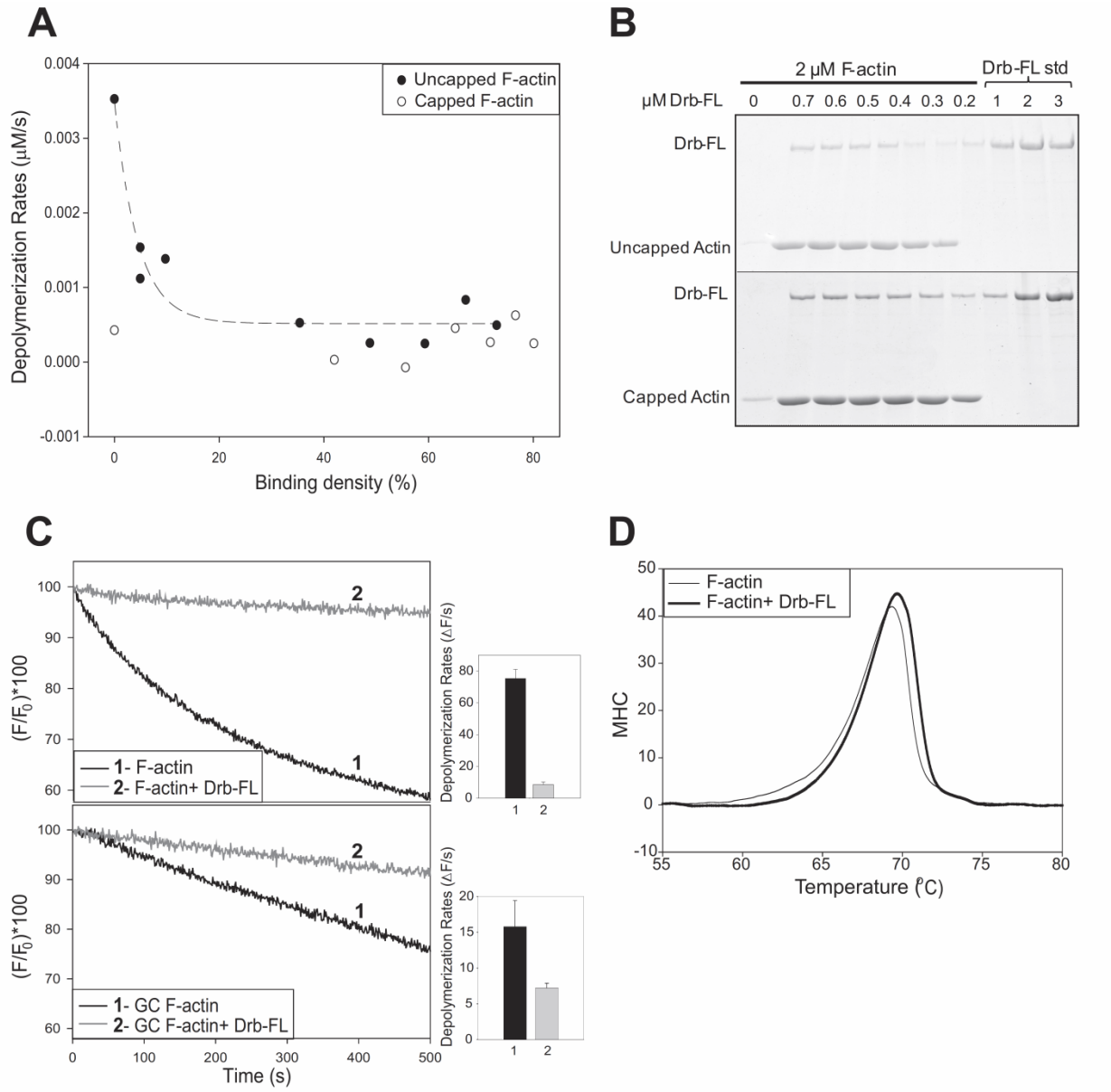

FIGURE 1. **Drebrin-A inhibits F-actin depolymerization and increases the thermal stability of F-actin.** *A*, 2 μM 5% pyrenyl-labeled skeletal F-actin was depolymerized in the presence of Lat-A (20 μM) and increasing concentrations of Drb-FL. Depolymerization rates (micromolar/second) of uncapped F-actin (●) and F-actin capped with 10 nM CAP-G (○) are shown plotted *versus* Drb-FL binding densities. *B*, SDS-PAGE patterns of high-speed centrifugation pellets of F-actin after its depolymerization (± Drb-FL). Pellets from samples containing uncapped filaments are shown in the *top panel*. Pellets obtained from samples containing filaments capped with 10 nM CAP-G are shown in the *bottom panel*. For detection purposes, the pellets were concentrated by resuspending them in a volume 2.5× smaller than the original one. Known concentrations of Drb-FL (*Drb-FL std*, 1, 2, and 3 μM) were loaded on the gels for quantification purposes. *C*, *top panel*, *graph*, 2 μM 5% pyrenyl-labeled skeletal F-actin was depolymerized in the presence of Lat-A (20 μM) only (*trace 1*) or with the additional presence of 0.8 μM Drb-FL (*trace 2*). The *bar plot* in the *right panel* shows the corresponding initial depolymerization rate of F-actin alone (*black bar*, *1*) or in the presence of 0.8 μM Drb-FL (*gray bar*, *2*). *Bottom panel*, *graph*, gelsolin-capped, 2 μM 5% pyrenyl-labeled skeletal F-actin depolymerized in the presence of Lat-A (20 μM) only (*trace 1*) or with Lat-A in the presence of 0.8 μM Drb-FL added (*trace 2*). The *bar plot* in the *right panel* shows the corresponding initial depolymerization rate of GC-F-actin alone (*black bar*) or in the presence of 0.8 μM Drb-FL (*gray bar*). The rates are the average of six separate measurements of the initial depolymerization over 60 s for all conditions. *D*, DSC scans showing molecular heat capacity (*MHC*) of 20 μM skeletal F-actin alone (*thin trace*) and in the presence of 4 μM drebrin A (*thick trace*). Similar results were reproduced over two independent experiments. Representative plots are shown.

a fraction of drebrin remains bound to the filaments under the conditions of our DSC experiments. Thus, it is likely that the stabilizing effect of drebrin is underestimated in this assay.

Effects of the Actin-binding Domain (DrbABD) of Drebrin on Longitudinal and Lateral Contacts in F-actin—Our previous study on the actin-binding domain of drebrin, DrbABD,

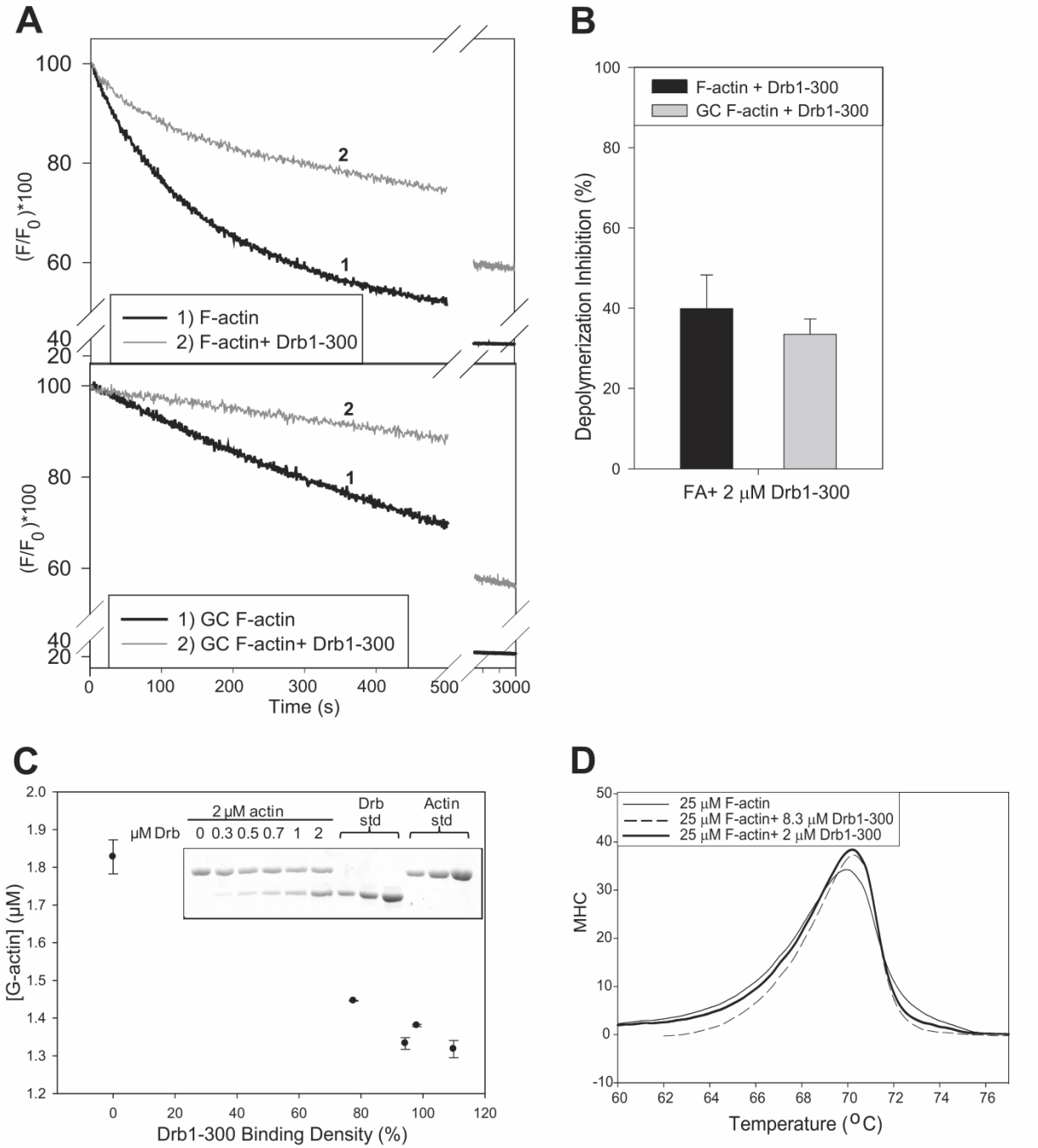

FIGURE 2. **Drb1–300 inhibits F-actin depolymerization from both barbed and pointed ends and increases the thermal stability of F-actin.** *A*, *top panel*, 2 μM 25% pyrenyl-labeled skeletal F-actin was depolymerized in the presence of Lat-A (20 μM) only (*trace 1*) or with LatA and 2 μM Drb1–300 (*trace 2*). *Bottom panel*, gelsolin-capped 2 μM 5% pyrenyl-labeled skeletal F-actin depolymerized in the presence of Lat-A (20 μM) only (*trace 1*) or with Lat-A and 2 μM Drb1–300 as well (*trace 2*). *B*, the *bar plot* shows the depolymerization inhibition percentage by 2 μM Drb1–300 on uncapped F-actin (*black bar*) and on GC-F-actin (*gray bar*). *C*, concentrations of G-actin *versus* Drb1–300 binding density after 2 μM F-actin was depolymerized by Lat-A (20 μM), alone or with different amounts of Drb1–300 present, overnight at 4 °C. The *inset* shows the SDS-PAGE patterns of the high-speed centrifugation supernatants of F-actin ± Drb-1–300. A Drb-1–300 and an actin standards (*Drb std* and *Actin std*) at three different concentrations (1, 2, and 4 μM for both) were loaded for quantification purposes. *D*, DSC scans of 25 μM skeletal F-actin alone (*thin trace*) and in the presence of 2 μM Drb1–300 (*thick trace*) and 8.3 μM Drb1–300 (*dashed trace*). Similar results were reproduced over two independent experiments. Representative plots are shown. *MHC*, molecular heat capacity.

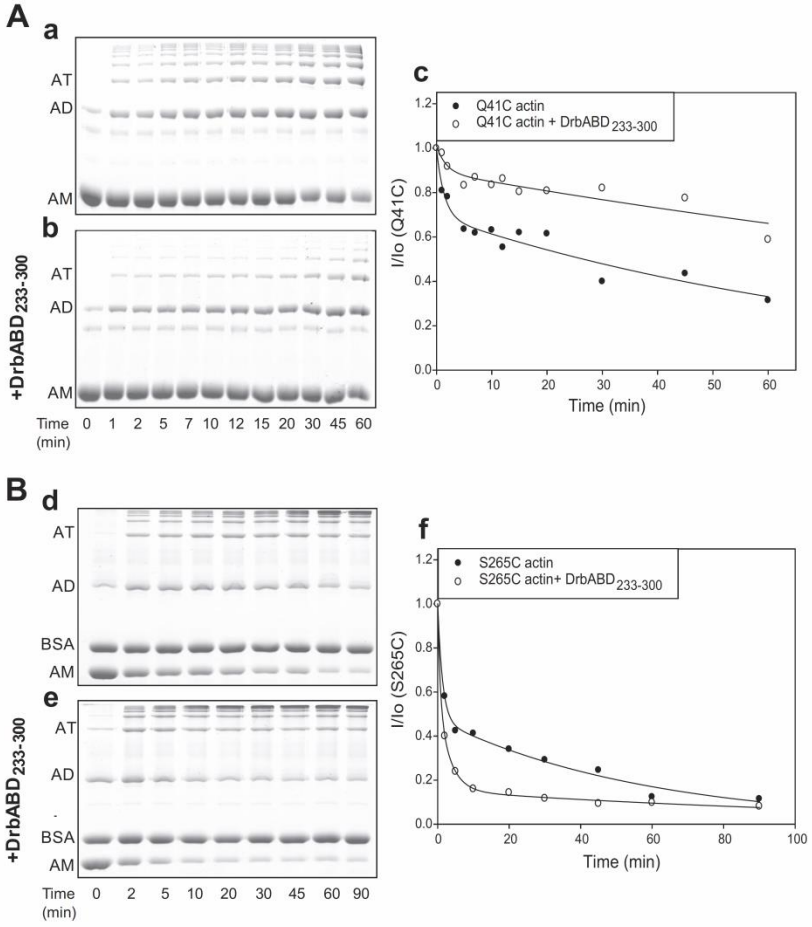

FIGURE 3. **Disulfide cross-linking of Q41C and S265C F-actin.** *A*, disulfide cross-linking of Q41C F-actin. Shown are SDS-PAGE patterns of F-actin (10 μM) cross-linked in the absence (*a*) and presence (*b*) of DrbABD$_{233-300}$. Lanes are for reaction aliquots taken after 0, 1, 2, 5, 7, 10, 12, 15, 20, 30, 45, and 60 min of the cross-linking reaction. *AM*, actin monomer; *AD*, disulfide cross-linked actin dimer; *AT*, disulfide cross-linked actin trimer. Reaction conditions were as described under "Experimental Procedures." *c*, plots of monomer actin band decay (I/I_0) on SDS-PAGE with time of the reaction. The data were taken from *a* for the reaction in the absence of DrbABD$_{233-300}$ (●) and from *b* for the reaction in the presence of DrbABD$_{233-300}$ (○). *B*, disulfide cross-linking of S265C F-actin. Shown are SDS-PAGE patterns of F-actin (10 μM) cross-linked in the absence (*d*) and presence (*e*) of DrbABD233–300. Lanes are for reaction aliquots taken after 0, 2, 5, 10, 20, 30, 45, 60, and 95 min of the cross-linking reaction. BSA was used as a loading control. Reaction conditions were as described under "Experimental Procedures." *f*, plots of monomer actin band decay on SDS-PAGE with time of the reaction in the absence of DrbABD$_{233-300}$ (●, from *d*) and in its presence (○, from *b*). The experiments were done in triplicate and yielded similar results. A representative plot of each actin mutant is shown.

revealed that it bridged two actin protomers and was the strongest actin-interacting module within the drebrin molecule (23), which was in good agreement with the reported *in vivo* data (30). The fact that DrbABD bridges two adjacent actin protomers calls for assessing its effect on interprotomer contacts and its contribution to overall F-actin stabilization. We showed that both drebrin constructs act as the actin binding domain, DrbABD (residues 233–317) and DrbABD$_{233-300}$ (residues 233–300), and have very similar binding affinities to F-actin (23). Conveniently, DrbABD$_{233-300}$ does not contain any endogenous cysteines, which makes it easier to assess its effect on interprotomer contacts in F-actin via actin cross-linking studies. Copper-catalyzed cross-linking has been used previously to examine the longitudinal and lateral interfaces in F-actin, employing the double cysteine actin mutants Q41C and S265C, respectively (31). In these actins, a cysteine is introduced at either residue 41 or 265 while retaining the endogenous cysteine 374. Here we used a similar approach and monitored the protomer-protomer cross-linking reactions in these mutant actin filaments via SDS-PAGE, where actin monomer depletion because of F-actin cross-linking was monitored. Different gel patterns were obtained in the presence and absence of DrbABD$_{233-300}$. DrbABD$_{233-300}$ slowed the longitudinal cross-linking between actin residues Q41C (D-loop) and Cys-374 (C terminus) (Fig. 3*A*), whereas it accelerated the lateral cross-linking between the residues Cys-265 (hydrophobic plug) and Cys-374 (Fig. 3*B*). The inhibition or acceleration of disulfide formation in the presence of drebrin could be due to the change in the mean distance between the residues on adjacent actin protomers in F-actin. In pyrene actin fluorescence assays, Drb-

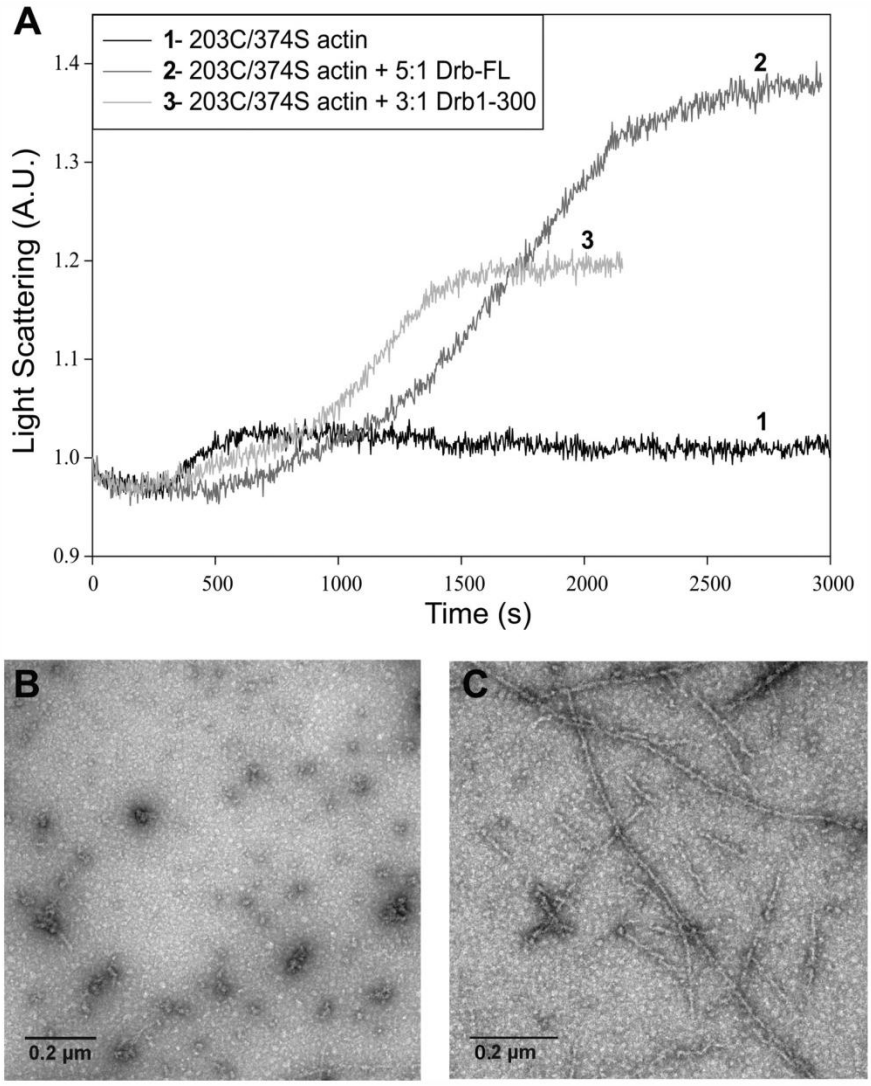

FIGURE 4. **Drb-FL and Drb1–300 rescue the polymerization of the T203C/C374A yeast actin mutant.** The experiments were done in triplicate with both drebrin constructs and yielded similar results. Representative plots are shown. *A*, light scattering results showing the polymerization of 10 μM actin with 3 mM $MgCl_2$ alone (*trace 1*) and in the presence of 2 μM Drb-FL (*trace 2*) or 3.3 μM Drb1–300 (*trace 3*). *A.U.*, arbitrary unit. *B*, EM image showing mainly aggregates of actin when polymerized on its own with 3 mM $MgCl_2$. *C*, EM image of actin filaments for the same actin polymerized with 3 mM $MgCl_2$ in the presence of 2 μM Drb-FL.

ABD showed an insignificant inhibition of depolymerization (~5% calculated at full saturation), suggesting that it does not stabilize actin filaments (data not shown).

Our results suggested that drebrin may stabilize the lateral interface in F-actin, which needed to be confirmed with the full-length protein and/or its "actin-interacting core," Drb1–300. To this end, we employed actins with perturbed lateral or longitudinal interfaces and monitored the effect of longer constructs (Drb-FL, Drb1–300, and Drb2–252) on the intra-protomer contacts in F-actin.

Effects of Drebrin on the Polymerization of Actin with an Impaired Ability to Form Longitudinal Contacts—Substituting Thr-203 to cysteine and Cys-374 to a serine (TC/CS-actin) in yeast actin inhibits its spontaneous filament formation upon salt addition (32). Similarly, cleaving skeletal actin with grimelysin (previously known as *E. coli* protease ECP) between residues 42 and 43 inhibits its polymerization (26, 33, 34). On the basis of the Fujii *et al.* model (35), these residues are part of the longitudinal interface in F-actin, and the (Thr-203) mutation inhibits actin polymerization, most likely by weakening longitudinal contacts among actin protomers. The polymerization activity of TC/CS actin can be restored by cofilin, which bridges two adjacent actin protomers by interacting with subdomain 1 (SD1) and SD3 on the "upper protomer" and SD2 on the lower one (36). To test whether drebrin could "correct for" a weakened longitudinal F-actin interface, TC/CS actin was polymerized in the presence of saturating amounts of Drb-FL or Drb1–300. Light scattering experiments show that, like cofilin (32), both constructs rescue the polymerization of this actin mutant (Fig. 4), although many rescued filaments are short. We con-

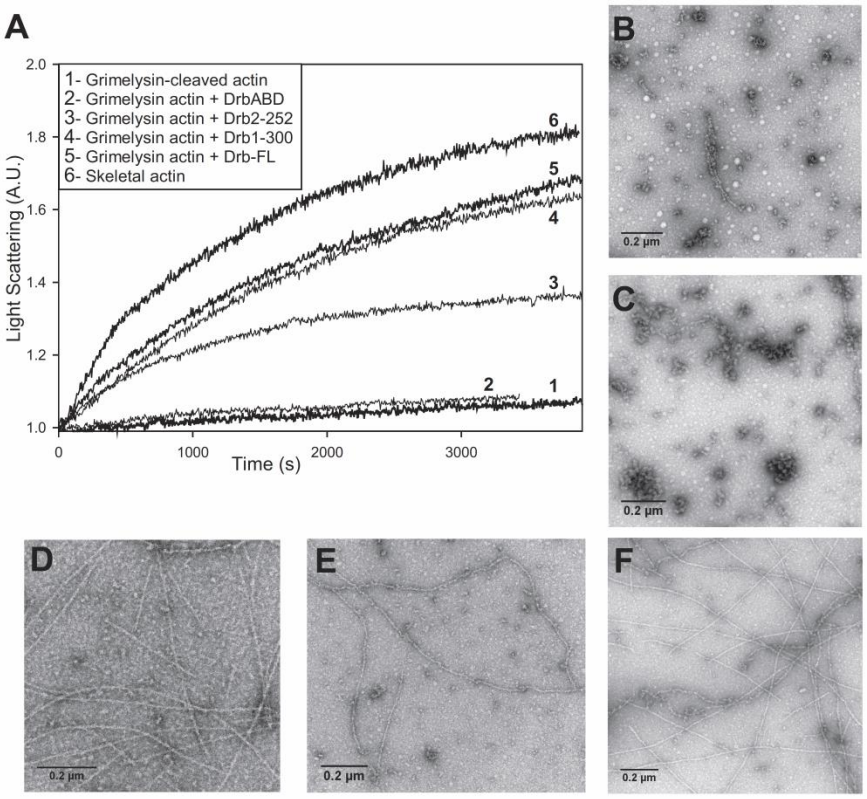

FIGURE 5. **Drb-FL, Drb1–300, and Drb2–252 rescue the polymerization of grimelysin-cleaved skeletal actin.** The experiments were done in triplicate with all drebrin constructs mentioned and yielded similar results. A representative plot is shown for each construct. *A*, light scattering results showing the polymerization of 5 μM cleaved Mg^{2+} actin with 2 mM $MgCl_2$ and 50 mM KCl alone (*trace 1*) and with the additional presence of 50 μM DrbABD (*trace 2*), 25 μM Drb2–252 (*trace 3*), 1.7 μM Drb1–300 (*trace 4*), and 1 μM Drb-FL (*trace 5*). Polymerization of 5 μM uncleaved skeletal actin is shown in *trace 6*. *A.U.*, arbitrary unit. *B*, EM image of aggregates of cleaved actin polymerized with 3 mM $MgCl_2$ only. *C*, EM image of actin polymerized in the presence of DrbABD. *D*, EM image of actin filaments obtained in the presence of Drb2–252. *E*, EM image of actin filaments formed in the presence of Drb1–300. *F*, EM image of actin filaments polymerized with 2 mM $MgCl_2$ and 50 mM KCl in the presence of 1 μM Drb-FL.

firmed the effect of drebrin on the longitudinal interface using grimelysin-cleaved skeletal actin. Again, the increase in light scattering signal suggested that addition of Drb-FL, Drb1–300, or Drb2–252 rescues the polymerization of grimelysin cleaved-actin, and EM images confirmed the formation of actin filaments (Fig. 5, *A–F*). However, the addition of DrbABD to the cleaved actin does not rescue its polymerization because there was no observed increase in light scattering, and actin filaments were not present in the EM images, which is consistent with our depolymerization results (Fig. 5, *A* and *C*).

Drb-FL and Drb1–300 Restore the Polymerization of the GG-Actin Mutant—The mutation of two actin residues, Val-266 and Leu-267, at the amino-terminal end of the hydrophobic loop, was shown previously to cause a polymerization defect in this yeast actin mutant, GG-actin (37). According to the model by Fujii *et al.* (35), the hydrophobic plug contacts four regions on the opposite strand, including amino acids 201–203 and 39–42 of one subunit and amino acids170–174 and 285–286 of an adjacent subunit. Mutating both Val-266 and Leu-267 to glycines reduces the hydrophobicity of the plug by two thirds and disrupts the contacts needed for actin polymerization (35). This mutant was used for prior tropomyosin studies and is a suitable tool for testing the effects of interacting factors on the lateral interface in F-actin (37). As shown in Fig. 6, the addition of salts to GG-actin causes a slight but steady increase in light scattering. EM shows that this change in signal is due to actin aggregation rather than its polymerization into stable filaments (Fig. 6*C*). Under the same conditions, the addition of saturating amounts of either Drb-FL or Drb1–300 induces a stable increase in light scattering, and the EM shows that this change in signal reflects actin filament formation (Fig. 6, *D–F*). EM images show that the addition of Drb1–300 induces the formation of long filaments, whereas Drb-FL samples show filaments along with some bundle and/or aggregate formation, which might be an artifact of the negative staining.

Previously documented rescue of GG-actin mutant polymerization by tropomyosin exhibited cold sensitivity because of the hydrophobic nature of the contacts (37). We observed a similar effect with drebrin. As shown in Fig. 6, *A* and *B*, GG-actin was polymerized in the presence of the Drb-FL, Drb1–300, or Drb2–252 construct until the light scattering signal reached a plateau, indicating a completion of the drebrin-induced GG-actin polymerization. The temperature was then lowered to 4 °C over a 30-min period. The light scattering of the sample decreased during that time, indicating actin depolymerization. EM images showed few small aggregates and some remaining

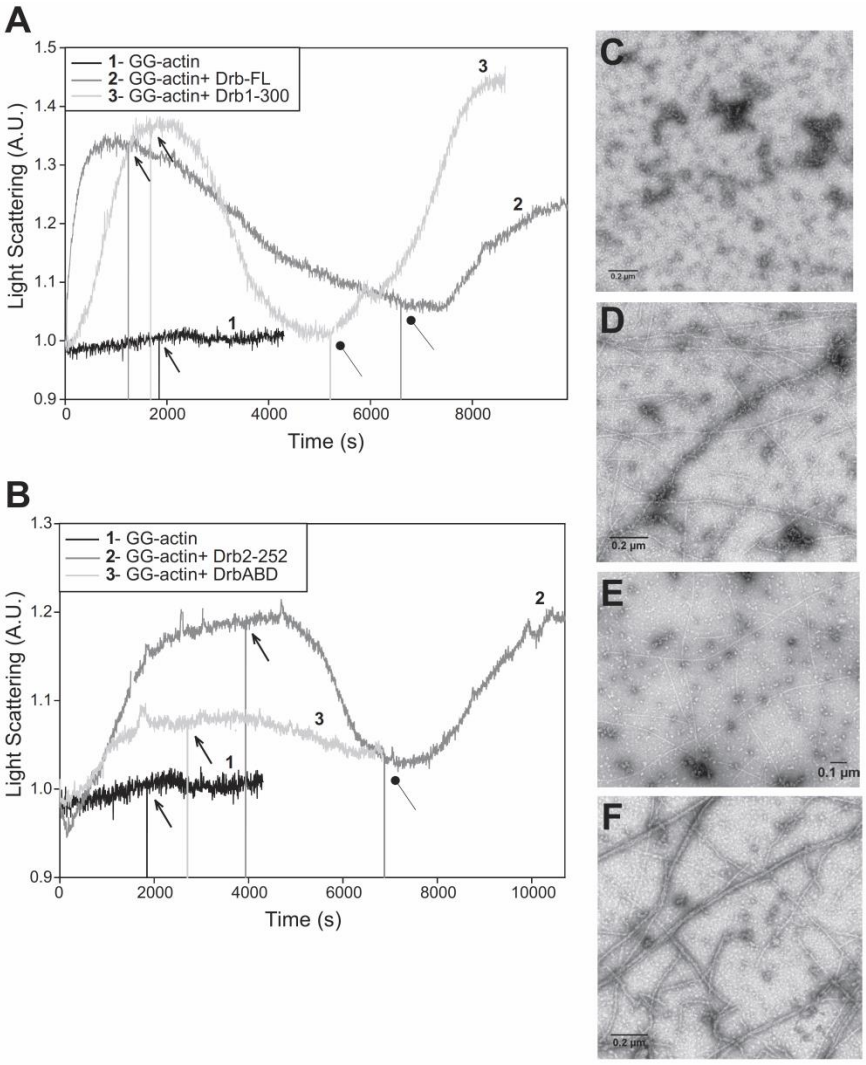

FIGURE 6. **Drb-FL, Drb1–300, and Drb2–252 restore the polymerization of the GG-yeast actin mutant.** The experiments with Drb-FL and Drb 1–300 were repeated six times. Those with Drb2–252 were repeated three times. These experiments were carried out with different GG-yeast actin mutant preparations yielding similar results. Representative plots are shown. *A*, for these experiments, 12 μM Mg-GG-actin was polymerized at 25 °C with 2 mM $MgCl_2$ and 50 mM KCl alone (*trace 1*), in the presence of 2.4 μM Drb-FL (*trace 2*), or in the presence of 4 μM Drb1–300 (*trace 3*). At the time points indicated by *arrows*, the temperature was lowered to 4 °C (*pointed arrows*), and the decrease in light scattering for each sample was recorded. The temperature was then raised back to 25 °C (● *arrows*), and the increase in light scattering for each sample was followed. *A.U.*, arbitrary unit. *B*, for these experiments, 12 μM Mg-GG-actin was polymerized at 25 °C with 2 mM $MgCl_2$ and 50 mM KCl alone (*trace 1*), in the presence of 60 μM Drb2–252 (*trace 2*), or in the presence of 120 μM DrbABD (*trace 3*). Shown are EM images of actin alone (*C*) and in the presence of Drb-FL (*D*), Drb1–300 (*E*), or Drb2–252 (*F*), respectively.

filaments in the sample (data not shown). A subsequent increase in temperature caused repolymerization of actin into filaments. The light scattering signal increased again (Fig. 6, *A* and *B*), and EM images confirmed the presence of actin filaments. The addition of DrbABD to GG-actin causes a small increase in light scattering, pointing to the formation of higher-order actin oligomers (Fig. 6*B*). These structures are, however, not temperature-sensitive because the signal remains almost unchanged, even after the sample is brought to 4 °C (Fig. 6*B*). We conclude that DrbABD does not restore the polymerization of GG-actin mutant, unlike the longer drebrin constructs.

DISCUSSION

Using depolymerization assays, DSC, and polymerization deficient actins as tools, we demonstrated that drebrin binding inhibits F-actin depolymerization and facilitates the assembly of polymerization-impaired actin by stabilizing both lateral and longitudinal contacts in filaments. We also clarified the domain requirements for the observed effects.

Drebrin Inhibits Depolymerization of Actin Filaments from B-ends Stronger Than from P-ends—Drb-FL causes an ~90% decrease in the depolymerization rates of uncapped filaments, in which B-end depolymerization predominates. This points to a strong barbed end protection by Drb-FL because the B-end is

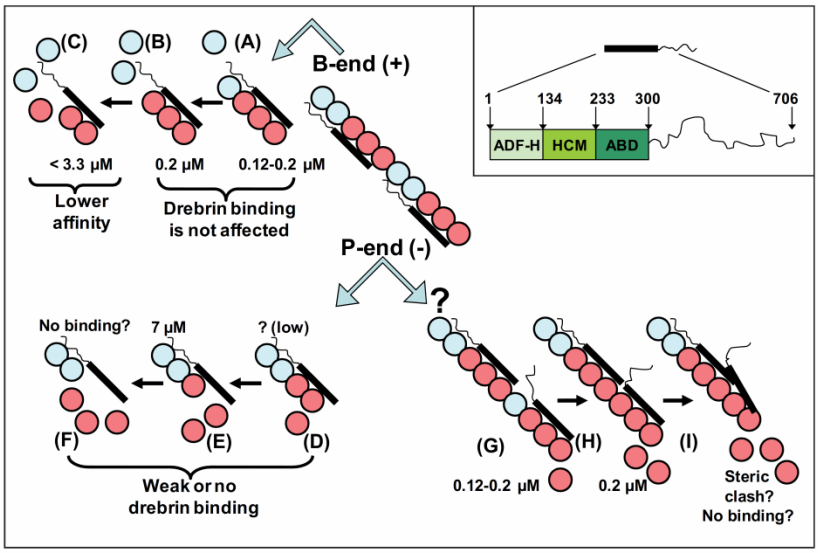

FIGURE 7. **Effect of drebrin on B-end and P-end actin depolymerization.** *Center*, schematic representation of an actin filament in complex with full-length drebrin. Individual actin protomers are represented by *spheres*. Protomers proposed to interact with the actin-binding core of drebrin (seq. 1–300) are shown in *red*. Protomers bound/protected by the C-terminal part of drebrin molecule are colored in *light blue*. For simplicity, only one strand is shown in *A–I*. On the basis of the presented results and the available interface mapping data, drebrin is proposed to bind to the filament with its C-terminal sequence oriented toward the B-end. *A–C* represent the scenario of B-end depolymerization and the subsequent effect on drebrin binding. *D–F* depict the scenario of P-end depolymerization and the subsequent effect on drebrin binding. *G–I* represent another P-end depolymerization possibility when drebrin-binding sites partially overlap on F-actin. See details in text ("Discussion"). A schematic representation of the drebrin molecule is shown in the *inset*. The ADF-H, helical charged motif, and ABD of drebrin (DrbABD) are represented by *rectangles*. The C-terminal part of the molecule (predicted to be unstructured) is represented by a *curvy line*. Numbers correspond to the K_ds for different constructs determined in cosedimentation experiments: Drb-FL, 0.12 μM; Drb1–300, 0.2 μM; Drb2–252, ~3.3 μM; DrbABD, ~7 μM (18, 23).

the faster depolymerizing end of the filament. Using gelsolin-capped filaments, we were able to estimate the effect of drebrin on pointed end depolymerization. Saturating concentrations of Drb-FL and Drb1–300 caused an ~50 and ~40% decrease in the depolymerization rate of GC filaments, respectively. This observation implies a lower affinity of drebrin to the P-ends compared with the B-ends.

Drb1–300 caused a similar ~40% decrease in depolymerization rates of both capped and uncapped filaments. The Drb1–300 construct showed a weaker inhibition of uncapped filament depolymerization than Drb-FL despite the fact that their affinities for F-actin are similar (K_d = 0.2 and 0.12 μM, respectively, for Drb1–300 and Drb-FL). The simplest explanation would be that the weakly interacting C-terminal part of Drb-FL reduces the protomer off rate at the B-end, further contributing to the overall inhibition of actin depolymerization (Fig. 7, *A–C*).

As shown in Fig. 7 (*top right corner*), the drebrin molecule consists of an ADF-H domain, a helical/charged motif, an actin binding domain (DrbABD), and an intrinsically disordered C-terminal part. Structural information available on F-actin-ADF/cofilin interactions (38–40), together with drebrin-actin interface mapping results (23), suggest that the C-terminal part of drebrin may be oriented toward the B-end of the filament (as shown in Fig. 7). Because the actin binding "core" of drebrin is localized within the N-terminal part of the molecule, we speculate that the dissociation of the actin monomers will shorten the lifespan of the drebrin·F-actin complex more drastically at the P-end than at the B-end (Fig. 7, *D–F, versus A–C*). Several possible scenarios can explain the lower affinity of Drb-FL to the P-end of filaments (Fig. 7).

1) Assuming that drebrin binding sites on F-actin do not overlap, five actin protomers are required for the binding of one Drb-FL molecule (Fig. 7, *F–D*). This would imply that, because of a steric clash, Drb-FL is not able to rebind with high affinity to a shorter filament stretch (less than five protomers) after its dissociation from the filament. In such a case, the dissociation of the first terminal actin protomer (of five) at the P-end of the Drb-FL binding site impairs the binding sites for ADF-H, which is critical for filament binding (on the basis of the data reported for N-terminal truncations of homologous Abp1 (41)). Dissociation of a second subunit from the P-end will only allow for the binding of DrbABD, which did not inhibit depolymerization in our assays. Loss of another protomer at the P-end will abolish drebrin binding, allowing for the F-actin depolymerization step with the rate characteristic of the uncomplexed F-actin.

2) Assuming that Drb-FL is able to interact with filament segments shorter than five protomers, unless precluded by a steric clash, the scenario shown in Fig. 7, *G* and *H*, is feasible. Because saturating amounts of Drb-FL and Drb1–300 show similar levels of P-end protection (Figs. 1*C*, *lower panel, bar plot*, and 2*B*), it is possible that the intrinsically disordered C-terminal region does not clash with the neighboring drebrin molecule when its 1–300 region is interacting with the last three to four protomers (of five forming the Drb-FL binding site) at the P-end (Fig. 7). Upon dissociation of the first and second actin protomers from the P-end, Drb-FL might be able to rebind to the remaining three- or four-protomer stretch with its C-terminal region pushed aside. However, it is expected that drebrin will be unable to interact with the two remaining actin

protomers (of five protomers) at the P-end because of a steric clash with the N-terminal part of a neighboring drebrin molecule (Fig. 7*I*) and will dissociate from the P-end.

According to the scheme proposed in Fig. 7, *A–C*, no steric clash occurs at the B-end because of the arrangement of drebrin molecules. Dissociation of the first three actin protomers will still allow for a weak binding of the ADF-H of drebrin and its helical/charged motif to the B-end and the inhibition of depolymerization.

It should be noted that the scenarios proposed above do not take into account the "on" and "off" rates of the interaction of drebrin with actin filaments (yet to be determined). The simplified scheme in Fig. 7 presents a case in which the five-promoter actin stretch adjacent to the terminal drebrin binding site at the ends is always occupied by another drebrin molecule. However, this will only be true in case of very slow Drb-FL off rates from actin filaments. If drebrin off rates are fast, the binding modes proposed in scenarios 1 and 2, and at the B-end, will alternate with high affinity drebrin binding modes, because of the dissociation of the neighboring drebrin molecule, which in turn will cause transient availability of longer undecorated F-actin stretches at the filament ends.

In light of the differences in drebrin stabilization effects on P- and B-ends, we considered several factors that contribute such differences. 1) A reduced affinity of Drb-FL for P-ends could also be due to a difference in its affinity for ADP+P_i *versus* ADP-actin. However, our unpublished results indicate that drebrin does not have a preference for a specific nucleotide state of filament (Grintsevich EE *at al.*, to be published elsewhere), excluding this possibility. 2) Facilitated cofilin binding to GC-filaments suggests that gelsolin alters the morphology of F-actin in a cooperative manner (42). It is possible that gelsolin-induced allosteric changes can lead to a weaker binding of drebrin to GC-F-actin. Co-sedimentation of Drb-FL with gelsolin-capped and uncapped actin filaments showed no differences in drebrin binding. Measurements of drebrin binding kinetics to GC-F-actin will be needed to rule out the less likely possibility that both "on" and "off" rates of drebrin interaction with GC-actin filaments are changed.

At a cellular level, a different affinity of drebrin for the two filament ends will translate into the P-end of drebrin-decorated-F-actin being available to interact with P-end capping proteins. For example, tropomodulins (Tmods) regulate the dynamics of the slow-growing pointed end of the actin filament and require tropomyosins (TM) for optimal function as TMs greatly enhance Tmods pointed-end capping activity (43, 44). However, drebrin binding to actin filaments may interfere with the subsequent binding and effect of B-end cappers and/or elongation factors. In line with this possibility, a potential cross-talk between neuronal B-end capper Eps8 and drebrin E was reported recently (45). Moreover, our findings are consistent with an earlier report (46) showing that drebrin-expressing fibroblasts were resistant to cytochalasin D, which causes depolymerization of actin filaments trough B-end capping and monomer sequestration. Inhibition of depolymerization could be a mechanism used by drebrin to protect actin filaments and, thereby, the size and morphology of dendritic spines.

The effect of Drebrin on Longitudinal Contacts in F-actin and Domain Requirements—Drb-FL and its actin-binding core, Drb1–300, both rescue the polymerization of the TC/CS yeast actin mutant (impaired polymerization because of the mutation in the SD4 of actin), as observed by light scattering and EM. A similar effect was observed with grimelysin-cleaved actin. Drb FL, Drb1–300, and Drb2–252 all induced the formation of actin filaments (Fig. 5, *A* and *D--F*). However, the strongest actin interacting unit of the drebrin molecule, DrbABD, failed to rescue, on its own, the polymerization of grimelysin-cleaved actin (Fig. 5, *A* and *C*). These results are in line with the Cu^{2+} catalyzed cross-linking of the yeast actin mutant Q41C, in which we observed an inhibition of cross-linking between residues 41 (in SD2) and the native Cys-374 on F-actin in the presence of $DrbABD_{233–300}$. The inhibition of disulfide formation by $DrbABD_{233–300}$ suggests an increase in the mean distance between Cys-374 and the DNase I binding loop on adjacent actin protomers in F-actin. It is tempting to speculate that the observed inhibition of Cys-41-Cys-374 cross-linking by $DrbABD_{233–300}$, together with its inability to rescue the polymerization of actins with a perturbed longitudinal interface, can be explained by DrbABD-induced "under-twisting" of F-actin (the helical pitch is 40 nm *versus* 36 nm in bare actin (18)). It is possible that this "stretched" conformation is stabilized by binding of N-terminal drebrin domains (ADF-H and predicted coil-coiled region, seq. 2–252) to the filament. However, it is also possible that the inhibition of cross-linking by $DrbABD_{233–300}$ may be caused by steric hindrance because of the proposed binding to subdomain 2 of actin of DrbABD (23).

The Effect of Drebrin on Lateral Contacts in F-actin and Domain Requirements—An increase in the cross-linking rate between Cys-265 and Cys-374 in the presence of $DrbABD_{233–300}$ suggested its stabilization of interstrand contacts in F-actin. We employed the GG-yeast actin mutant to test this possibility. This particular mutant has two hydrophobic residues, Val-266 and Leu-267, substituted to glycines and a high critical concentration > 20 μM (37). Similar to the effect of drebrin on the longitudinal interface of F-actin, the N-terminal constructs Drb1–300 and Drb2–252, and full-length protein rescued the polymerization of GG-actin. DrbABD alone was not sufficient to rescue actin polymerization (Fig. 6).

The observed filament stabilization would be consistent with drebrin binding in the area of interstrand contacts and restoring the impaired interface and/or compensating for the missing contacts by binding to several protomers. According to the mapping reported previously (23), DrbABD is centered on SD2 of actin and makes an interstrand contact only in a minor binding mode. Together with its inability to protect actin filaments from depolymerization and rescue the polymerization of GG-actin, this suggests that the enhanced cross-linking in the presence of $DrbABD_{233–300}$ most likely reports on its allosteric effect on the lateral interface in F-actin. Taking into account the reported data on ADF/cofilin interactions with actin filaments, the N-terminal ADF-H domain of drebrin is an unlikely candidate for direct stabilization of the lateral interface (36). Moreover, control experiments performed with the GG-mutant in the presence of yeast cofilin showed no rescue of its polymerization (data not shown). This leaves the helical/charged region

(amino acids134–233) of drebrin as a possible candidate for direct stabilization of the lateral interface of actin. Our hypothesis is that the drebrin molecule wraps around the filament, "stapling" two protofilaments by its helical/charged motif. High-resolution EM reconstruction and detailed interface mapping is needed to confirm or rule out this hypothesis. It should be noted that the time scales of GG-actin polymerization rescue by drebrin are similar to those reported previously for several tropomyosins (37). In the case of TMs, it was shown that the rescue efficiency is proportional to the number of quasirepeats in the TM molecule. As shown in Fig. 6, we observed a similar effect with Drb-FL addition (5:1 stoichiometry), yielding faster polymerization kinetics than Drb1–300 (3:1 stoichiometry) or Drb2–252 (2:1 stoichiometry).

Lowering the temperature of GG-actin filaments to 4 °C in the presence of drebrin constructs caused their partial depolymerization but not as complete as reported previously for TM. Lack of complete GG-actin depolymerization at 4 °C in the presence of drebrin indicates that its overall stabilization effect (taking into consideration the additional stabilizing effects on the longitudinal contacts of F-actin reported earlier) is stronger than that of TMs tested in the same system. Repolymerization of GG-actin in the presence of drebrin was not detected below 20 °C, indicating a similar temperature sensitivity to tropomyosins in stabilization of the lateral interface of actin.

Our combined results provide evidence for filament stabilization of actin by drebrin and analyze its structural basis. These results point to the likely role and mode of action of drebrin in preserving the integrity of F-actin structures in dendritic spines. In conclusion, drebrin inhibits F-actin depolymerization from both B- and P-ends. The P-end of actin is protected by drebrin to a lesser degree than the B-end. Results obtained with the Drb-FL and Drb 1–300 constructs suggest that the intrinsically disordered C-terminal part of the drebrin molecule is responsible for the stronger inhibition of B-end than P-end depolymerization (Figs. 1*C* and 2*B*). Despite being the strongest binding module within the drebrin molecule, DrbABD alone does not rescue the polymerization of actins with an impaired ability to form an interface between protomers.

Acknowledgments—We thank Dr. Peter Rubenstein for the yeast cell line-expressing actin mutant V266G/L267G. We also thank Dr. M. Quinlan for the heterodimeric capping protein, Dr. S. Khaitlina for grimelysin, and the Electron Imaging Center for NanoMachines at the California NanoSystems Institute, University of California Los Angeles, for the use of instruments (supported in part by National Institutes of Health Grant 1S10RR23057).

REFERENCES

1. Sekino, Y., Kojima, N., and Shirao, T. (2007) Role of actin cytoskeleton in dendritic spine morphogenesis. *Neurochem. Int.* **51,** 92–104
2. Hering, H., and Sheng, M. (2001) Dendritic spines. Structure, dynamics and regulation. *Nat. Rev. Neurosci.* **2,** 880–888
3. Moser, M. B., Trommald, M., and Andersen, P. (1994) An increase in dendritic spine density on hippocampal CA1 pyramidal cells following spatial learning in adult rats suggests the formation of new synapses. *Proc. Natl. Acad. Sci. U.S.A.* **91,** 12673–12675
4. Purpura, D. P. (1974) Dendritic spine "dysgenesis" and mental retardation. *Science* **186,** 1126–1128
5. Irwin, S. A., Galvez, R., and Greenough, W. T. (2000) Dendritic spine structural anomalies in fragile-x mental retardation syndrome. *Cereb. Cortex.* **10,** 1038–1044
6. Wisniewski, K. E., Segan, S. M., Miezejeski, C. M., Sersen, E. A., and Rudelli, R. D. (1991) The fra(X) syndrome. Neurological, electrophysiological, and neuropathological abnormalities. *Am. J. Med. Genet.* **38,** 476–480
7. Capani, F., Ellisman, M. H., and Martone, M. E. (2001) Filamentous actin is concentrated in specific subpopulations of neuronal and glial structures in rat central nervous system. *Brain Res.* **923,** 1–11
8. Fifková, E., and Delay, R. J. (1982) Cytoplasmic actin in neuronal processes as a possible mediator of synaptic plasticity. *J. Cell Biol.* **95,** 345–350
9. Matus, A., Ackermann, M., Pehling, G., Byers, H. R., and Fujiwara, K. (1982) High actin concentrations in brain dendritic spines and postsynaptic densities. *Proc. Natl. Acad. Sci. U.S.A.* **79,** 7590–7594
10. Matus, A. (2000) Actin-based plasticity in dendritic spines. *Science* **290,** 754–758
11. Takahashi, H., Sekino, Y., Tanaka, S., Mizui, T., Kishi, S., and Shirao, T. (2003) Drebrin-dependent actin clustering in dendritic filopodia governs synaptic targeting of postsynaptic density-95 and dendritic spine morphogenesis. *J. Neurosci.* **23,** 6586–6595
12. Aoki, C., Sekino, Y., Hanamura, K., Fujisawa, S., Mahadomrongkul, V., Ren, Y., and Shirao, T. (2005) Drebrin A is a postsynaptic protein that localizes *in vivo* to the submembranous surface of dendritic sites forming excitatory synapses. *J. Comp. Neurol.* **483,** 383–402
13. Hayashi, K., Ishikawa, R., Ye, L. H., He, X. L., Takata, K., Kohama, K., and Shirao, T. (1996) Modulatory role of drebrin on the cytoskeleton within dendritic spines in the rat cerebral cortex. *J. Neurosci.* **16,** 7161–7170
14. Kojima, N., and Shirao, T. (2007) Synaptic dysfunction and disruption of postsynaptic drebrin-actin complex. A study of neurological disorders accompanied by cognitive deficits. *Neurosci. Res.* **58,** 1–5
15. Shim, K. S., and Lubec, G. (2002) Drebrin, a dendritic spine protein, is manifold decreased in brains of patients with Alzheimer's disease and Down syndrome. *Neurosci. Lett.* **324,** 209–212
16. Weitzdoerfer, R., Dierssen, M., Fountoulakis, M., and Lubec, G. (2001) Fetal life in Down syndrome starts with normal neuronal density but impaired dendritic spines and synaptosomal structure. *J. Neural. Transm. Suppl.* **61,** 59–70
17. Ishikawa, R., Hayashi, K., Shirao, T., Xue, Y., Takagi, T., Sasaki, Y., and Kohama, K. (1994) Drebrin, a development-associated brain protein from rat embryo, causes the dissociation of tropomyosin from actin filaments. *J. Biol. Chem.* **269,** 29928–29933
18. Sharma, S., Grintsevich, E. E., Phillips, M. L., Reisler, E., and Gimzewski, J. K. (2011) Atomic force microscopy reveals drebrin induced remodeling of F-actin with subnanometer resolution. *Nano Lett.* **11,** 825–827
19. Ishikawa, R., Katoh, K., Takahashi, A., Xie, C., Oseki, K., Watanabe, M., Igarashi, M., Nakamura, A., and Kohama, K. (2007) Drebrin attenuates the interaction between actin and myosin-V. *Biochem. Biophys. Res. Commun.* **359,** 398–401
20. Sasaki, Y., Hayashi, K., Shirao, T., Ishikawa, R., and Kohama, K. (1996) Inhibition by drebrin of the actin-bundling activity of brain fascin, a protein localized in filopodia of growth cones. *J. Neurochem.* **66,** 980–988
21. Kojima, N., Shirao, T., and Obata, K. (1993) Molecular cloning of a developmentally regulated brain protein, chicken drebrin A and its expression by alternative splicing of the drebrin gene. *Brain Res. Mol. Brain Res.* **19,** 101–114
22. Shirao, T., and Obata, K. (1986) Immunochemical homology of 3 developmentally regulated brain proteins and their developmental change in neuronal distribution. *Brain Res.* **394,** 233–244
23. Grintsevich, E. E., Galkin, V. E., Orlova, A., Ytterberg, A. J., Mikati, M. M., Kudryashov, D. S., Loo, J. A., Egelman, E. H., and Reisler, E. (2010) Mapping of drebrin binding site on F-actin. *J. Mol. Biol.* **398,** 542–554
24. Spudich, J. A., and Watt, S. (1971) The regulation of rabbit skeletal muscle contraction. I. biochemical studies of the interaction of the tropomyosin-troponin complex with actin and the proteolytic fragments of myosin. *J. Biol. Chem.* **246,** 4866–4871
25. Kim, E., Wriggers, W., Phillips, M., Kokabi, K., Rubenstein, P. A., and Reisler, E. (2000) Cross-linking constraints on F-actin structure. *J. Mol.*

Biol. **299,** 421–429
26. Pivovarova, A. V., Khaitlina, S. Y., and Levitsky, D. I. (2010) Specific cleavage of the DNase-I binding loop dramatically decreases the thermal stability of actin. *FEBS J.* **277,** 3812–3822
27. Kurokawa, H., Fujii, W., Ohmi, K., Sakurai, T., and Nonomura, Y. (1990) Simple and rapid purification of brevin. *Biochem. Biophys. Res. Commun.* **168,** 451–457
28. Kuhn, J. R., and Pollard, T. D. (2005) Real-time measurements of actin filament polymerization by total internal reflection fluorescence microscopy. *Biophys. J.* **88,** 1387–1402
29. Pollard, T. D. (1986) Rate constants for the reactions of ATP- and ADP-actin with the ends of actin filaments. *J. Cell Biol.* **103,** 2747–2754
30. Hayashi, K., Ishikawa, R., Kawai-Hirai, R., Takagi, T., Taketomi, A., and Shirao, T. (1999) Domain analysis of the actin-binding and actin-remodeling activities of drebrin. *Exp. Cell Res.* **253,** 673–680
31. Bobkov, A. A., Muhlrad, A., Kokabi, K., Vorobiev, S., Almo, S. C., and Reisler, E. (2002) Structural effects of cofilin on longitudinal contacts in F-actin. *J. Mol. Biol.* **323,** 739–750
32. Kudryashov, D. S., Galkin, V. E., Orlova, A., Phan, M., Egelman, E. H., and Reisler, E. (2006) Cofilin cross-bridges adjacent actin protomers and replaces part of the longitudinal F-actin interface. *J. Mol. Biol.* **358,** 785–797
33. Bozhokina, E., Khaitlina, S., and Adam, T. (2008) Grimelysin, a novel metalloprotease from *Serratia grimesii*, is similar to ECP32. *Biochem. Biophys. Res. Commun.* **367,** 888–892
34. Klenchin, V. A., Khaitlina, S. Y., and Rayment, I. (2006) Crystal structure of polymerization-competent actin. *J. Mol. Biol.* **362,** 140–150
35. Fujii, T., Iwane, A. H., Yanagida, T., and Namba, K. (2010) Direct visualization of secondary structures of F-actin by electron cryomicroscopy. *Nature* **467,** 724–728
36. Galkin, V. E., Orlova, A., Lukoyanova, N., Wriggers, W., and Egelman, E. H. (2001) Actin depolymerizing factor stabilizes an existing state of F-Actin and can change the tilt of F-Actin subunits. *J. Cell Biol.* **153,** 75–86
37. Wen, K. K., Kuang, B., and Rubenstein, P. A. (2000) Tropomyosin-dependent filament formation by a polymerization-defective mutant yeast actin (V266G,L267G). *J. Biol. Chem.* **275,** 40594–40600
38. Galkin, V. E., Orlova, A., Kudryashov, D. S., Solodukhin, A., Reisler, E., Schröder, G. F., and Egelman, E. H. (2011) Remodeling of actin filaments by ADF/cofilin proteins. *Proc. Natl. Acad. Sci. U.S.A.* **108,** 20568–20572
39. Paavilainen, V. O., Oksanen, E., Goldman, A., and Lappalainen, P. (2008) Structure of the actin-depolymerizing factor homology domain in complex with actin. *J. Cell Biol.* **182,** 51–59
40. Grintsevich, E. E., Benchaar, S. A., Warshaviak, D., Boontheung, P., Halgand, F., Whitelegge, J. P., Faull, K. F., Loo, R. R., Sept, D., Loo, J. A., and Reisler, E. (2008) Mapping the cofilin binding site on yeast G-actin by chemical cross-linking. *J. Mol. Biol.* **377,** 395–409
41. Quintero-Monzon, O., Rodal, A. A., Strokopytov, B., Almo, S. C., and Goode, B. L. (2005) Structural and functional dissection of the Abp1 ADFH actin-binding domain reveals versatile *in vivo* adapter functions. *Mol. Biol. Cell* **16,** 3128–3139
42. Ressad, F., Didry, D., Xia, G. X., Hong, Y., Chua, N. H., Pantaloni, D., and Carlier, M. F. (1998) Kinetic analysis of the interaction of actin-depolymerizing factor (ADF)/cofilin with G- and F-actins. *J. Biol. Chem.* **273,** 20894–20902
43. Kostyukova, A. S. (2008) Tropomodulin/tropomyosin interactions regulate actin pointed end dynamics. *Adv. Exp. Med. Biol.* **644,** 283–292
44. Yamashiro, S., Gokhin, D. S., Kimura, S., Nowak, R. B., and Fowler, V. M. (2012) Tropomodulins: Pointed-end capping proteins that regulate actin filament architecture in diverse cell types. *Cytoskeleton (Hoboken)* **6,** 337–370
45. Cheng, C. Y., Lie, P. P., Wong, E. W., Mruk, D. D., and Silvestrini, B. (2011) Adjudin disrupts spermatogenesis via the action of some unlikely partners. Eps8, Arp2/3 complex, drebrin E, PAR6 and 14GÇô3-3. *Spermatogenesis* **1,** 291–297
46. Ikeda, K., Kaub, P. A., Asada, H., Uyemura, K., Toya, S., and Shirao, T. (1996) Stabilization of adhesion plaques by the expression of drebrin A in fibroblasts. *Brain Res. Dev. Brain Res.* **91,** 227–236

CHAPTER 4

The Effects of Coronin on the Structure and Dynamics of Actin Filaments.

INTRODUCTION

Coronin is one of the conserved actin-binding proteins and its different isoforms have been identified in many eukaryotic organisms including yeast, fish and mammals **(1, 2, 3)**. Functional studies in these organisms have shown coronins to be important regulators of actin based processes such as cytokinesis, cell migration and lamellopodia formation. *S.Cerevisiae'*s coronin, along with other coronins of the Type I class, has a structure that consists of three domains. The defining feature of this structure is the presence of a β-propeller domain containing 7 WD40 repeats at the N-terminal part of the protein, generally believed to be a scaffold to support protein–protein interaction. A highly variable "unique region" in the middle segment links the β-propeller to a coiled coil (CC) structure at the C-terminal segment of coronin.

Coronin's mode of influencing actin dynamics in the cell is not well understood yet, but its involvement in the rearrangement of the actin cytoskeleton is substantial and physiologically important. Type I coronins interact with and inhibit the Arp2/3 complex—which nucleates the formation of new branches of actin filaments off the sides of existing ones, at an angle of ~70° to the original filament **(1, 4, 5).** Another study showed that yeast coronin not only inhibits but can also activate Arp2/3 nucleating activity. These dual modes of regulation by Crn1 showed a concentration-dependent switch between activating Arp2/3 nucleating activity —by enhancing its filament binding at low coronin concentrations, and inhibiting the nucleation— by blocking its binding at higher coronin concentrations **(6)**. The activation function relies on a sequence called CA located in the "unique region" of Crn1. This sequence is conserved in WASp/Scar proteins (the prototypical activators of Arp2/3 complex) and point mutations in it abolished the activation of Arp2/3 complex by Crn1 in vitro.

There is also clear evidence for coronin's conserved function in regulating cofilin-dependent actin disassembly. The deletion of the yeast coronin gene, Crn1 does not produce aberrant defects in the cells; however, when the null-mutation is combined with another mutation that slows the actin turnover rate in the cell, like the example of *cof1-22*, it enhances the defective phenotype **(7).** Originally, contradicting regulatory effects of coronin on cofilin had been proposed **(4, 8, 9)**. This paradox was later addressed by Ghandi *et al.*, **(10)** who showed that the full length coronin (Crn1, Figure 4.1) synergizes with cofilin in the severing of ADP-F-actin (older filaments), but it antagonizes cofilin's severing of ATP/ADP+Pi-F-actins (newly formed filaments). Coronin and cofilin's cooperation in actin disassembly is therefore conditional and depends on the nucleotide state of actin, facilitating the disassembly of older filaments and inhibiting the disassembly of the newly formed ones. Furthermore, filaments were shorter in the presence of Crn1 alone, suggesting that it may sever ADP-F-actin filaments independently of cofilin. The same study showed that the C-terminal truncated construct lacking the CC domain (CrnΔCC, a.a.1-600, Figure 4.1) also increases cofilin's severing activity.

Figure 4.1- Schematic representation of coronin and coroninΔCC.
A- Full length coronin- Crn1.
B- The C-terminal truncated construct lacking the coiled-coil domain- CrnΔCC (a.a.1-600).

Actin interacting protein 1 (AIP1) was identified as a major co-factor that collaborates with cofilin to disassemble F-actin. AIP1 can bind to the cofilin–F-actin complex and strongly enhance the severing activity of cofilin on actin filaments by capping the barbed ends of the severed filaments, resulting in acceleration of actin depolymerization **(11)**. Evidence from microscopy indicates that AIP1 can actively disassemble cofilin-bound actin filaments **(11)**. Interestingly, the addition of AIP1 in a mixture of full length coronin, cofilin and F-actin increased the severing activity of cofilin the same way that CrnΔCC did (personal communication, unpublished results, Goode et al.). We can speculate that AIP1 blocks the inhibitory effect of Crn1's coiled-coil domain (perhaps by binding to it) and activates its synergistic role in the cofilin-mediated severing. In addition, class-average images of filament segments of actin filaments decorated with either full length coronin or CrnΔCC were indistinguishable by two-dimensional classification-averaging analysis **(12)**. Taken together, these results strengthen the significance of observations on the mechanism of CrnΔCC action on actin filaments, shedding light on the role of the full length protein.

Examining the direct effect of CrnΔCC on the structure and dynamics of actin filaments will allow for a basic understanding of the mechanisms by which coronin regulates the different actin-based processes in a cell, both independently and also in concert with other actin binding proteins, such as Arp2/3, cofilin and AIP1. In this chapter, using a combination of site-directed mutagenesis, solution biochemistry methods, electron and TIRF microscopy, we examined the effects of coronin on the structure of actin filaments by studying its impact on inter-protomer contacts in F-actin. We also examined how some of these effects compare to those induced by cofilin, studying how the two proteins act when they are both present and co-bound to actin. Our goal has been to shed light on the mechanism(s) by which coronin modulates cofilin's effects on actin filaments.

MATERIALS AND METHODS

Protein expression and purification :

GST fused CrnΔCC constructs were expressed in Rosetta 2 DE3 cells and recovered in soluble fractions. The protein was purified using Glutathione-Uniflow Resin (Clontech Laboratories). On-column thrombin cleavage was performed overnight at 4 °C and followed by gel filtration (Superdex 75). Skeletal actin was isolated from rabbit muscle **(13).** Yeast actins were purified as described before **(14)**.

Seeded polymerization of actin:

F-actin seeds were prepared by polymerizing 2 µM Mg-G-actin with 2 mM $MgCl_2$ and 50 mM KCl overnight, on ice. The seeds were incubated with CrnΔCC at different mole ratios to actin for 20 minutes at room temperature. 2 µM Mg-G-actin was then added under polymerizing conditions (10mM Hepes pH 7.4, 2 mM $MgCl_2$, 50 mM KCl, 0.2 mM ATP, 1 mM DTT) to the seeds. Pyrene fluorescence increase, which monitors actin's polymerization, was measured using TECAN microplate reader.

Total internal reflection fluorescence microscopy (TIRF):

Coronin severing was probed by mixing Alexa 488-labeled F-actin (5 µM, 25% Alexa488) and yeast CrnΔCC (7.5 µM, occupancy~0.8). After 30 min incubation at RT, the reaction mixtures were diluted to 5 nM actin in F-buffer (2mM $MgCl_2$, 50mM KCl in 20mM Pipes pH 6.8, 20mM Hepes pH 7.5 or 5mM Tris pH8.0), supplemented with 0.2 mM ATP and 100 mM DTT (imaging buffer), and applied on the polylysine-coated coverslips.

Filaments were imaged using DMI6000 TIRF microscope (Leica, Wetzlar, Germany). Filaments' length was analyzed using Fiji software.

Cross-linking of actin:

Free thiols were removed from yeast actin cysteine mutant samples using Sephadex G-50 spin columns equilibrated with G-buffer containing 10 mM Hepes pH 7.5, 0.2 mM $CaCl_2$ and 0.2 mM ATP. Actin was polymerized for 2 hours on ice with 3.0 mM $MgCl_2$ and 50mM KCl. When needed, actin was polymerized in the presence of 100 µM $BeCl_2$ and 50mM NaF, final to yield BeFx-actin. ADP-F-actin contained an extra 0.4 mM ADP added after polymerization. The molar ratio of CrnΔCC/Yeast Cofilin to F-actin was 1: 1. Disulfide cross-linking of actin mutants was catalyzed by 5 µM CuSO4 or 10 µM MTS reagents and the reaction was stopped with 2mM N-ethyl maleimide (NEM). The progress of disulfide cross-linking was monitored by SDS-PAGE under non-reducing conditions. The decay of the actin monomer band with cross-linking progress was quantified using Scion Image software.

Electron microscopy (EM):

Undiluted actin samples from each experiment were applied to carbon-coated grids and stained with 1% uranyl acetate. The grids were examined in a JEM1200-EX electron microscope (JEOL) under minimal-dose conditions at an accelerating voltage of 80 keV and a nominal magnification of 80,000.

Rhodamine phalloidin release from actin:

Phalloidin was obtained from Sigma and rhodamine phalloidin was obtained from Molecular Probes (Eugene, OR). Rhodamine phalloidin release from F-actin (5.0 µM) was measured on yeast F-actin solutions (in 10 mM Hepes, 3.0 mM $MgCl_2$, 50 mM KCl, 0.2 mM $CaCl_2$, 0.2 mM ATP, 1 mM DTT at pH 7.4) pre-incubated overnight on ice with 0.2 µM rhodamine phalloidin and 4.8 µM phalloidin. Rhodamine phalloidin fluorescence was monitored

at 575 nm (emission wavelength) before and after the addition of CrnΔCC and/or cofilin (5.5 μM).

Ɛ-ADP collisional quenching experiments:

Excess ATP was removed from yeast and skeletal actin samples using G-50 spin columns equilibrated with G-buffer (10 mM Hepes pH 7.5, 0.2 mM $CaCl_2$, 1 mM DTT). Actin was incubated then with 10X molar excess of Ɛ-ATP overnight on ice. Prior to experiments, excess Ɛ-ADTP was removed on another G-50 spin column and Mg-G- actin was polymerized with 3 mM $MgCl_2$ and 50 mM KCl for 2 hours on ice. By then Ɛ-ATP was hydrolyzed to Ɛ-ADP. Finally, F-actin was incubated with CrnΔCC or F-buffer for 20 minutes at RT before recoding the quenching of Ɛ-ADP by nitromethane using a PTI spectrofluorometer, with excitation wavelength set at 350 nm and the emission wavelength set at 420 nm.

Fluorescence spectroscopy:

Before measurements of the effect of CrnΔCC on cysteine reactivity to acrylodan in actin mutants, DTT was removed from G-actins by passing them through a Sephadex G-50 column equilibrated with G-buffer (10 mM Hepes pH 7.5, 0.2 mM $CaCl_2$ and 0.2 mM ATP). Subsequently, F-actin (5.0 μM) was prepared from DTT-free Ca-G-actin by incubating it with 0.05 mM $MgCl_2$ and 0.4 mM EGTA for 5 min at room temperature, followed by the addition of 3 mM $MgCl_2$ and 50 mM KCl. CrnΔCC (5.5 μM) was added to F-actin and the sample was incubated for at least 30 min on ice. Before acrylodan labeling experiments were conducted, the samples were incubated for 10 min at 25°C, but were kept on ice at all other times. Acrylodan labeling solution was prepared at 5.0 μM in dimethylformamide using an extinction coefficient of 20,000 at 391 nm (Molecular Probes Handbook). The pseudo-first-order labeling reactions

were carried out at a 1:100 acrylodan/actin molar ratio and were monitored via an increase in acrylodan emission at 465 nm, with the excitation wavelength set at 385 nm.

To record emission spectra of acrylodan-labeled actins, DTT-free G-actins were labeled with a 1.1- to 1.2-fold mole excess of acrylodan for 3 hours, at 4°C. The reactions were stopped with 1 mM DTT. Actin was polymerized with 3 mM $MgCl_2$ and 50 mM KCl in 20 mM Hepes, 0.2mM ATP and 1mM DTT at pH7.4. Fluorescence emission spectra of 5 µM F-actin +/- 5.5 µM CrnΔCC (400–650 nm) were recorded with the excitation wavelength set at 385 nm. All fluorescence experiments were carried out on a spectrofluorometer using FeliX32 Analysis, version 1.1 (Photon Technology International, Lawrenceville, NJ).

Differential scanning calorimetry

Differential scanning calorimetry (DSC) experiments were carried out in an N-DSC II calorimeter (CSC). Mg-ATP-G-actin in G buffer (20 mM Hepes, 0.2 mM $CaCl_2$, 0.2 mM ATP, 0.1 mM tris(2-carboxyethyl)phosphine (TCEP), 0.4 mM EGTA, 0.05 mM $MgCl_2$ (pH 7.4)) was polymerized with 3 mM $MgCl_2$ and 50 mM KCl. Final protein mixtures contained 20 mM Hepes, 0.2 mM $CaCl_2$, 0.2 mM ATP, 4mM βME, 3.0 mM $MgCl_2$, and 50 mM KCl (pH 7.4).

Binding of cofilin to BeFx-F-actin.

Yeast F-actin (4.0 µM) was prepared from Ca-G-actin by incubating it with 0.05 mM $MgCl_2$ and 0.4 mM EGTA for 5 min at room temperature, followed by the addition of 3 mM $MgCl_2$ and 50 mM KCl and incubated for 1 hour at room temperature (in 10 mM Hepes, 3.0 mM $MgCl_2$, 50 mM KCl, 0.2 mM $CaCl_2$, 0.2 mM ATP, 1 mM DTT at pH 7.4). F-actin was then incubated with 100 µM $BeCl_2$ and 50mM NaF for 6 hours, on ice, in the same buffer. Samples were created by the addition of yeast cofilin at different concentrations (0.5, 1, 1.5, 2, 3, and 4.0 µM) and 2.0 or 1 µM CrnΔCC, and incubated for 30 minutes at room temperature. The

samples were centrifuged at 312,500***g*** for 20 min, at 4 °C, in a Beckman TLA-100 rotor. The resulting pellets were solubilized in gel sample buffer and analyzed by SDS-PAGE. Gels were stained with Coomassie Blue. The intensities of the bands were estimated using Scion Image Software. To quantify the amount of cofilin co-sedimented with F-actin, we loaded 170–340 μg of the purified protein on each gel as the standards. Graphs were generated using SigmaPlot software.

RESULTS

To sever or not to sever?

In addition to the previously reported activity of coronin in regulating cofilin's severing activity, EM and atomic force microscopy (AFM) images (Reisler lab unpublished data) observations alluded to a severing activity of F-actin by CrnΔCC itself. Seeded polymerization assays were used to study coronin's possible severing of F-actin. In this assay, actin is polymerized for an hour at room temperature (RT). These pre-formed filaments serve as "F-actin seeds" when diluted to a 0.5 μM concentration in polymerizing buffer, which contains also 2 μM gel-filtered 5% pyrenyl monomeric yeast actin and/or CrnΔCC, yeast cofilin (Ycof) and human cofilin-1 (hCof1). Assembly rates, measured via increase in pyrene fluorescence, are faster in the presence of a severing protein because severing of existing filaments creates additional new barbed ends to which actin monomers can add and elongate these filaments. Different concentrations of CrnΔCC were used to determine if and how this activity varies, in addition to probing the effect at different pH settings (Figure 4.2). Addition of CrnΔCC does not produce a visible increase in the initial elongation rates compared to that when F-actin seeds are added alone. This result points to a lack of significant severing activity of coronin alone (Figure 4.2A, pink and red traces vs. the purple trace).

In a control type test of the above conclusion the addition of Ycof at two different sub-stoichiometric ratios to actin causes an increase in the initial elongation rates (Figure 4.2A, light green and cyan traces), as expected from the known severing activity of yeast cofilin on yeast F-actin **(16, 17, 18)**. CrnΔCC enhances this severing activity as the elongation rates are faster when the proteins are added together (Figure 4.2A, light green and cyan grey traces vs. the dark blue and maroon traces).

A previous report has shown that hCof1 does not sever yeast actin filaments (McCullough et al., 2011). This is reconfirmed in our assays as Hcof1, like CrnΔCC, does not increase initial elongation rates upon its mixing with F-actin seeds. A speculation that CrnΔCC may "switch on" yeast actins severing by hCof1 was not confirmed. As shown in Figure 4.2B CrnΔCC does not "activate" any yeast F-actin severing by Hcof1 (all fluorescence traces are superimposable with the red trace corresponding to the addition of F-actin seeds alone to G-actin).

In addition to the above, TIRF microscopy was used for a direct observation of coronin's possible severing of F-actin. If severing were taking place, there would be clear breaks seen in the filaments with some broken filament fragments diffusing away from the focal plane. This experiment was repeated several times but there were no severing events observed over a time frame of fifteen minutes (results not shown). TIRF was also used in companion experiments to measure the average filament lengths of F-actin in the presence of CrnΔCC, at different pH values. The average length was ~5.5 μm in the presence and absence of CrnΔCC (Figure 4.3). Thus, neither experiment showed any significant severing activity by coronin alone. We did confirm previous reports of CrnΔCC enhancing yeast cofilin's severing activity, showing that our CrnΔCC was indeed active.

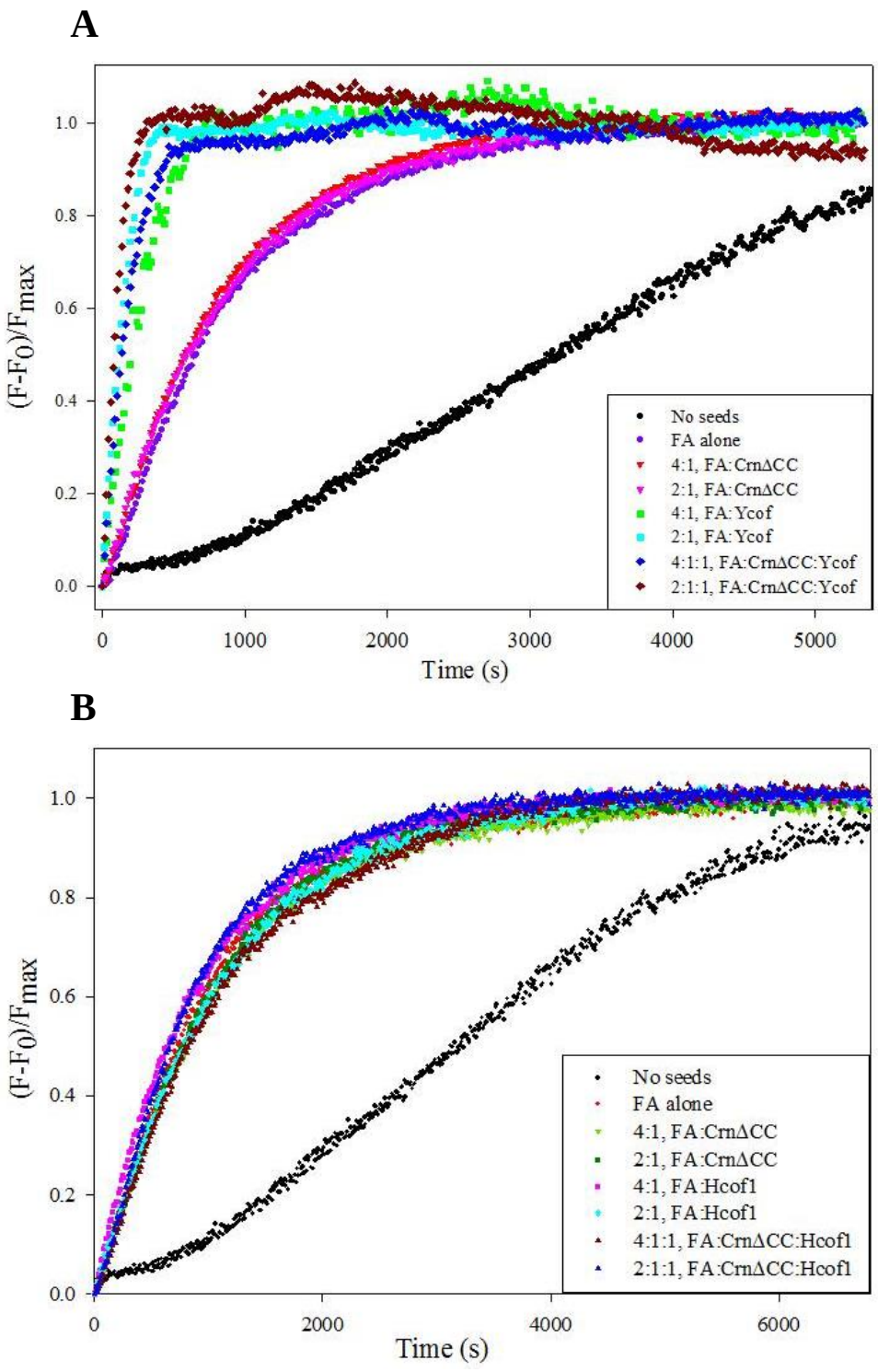

Figure 4.2- Investigating the potential severing activity of CrnΔCC.

A and B, Seeded polymerization assays: yeast F-actin was pre-polymerized for 1 hour at room temperature; to be used as "F-actin seeds", which were then diluted in polymerizing buffer with gel-filtered 5% pyrenyl monomeric yeast actin and different molar ratios of CrnΔCC and/or yeast cofilin (Ycof) **(A),** or CrnΔCC and/or human cofilin-1 (Hcof1) **(B).**

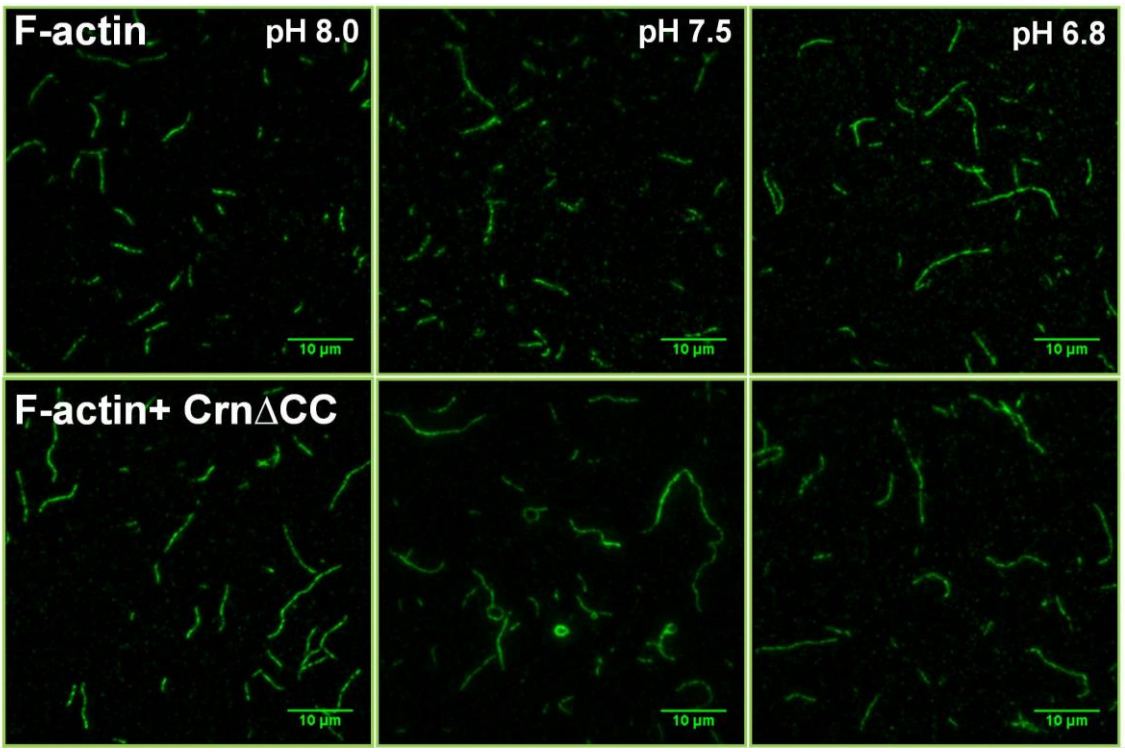

Figure 4.3- Investigating the potential severing activity of CrnΔCC by TIRF microscopy.
5 µM actin filaments labeled with Alexa-488 are incubated with 5.5 µM CrnΔCC for 30 min at room temperature at different pH values. The samples are carefully diluted 1000X, immobilized on poly-lysine slips and imaged by TIRF microscopy. The average filament length was ~5.5 µm ($^{+}$/$_{-}$ 1.8) for all samples.

CrnΔCC does not bind ATP or ADP.

The binding affinity to F-actin for human coronin1B is approximately 50-fold higher for freshly polymerized ATP/ADP+Pi F-actin compared with ADP-bound actin filaments **(4)**. Similar observations have been made for the budding-yeast coronin **(10)**. Due to the different binding affinities reported previously and because of its dual effect on F-actin severing by cofilin, it was almost imperative to eliminate the possibility of an intrinsic binding of ATP or ADP to coronin and its consequences on coronin's interaction with actin, as opposed to its recognition of the different states of actin and preferential binding to ATP/ADP+Pi bound actin over ADP-actin. To test whether coronin itself binds any of these nucleotides, fluorescent analogs of ATP and ADP, Ɛ-ATP and Ɛ-ADP, were used. Our results did not reveal any significant effect of coronin on Ɛ-ATP or Ɛ-ADP fluorescence, indicating that coronin lacks a high affinity nucleotide binding site (Figure 4.4). The negative results allowed for a further investigation of coronin related changes in the actin nucleotide phosphate site, discussed in a later section, as they relate to the effects of coronin on the structure of F-actin.

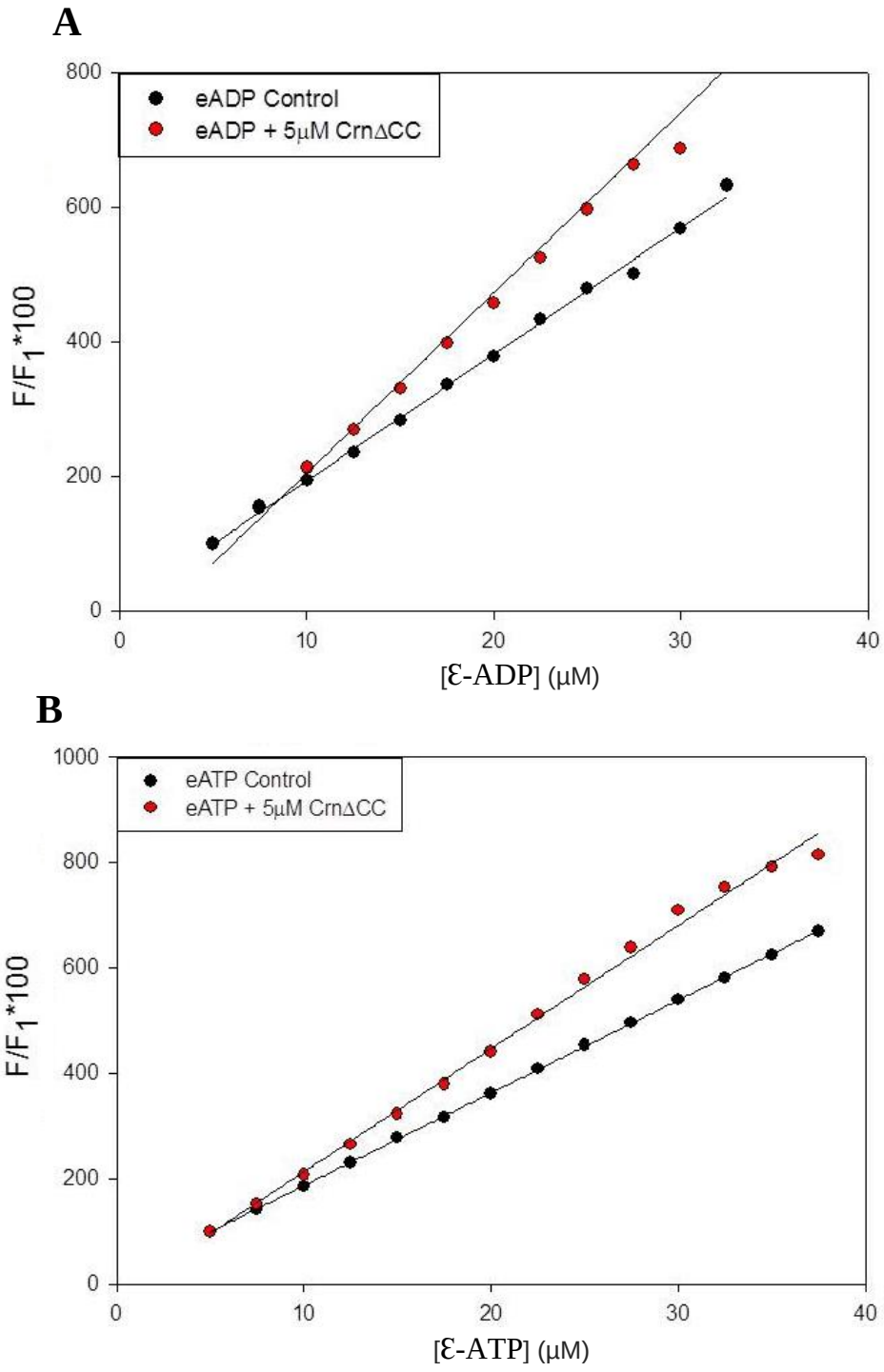

Figure 4.4- CrnΔCC does not bind ADP or ATP.

A, 5 μM CrnΔCC was incubated with increasing amounts of Ɛ-ADP: 5-37.5 μM, at 2.5 μM increments. **B,** 5 μM CrnΔCC was incubated with increasing amounts of Ɛ-ATP: 5-37.5 μM, at 2.5 μM increments. For all samples, the excitation wavelength was set at 325 nm and emission wavelength was read at 409 nm.

CrnΔCC affects the lateral and longitudinal interfaces of F-actin.

Cryo-EM reconstruction **(12)** shows CrnΔCC to bind between two longitudinally adjacent protomers in F-actin, making contacts with subdomain 1 (SD1) (C-terminal region) of the first actin protomer and SD1 and SD2 (DNAse I Binding loop, D-loop) of the next one. It also shows coronin to be in close proximity to SD4 of the laterally adjacent protomer; these contacts look more prominent with ADP vs. ATP-bound F-actin. This leads us to a hypothesis that coronin binding has an effect on the structure of F-actin by modulating its longitudinal and lateral interfaces. Conveniently, CrnΔCC does not contain any endogenous cysteines, which makes it easier to assess its effect on inter-protomer contacts in F-actin via actin cysteine based cross-linking studies. Double cysteine actin mutants Q41C and S265C were employed to analyze the extent of longitudinal (intra-strand) cross-linking between residues Cys41 (D-loop) and the endogenous Cys374 (C-terminus) and the lateral (inter-strand) cross-linking between Cys265 (hydrophobic loop, H-loop) and Cys374 in the presence and absence of CrnΔCC. In these actins, a cysteine was introduced at either residue 41 or 265 to create the corresponding mutants while retaining the endogenous cysteine 374. The copper-catalyzed cross-linking of these actins has been used previously to examine the longitudinal and lateral interfaces in F-actin **(18)**.

A similar approach was used in this work: the inter-protomer cross-linking reactions in the above mentioned mutant actin filaments were monitored via SDS-PAGE by quantifying actin monomer depletion resulting from un-catalyzed F-actin disulfide cross-linking. Different gel patterns are obtained in the presence and absence of CrnΔCC (Figure 4.5, 4.6 and 4.7). CrnΔCC accelerates the longitudinal cross-linking between actin residues Q41C (D-loop) and Cys374 (C-terminus) (Figure 4.4 and 4.5). Because cryo-EM reconstruction showed that CrnΔCC had more contacts in ADP-F-actin vs. BeFx F-actin, particularly in SD2, the Q41C cross-linking

experiments were done using both ADP and BeFx F-actin. Coronin's effect on the cross-linking of Q41C was the same regardless of the nucleotide state of F-actin (Figure 4.5 and 4.6).

The lateral cross-linking between residues Cys265 (hydrophobic loop, H-loop) and Cys374 is however inhibited by CrnΔCC (Figure 4.7), indicating that the time average mean distance between residues 265 and 374 is increased upon coronin binding.

Overall, these actin cross-linking studies show a direct effect of coronin on the lateral and longitudinal interfaces in F-actin.

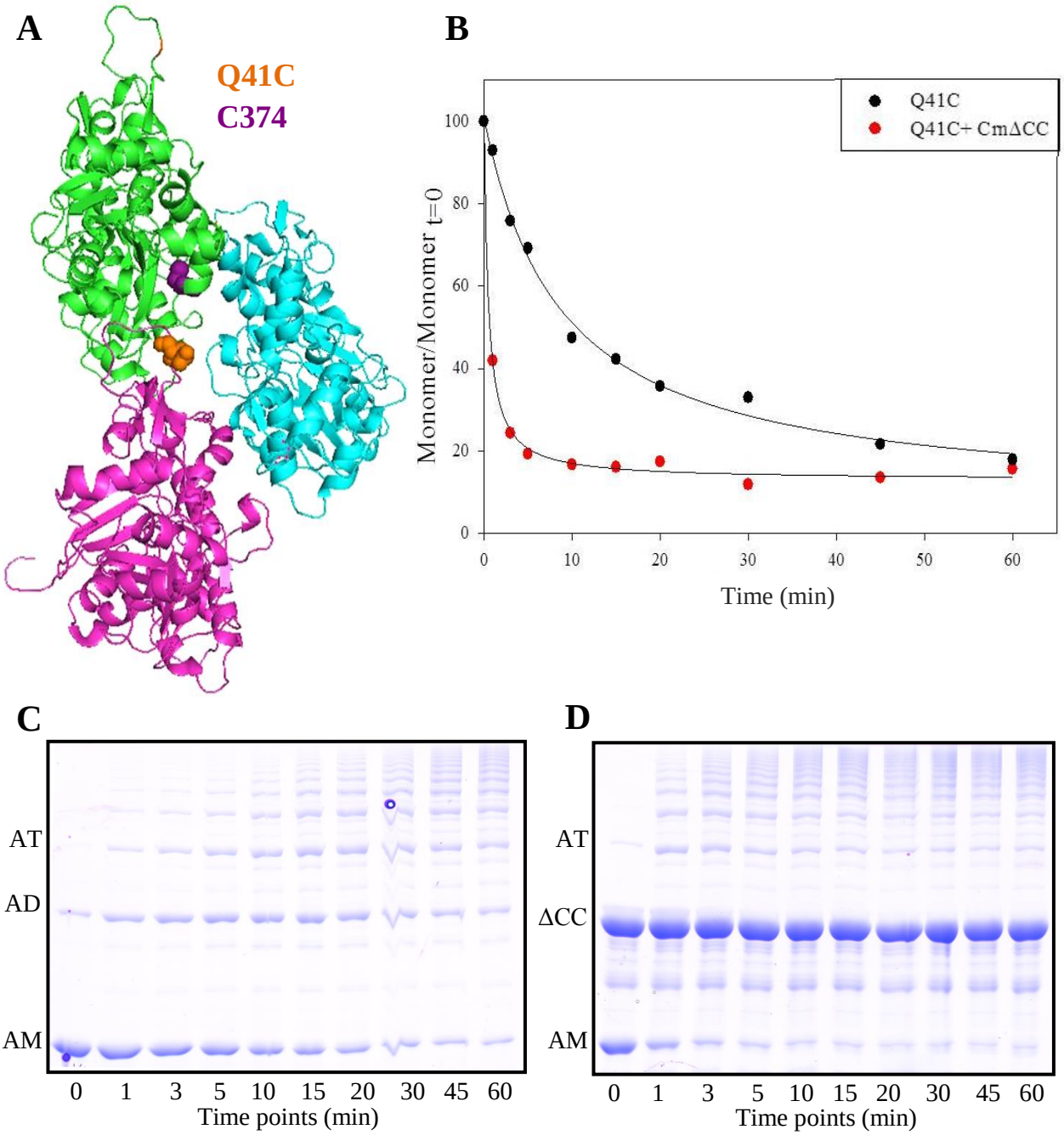

Figure 4.5- CrnΔCC accelerates the longitudinal cross-linking of Q41C in BeFx-F-actin.
A, F-actin model showing mutated residue Q41C and the endogenous Cys374. **B**, Plots of actin monomer band decay (*Monomer/Monomer*$_{t=0}$) with time of the cross-linking reaction. The data were taken from SDS-PAGE patterns shown in **(C)** and **(D)** for the reaction in the absence of CrnΔCC (●) and for the reaction in the presence of CrnΔCC (●), respectively. Symbols AM, AD, AT correspond to actin monomer, actin dimer and actin trimer disulfide-bonded species, respectively. ΔCC corresponds to CrnΔCC. All experiments were done in triplicate and yielded similar results; a representative plot of each actin mutant reaction is shown.

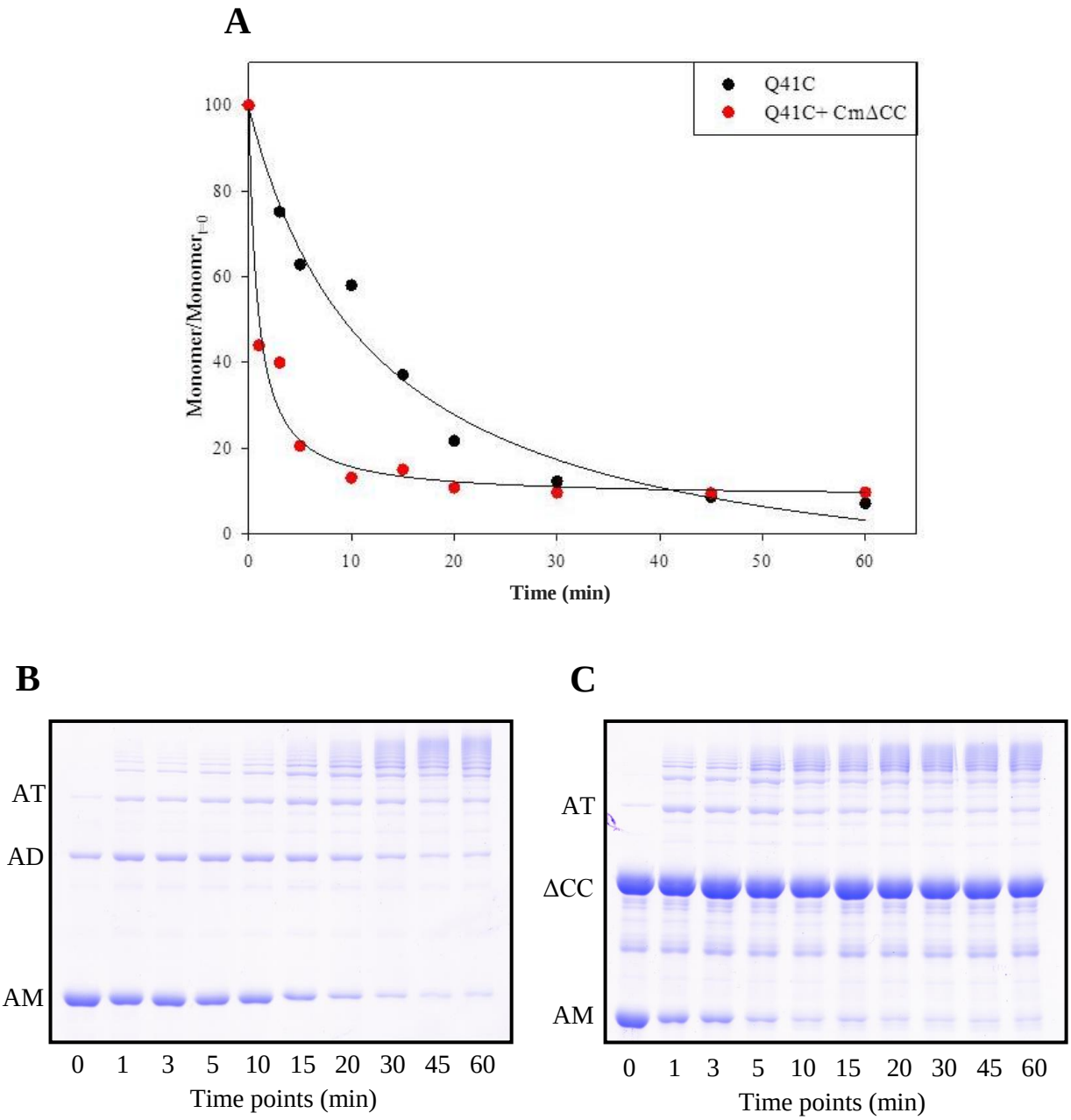

Figure 4.6- CrnΔCC accelerates the longitudinal cross-linking of Q41C in ADP F-actin.
A, Plots of actin monomer (AM) band decay (*Monomer/Monomer*$_{t=0}$) with time of the cross-linking reaction. The data were taken from SDS-PAGE patterns shown in **(B)** and **(C)** for the reaction in the absence of CrnΔCC (●) and for the reaction in the presence of CrnΔCC (●), respectively. Symbols AM, AD, AT correspond to actin monomer, actin dimer and actin trimer disulfide-bonded species, respectively. ΔCC corresponds to CrnΔCC.

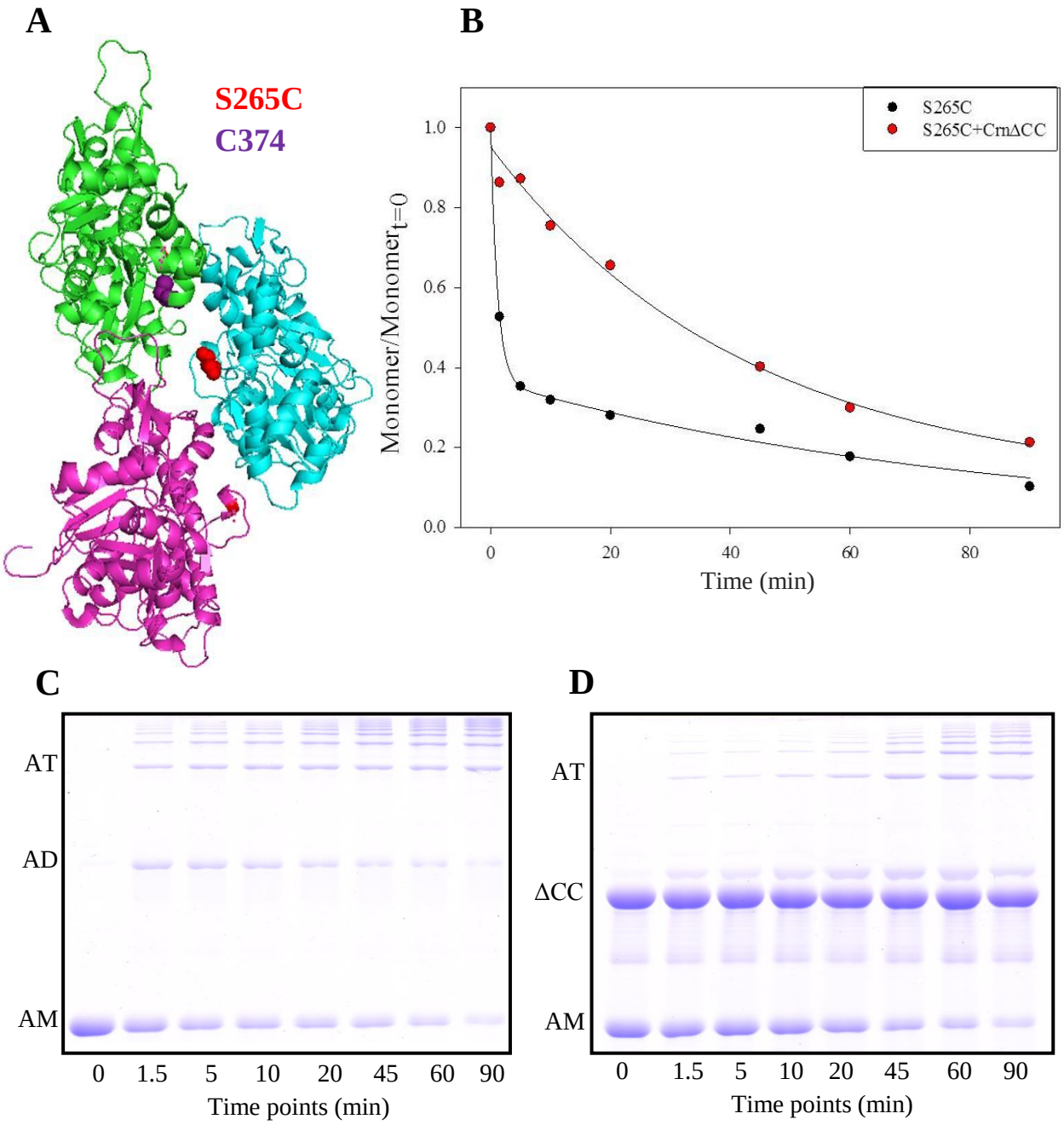

Figure 4.7- CrnΔCC affects the lateral cross-linking of S265C yeast actin mutant.
A, F-actin model showing mutated residue S265C and the endogenous Cys374. **B**, Plots of actin monomer band decay (*Monomer/Monomer*$_{t=0}$) with time of the reaction. The data were taken from SDS-PAGE patterns shown in **(C)** and (**D)** for the reaction in the absence of CrnΔCC (●) and for the reaction in the presence of CrnΔCC (●), respectively. Symbols AM, AD, AT correspond to actin monomer, actin dimer and actin trimer disulfide-bonded species, respectively. ΔCC corresponds to CrnΔCC. All experiments were done in triplicate and yielded similar results; a representative plot of each actin mutant reaction is shown.

To further probe coronin's effects on the lateral/longitudinal F-actin interfaces, we examined cross-linked actin filaments of co-polymers of two different single cysteine mutants, K50C/C374A co-polymerized with S265C/C374A and K50C/C374A co-polymerized with A167C/C374A. The first cross-linking involves the D-loop with the H-loop, whereas the second one involves the D-loop and the WH2-binding loop (W-loop). There is high level of conformational plasticity in the inter-protomer region as the D-loop can be cross-linked in F-actin by disulfide bonds to residues in the H-loop, C-terminus and the W-loop. However, some of these cross-linked co-polymers dismantle upon cross-linking, indicating that they "capture" and freeze intrinsically destabilizing dynamic states or fluctuations of these structural elements **(19)**. Cofilin increases the cross-linking of the D-loop with these three regions. Interestingly it also prevents the dismantling of filaments, while rescuing their formation if added after the cross-linking is induced (unpublished data, Reisler lab).

In our experiments filaments were formed by co-polymerizing two different single cysteine yeast mutants: K50C/C374A was co-polymerized at a 1:1 ratio with S265C/C374 (referred to as the C50/C265 co-polymer, for short) and K50C/C374A was co-polymerized at a 1:1 ratio with A167C/C374A (referred to as the C50/C167 co-polymer). Cross-linking between the different cysteines was induced by the addition of equimolar amounts of $CuSO_4$. Like cofilin, CrnΔCC rescues filament formation from the cross-linked actins, but inhibits the cross-linking reactions (Figure 4.8 and 4.10). SDS-PAGE gels analysis shows the actin dimer band (C50/C265 or C50/C167actins) appearing at a slower rate when CrnΔCC is added to the F-actin co-polymer (Figure 4.8A and figure 4.10A). The increase in light scattering after CrnΔCC is added to the cross-linked actins sample indicates a rescue of filament formation of C50/C265 mutant by CrnΔCC (Figure 4.9A, blue trace). The same rescue is seen with the C50/C167 mutant (Figure

4.11A, blue trace) and the inhibition of cross-linking by CrnΔCC can be deduced from the lack of signal decrease upon addition of cross-linking catalyst ($CuSO_4$) in the presence of CrnΔCC (Figure 4.11A, red trace). The effect of CrnΔCC was the same for both co-polymers and the results show decreased range of dynamic rearrangements which yield intrinsically destabilizing states. In the presence of coronin, these states are visited less frequently. Electron microscopy (EM) images were taken to confirm that the decrease and increase in light scattering was indeed due to the depolymerization and polymerization rescue of actin filaments, respectively (Figure 4.9B and 4.9C for the C50-C265 co-polymer and 4.11B for the C50-C167 co-polymer). The images of C50-C167 oxidized F-actin are not shown because of their poor quality.

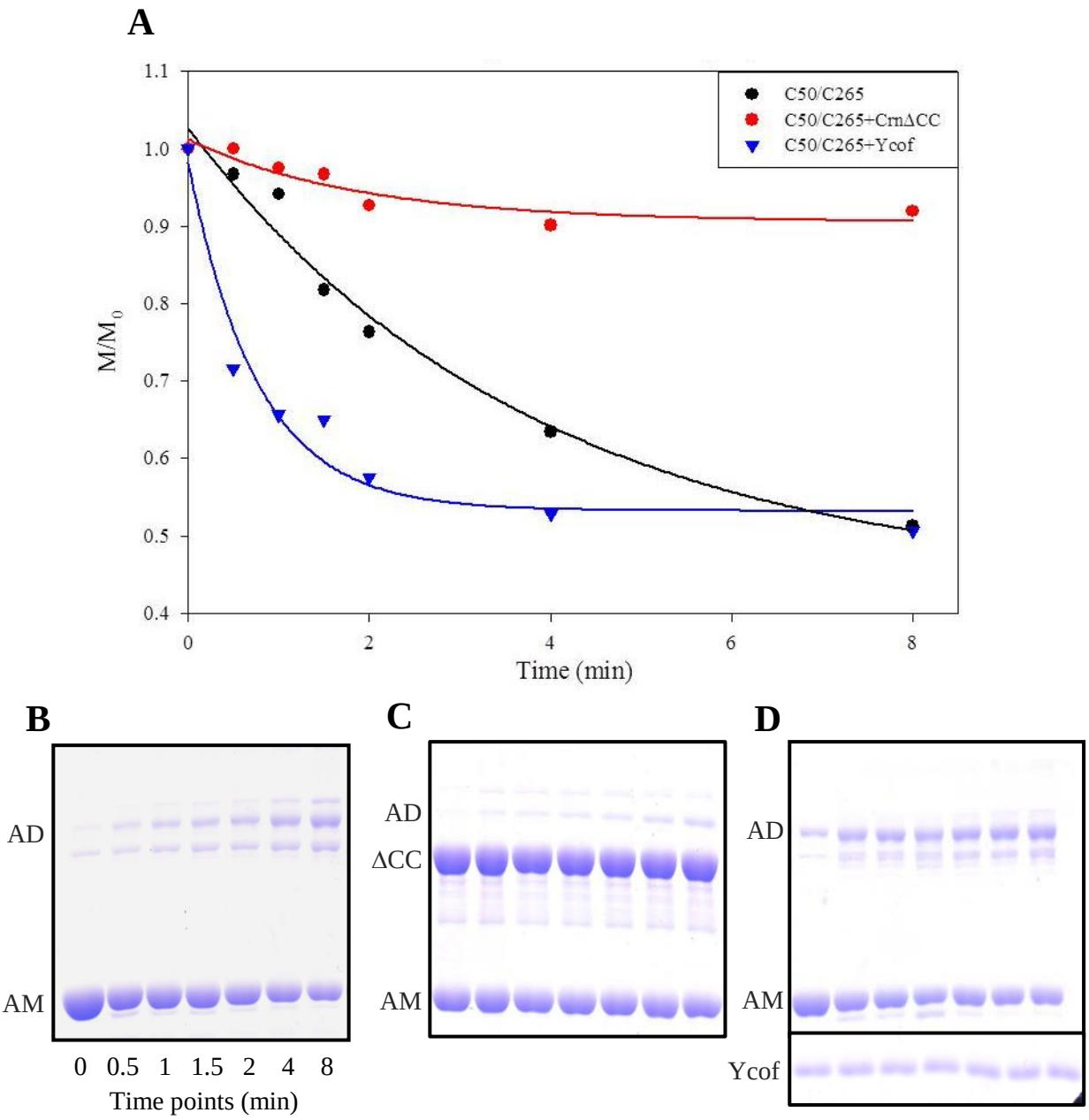

Figure 4.8- Effect of CrnΔCC on the C50-C265 co-polymer.

A, Plots of actin monomer band decay (M/M_0) with time of the disulfide cross-linking reaction. The data were taken from SDS-PAGE patterns shown in **(B)**, **(C)** and (D) for the reaction of C50-C265 alone (●), in the presence of CrnΔCC (●) or in the presence of yeast cofilin (▼), respectively. **B**, **C and D,** SDS-PAGE patterns of C50-C265 F-actin (10 µM) cross-linked alone **(B)**, in presence of 10 µM CrnΔCC **(C)** or 10 µM Ycof **(D)**. Reaction aliquots taken after 0, 0.5, 1, 1.5, 2, 4 and 8 min of the cross-linking reaction are analyzed in the corresponding lanes. Symbols AM, AD correspond to actin monomer and actin dimer disulfide-bonded species, respectively. ΔCC corresponds to CrnΔCC and Ycof to yeast cofilin.

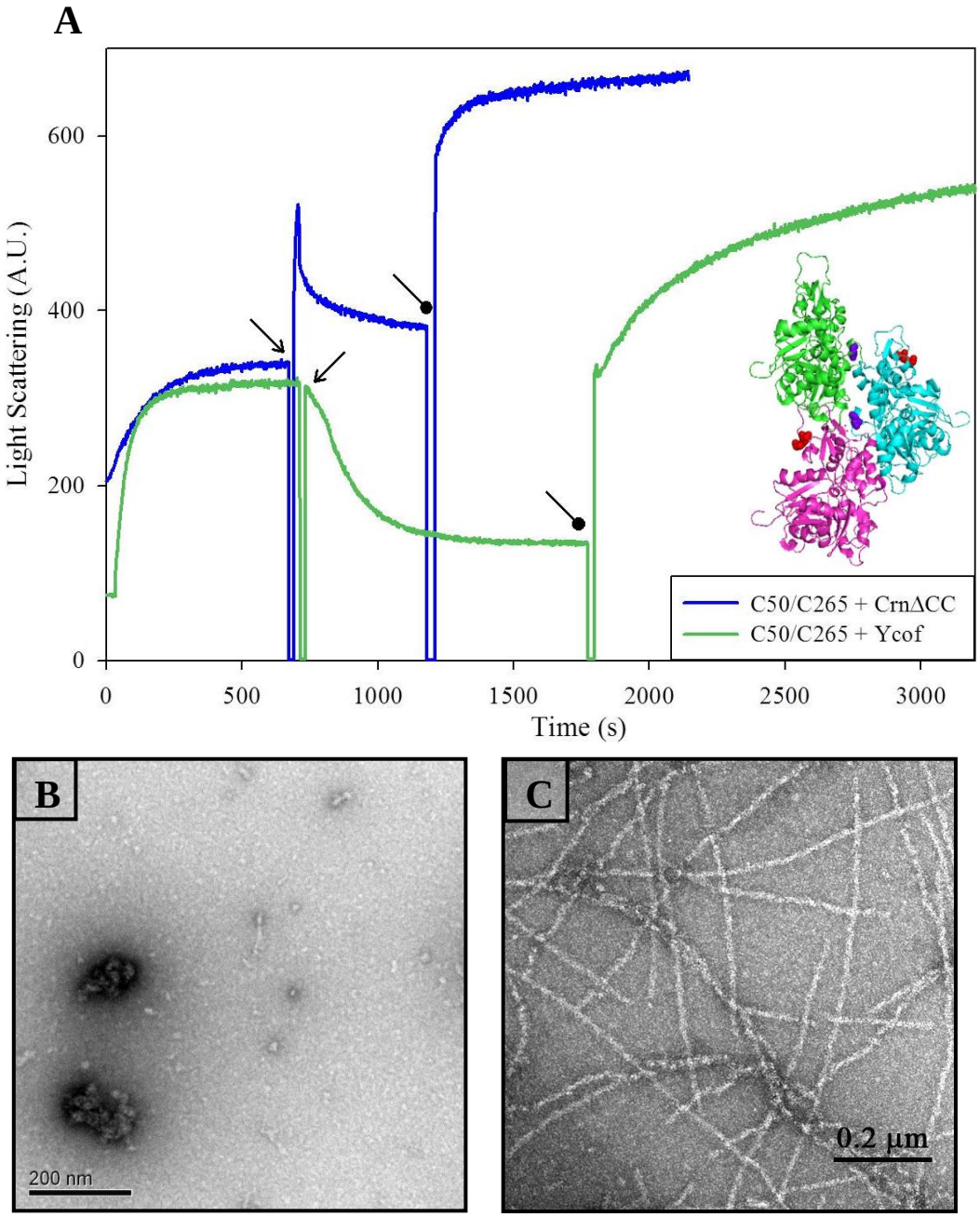

Figure 4.9- CrnΔCC rescues the polymerization of the C50-C265 cross-linked co-polymer. **A**, 10 µM C50-C265-actin was polymerized at 25 °C with 3 mM $MgCl_2$ and 50 mM KCl. At the time points indicated by (*arrows)*, 20 µM $CuSO_4$ was added and the decrease in light scattering for each sample was recorded. At the time points indicated by (● *arrows*), 10 µM CrnΔCC *(blue trace)* or 10 µM Ycof *(green trace)* was added and the increase in light scattering indicates rescue of filaments formation. *A.U.*, arbitrary units**.** ***Inset***, F-actin model showing mutated residues K50C (*purple dots*) and S265C (*red dots*). **B**, EM image showing C50-C265 F-actin cross-linked alone. **C**, EM image showing the sample from **(B)** after CrnΔCC addition.

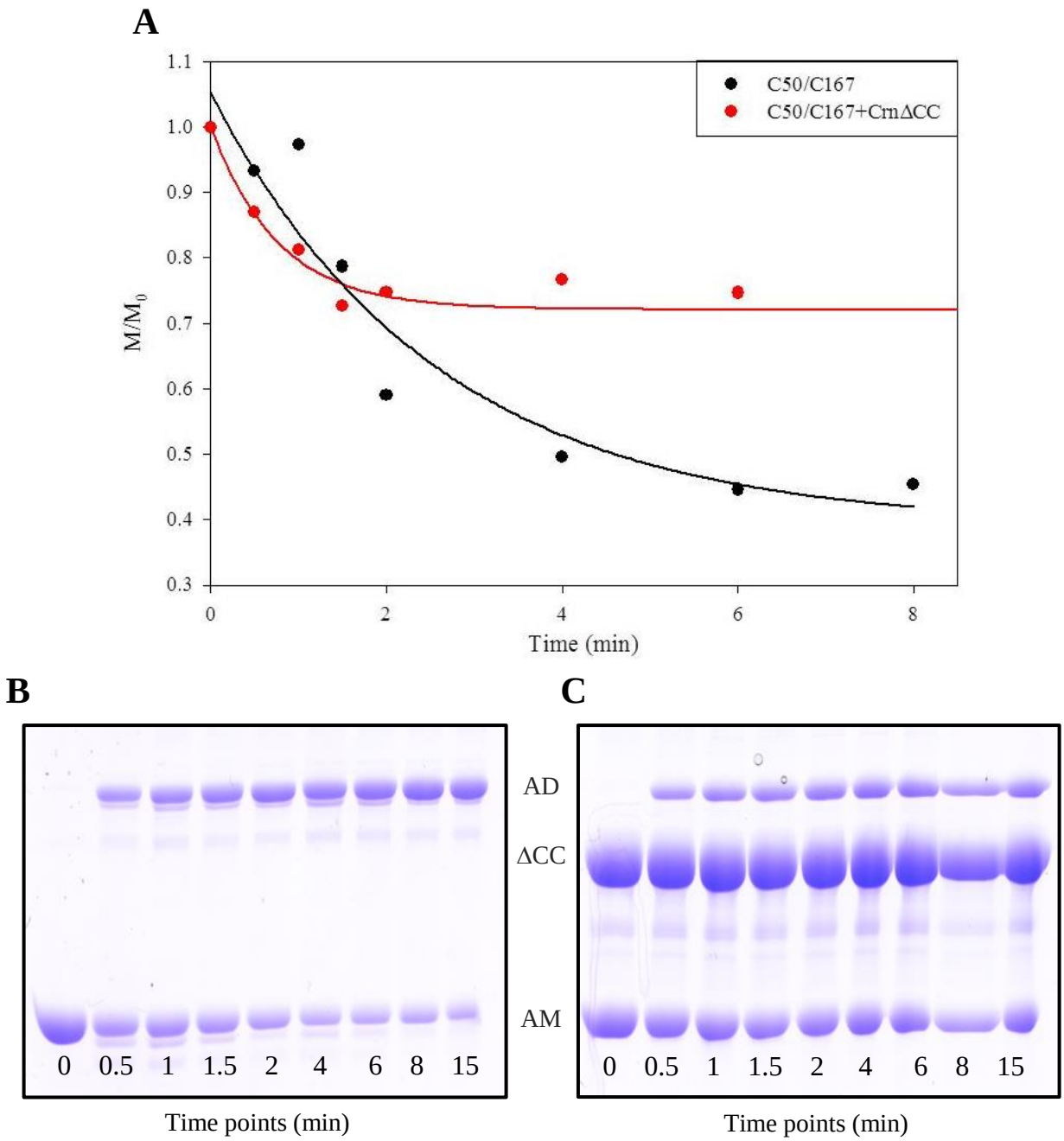

Figure 4.10- Effect of CrnΔCC on the C50-C167 co-polymer.

A, Plots of actin monomer band decay (M/M_0) with time of the cross-linking reaction. The data were taken from SDS-PAGE patterns shown in **(B)**, (**C)** and (D) for the reaction of C50-C265 alone (●), in the presence of CrnΔCC (●), respectively. **B** and **C,** SDS-PAGE patterns of C50-C265 F-actin (10 µM) cross-linked alone **(B)**, in presence of 10 µM CrnΔCC **(C)**. Reaction aliquots taken after 0, 0.5, 1, 1.5, 2, 4, 6, 8 and 15 min of the cross-linking reaction are analyzed in the corresponding lanes. Symbols AM, AD correspond to actin monomer and actin dimer disulfide-bonded species, respectively. ΔCC corresponds to CrnΔCC.

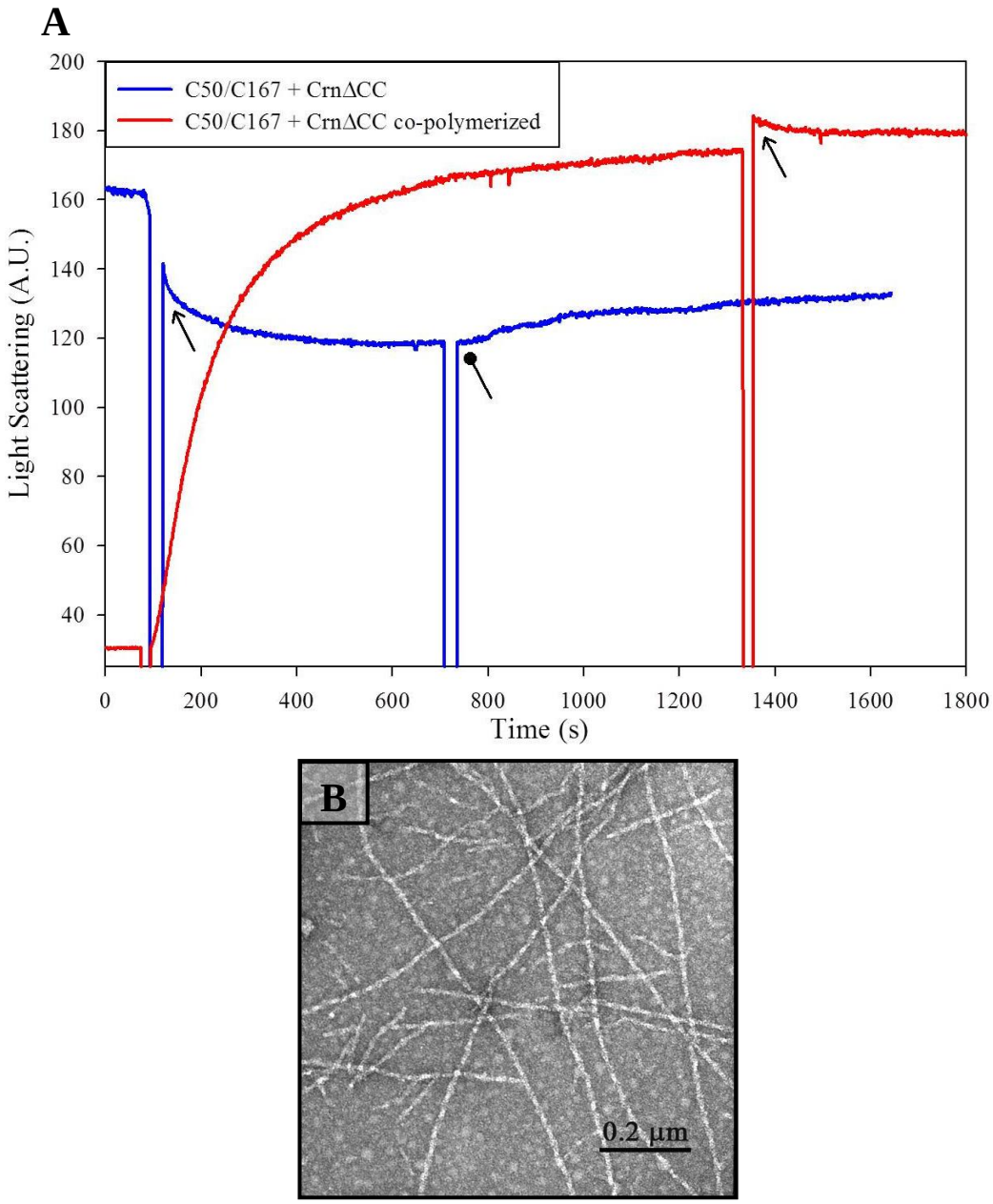

Figure 4.11- CrnΔCC rescues the polymerization of the C50-C167 cross-linked co-polymer. **A**, *Blue trace*, 10 µM C50-C167-actin was pre-polymerized at 25 °C with 3 mM $MgCl_2$ and 50 mM KCl. At the time point indicated by (*arrow)*, 20 µM $CuSO_4$ was added and the decrease in light scattering was recorded. At the time point indicated by (● *arrow*), 10 µM CrnΔCC was added and the rescue in polymerization was observed via the increase in light scattering. *Red trace*, 10 µM C50-C167-actin was polymerized with CrnΔCC at 25 °C with 3 mM $MgCl_2$ and 50 mM KCl. At the time point indicated by (*arrow)*, 20 µM $CuSO_4$ was added and no decrease in light scattering was observed. *A.U.*, arbitrary units. **B**, EM image showing C50-C167 cross-linked co-polymer after the addition of CrnΔCC.

The fungus toxin, phalloidin, binds to three actin protomers in two filament strands **(20, 21)**. It stabilizes the lateral contacts and the structure of F-actin, reducing the critical concentration for actin polymerization by two orders of magnitude **(22)**. Thus, to shed more light on coronin effects on lateral contacts in F-actin, we used rhodamine phalloidin (phalloidin conjugated to the red-orange fluorescent dye, tetramethylrhodamine) as a probe for the state of the inter-strand interface. It was previously demonstrated that cofilin binds weakly to F-actin saturated with a rhodamine phalloidin/phalloidin mixture, and produces subsequent conformational changes that result in phalloidin release from F-actin **(23)**. This was due to cofilin's effect on lateral inter-protomer contacts and its weakening of the inter-strand coupling in actin filaments. CrnΔCC does not cause similar release of rhodamine phalloidin, indicating that it does not induce major conformational changes in the lateral interface of the actin filament which would not accommodate the binding of phalloidin (Figure 4.12, red trace). Interestingly, CrnΔCC does however increase the rate at which cofilin induces the release of rhodamine phalloidin from a fraction of F-actin (Figure 4.12, black trace *vs.* blue trace). This effect could be due to a combined perturbation of phalloidin stabilized F-actin structure, resulting in the accelerated release of phalloidin from the filament.

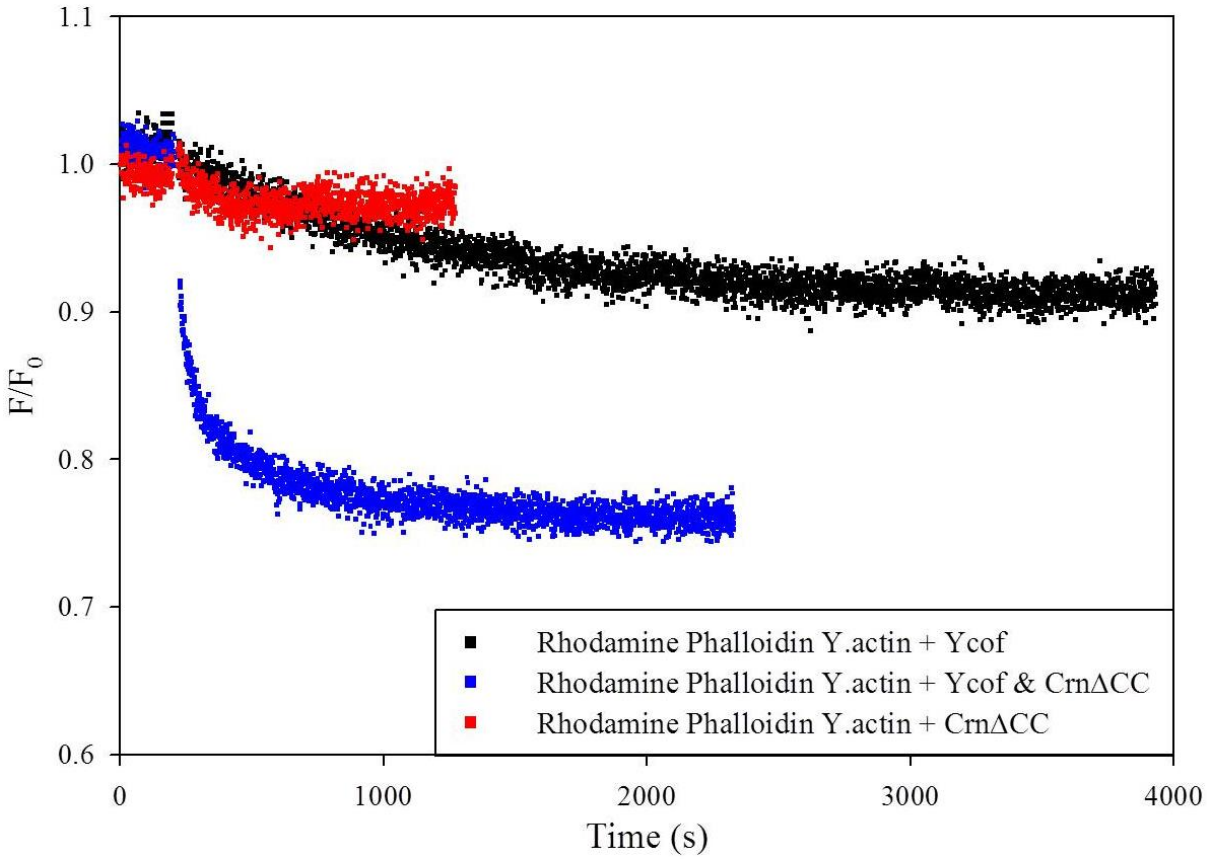

Figure 4.12- Rhodamine phalloidin release from F-actin by CrnΔCC and cofilin.
Yeast F-actin (5.0 μM) was stabilized with a rhodamine phalloidin/phalloidin mixture and after recording the initial rhodamine phalloidin fluorescence, the release of rhodamine phalloidin was monitored *via* a decrease in its fluorescence intensity (λ_{em}=575 nm) upon the addition of cofilin (5.5 μM, black curve), CrnΔCC (5.5 μM, red curve), or both (5.5 μM both, blue curve).

Crn∆CC decreases the accessibility of the nucleotide binding cleft.

Furthermore, we probed coronin's effect on another major structural element of F-actin, the nucleotide binding cleft site and the related intra-molecular rearrangements in actin protomers. It is possible that coronin induced changes in the nucleotide binding cleft, and/or in the sites impacted by the nucleotide cleft state, if present, are related to the increase in cofilin's severing activity. To assess whether such changes indeed occur in F-actin, we examined the effect of CrnΔCC on the nitromethane quenching of etheno-ADP (Ɛ-ADP) in F-actin (Figure 4.13). Stern-Volmer quenching constant (K_{SV}) values obtained in the absence and presence of CrnΔCC were 5.4 M^{-1} and 3.3 M^{-1}, respectively, which indicates that CrnΔCC induces perturbation in the nucleotide binding cleft and decreases the accessibility of the F-actin bound nucleotide to collisional quenchers. This effect was slightly more pronounced than that of cofilin (K_{SV}= 3.9 M^{-1}) and did not change significantly in the presence of both proteins (K_{SV}= 3.1 M^{-1}), suggesting a more dominant effect of coronin.

We also tested for the nucleotide binding cleft "closing" in the presence of coronin using two double cysteine yeast actin mutants, Q59C/D211C and S60C/D211C and homo-bi-functional, thiol specific reagents, methanothiosulfonates (MTS). MTS reagents have different spacer arm lengths and can therefore be used as molecular rulers. Residues 59 and 60 are located in subdomain 2 (SD2), on one side of the nucleotide cleft, whereas residue 211 is located in SD4 on the other side of the cleft (Figure 4.14A, inset). CrnΔCC decreases the cross-linking rates between residues S60C and D211C when any of the MTS reagents is used (data not shown). Results are however different with the Q59C/D211C mutant: Less cross-linking is observed on CrnΔCC decorated F-actin vs. bare F-actin in the presence of MTS1, whereas the opposite is true when MTS2 is used. MTS3 shows no significant difference in cross-linking percentage +/-

CrnΔCC (Figure 4.14A and B). These results suggest that CrnΔCC tightens the nucleotide binding cleft by stabilizing it in a particular semi-open conformation.

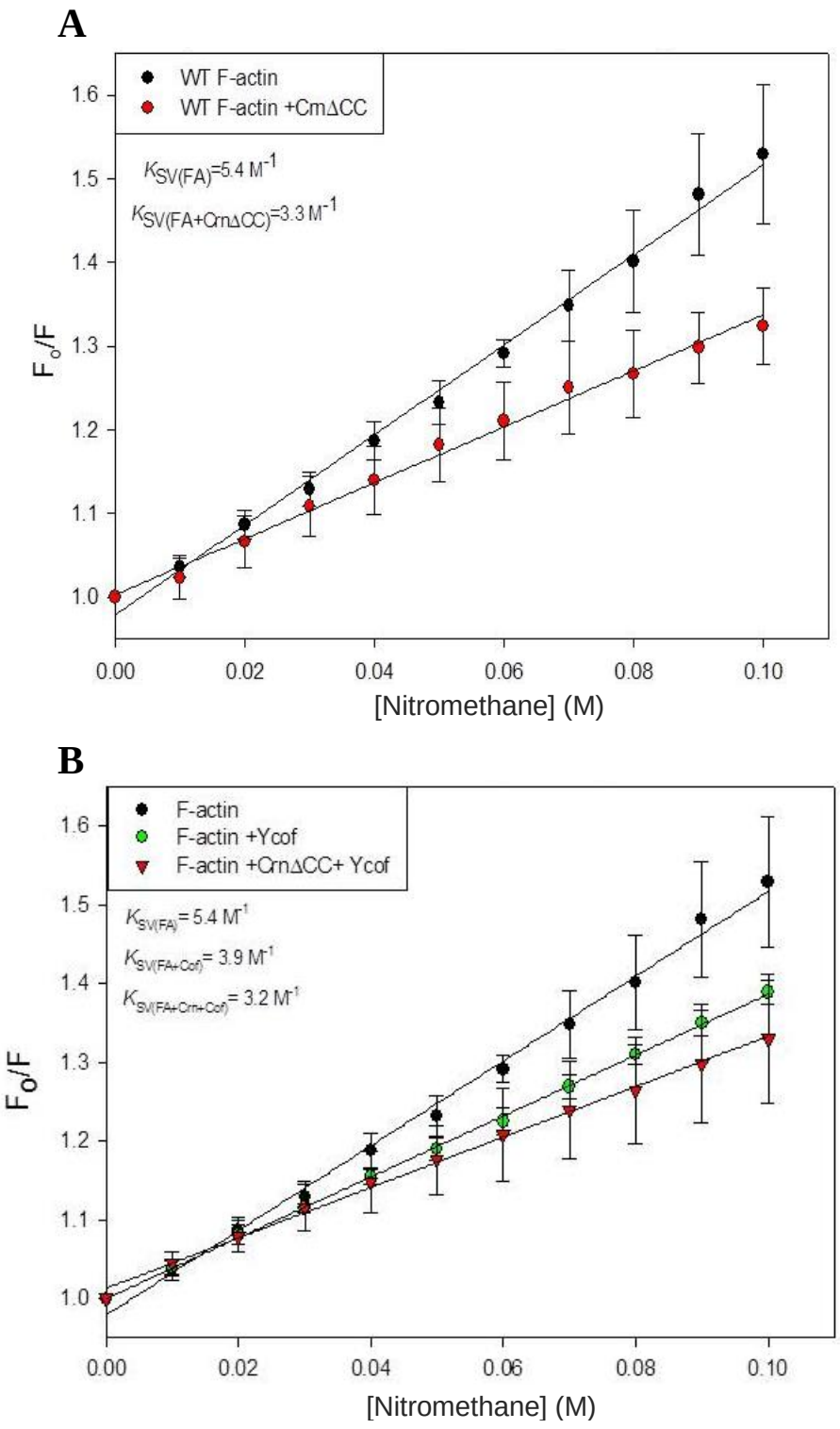

Figure 4.13- Effect of CrnΔCC on the nucleotide binding cleft of yeast F-actin. **A**, nitromethane quenching of Ɛ-ADP in 5 µM F-actin alone (●) and in the presence of 5.5 µM CrnΔCC (●). **B**, nitromethane quenching of Ɛ-ADP in 5 µM F-actin alone (●), in the presence of 5.5 µM Ycof (●), and 5.5 µM Ycof + CrnΔCC (▼).

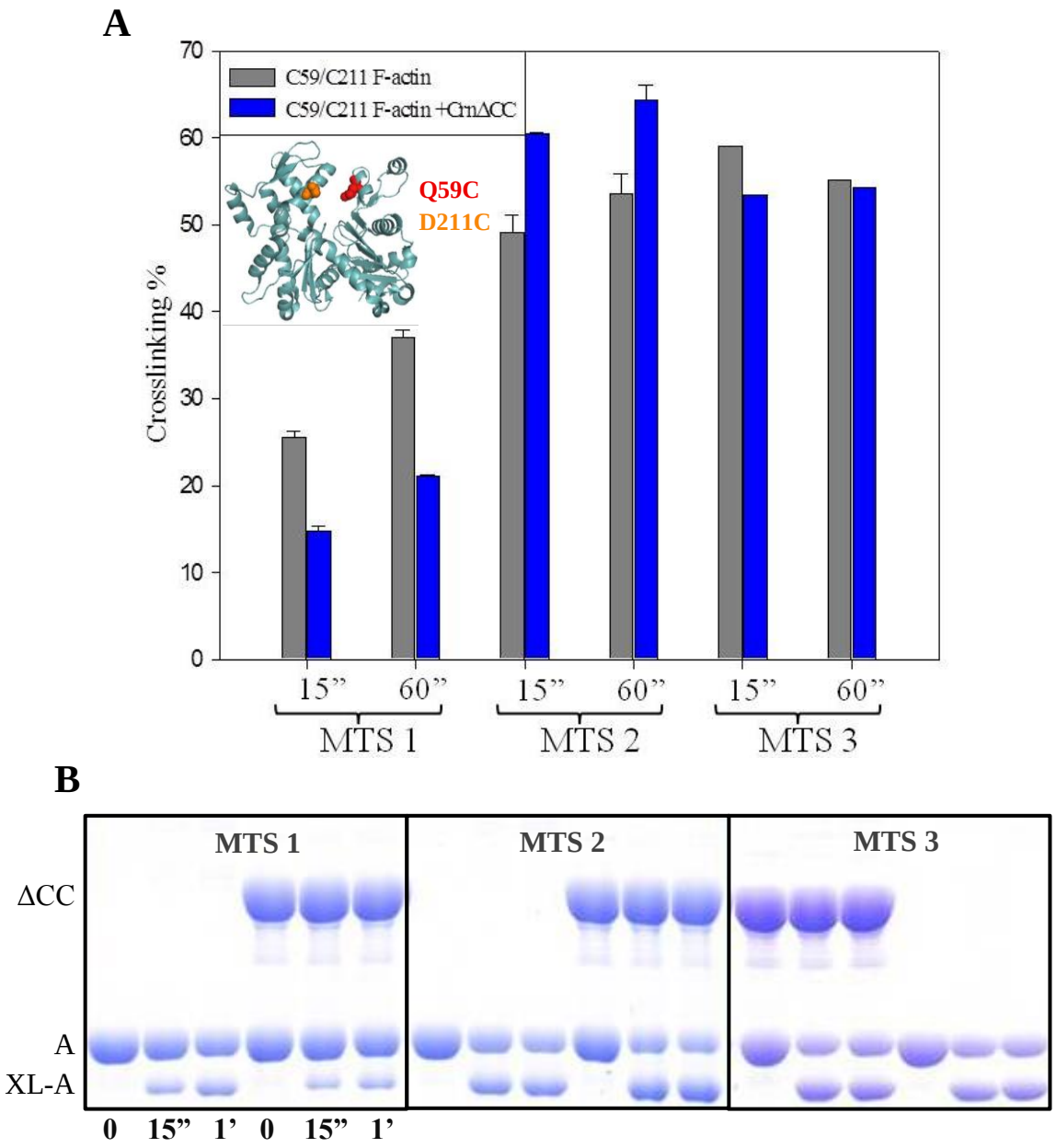

Figure 4.14- Effect of CrnΔCC on the nucleotide binding cleft of yeast F-actin.
A, cross-linking (%) of Q59C/D211C F-actin in the absence (grey bars) and presence (blue bars) of CrnΔCC using three different MTS reagents, MTS1 (5.4Å), MTS2 (5.9Å) and MTS3 (6.4Å). Cross-linking (%) was estimated as follows: [actin total (before the reaction) – uncross-linked actin monomer left after cross-linking time]/total actin, %.]; ***inset***, G-actin model showing mutated residue Q59C and D211C. **B,** SDS-PAGE patterns of the cross-linking reactions of C59/C211 yeast actin mutant; the final concentrations of actin and CrnΔCC were 10 μM each. The reactions were stopped with NEM after 15 sec and 1 min. Symbols A, XL-A and ΔCC correspond to actin, cross-linked actin and CrnΔCC, respectively. Relative intensities of protein bands were determined by densitometric analysis.

Effect of Crn∆CC on the structural elements of the actin filament.

To further study the effects of coronin on inter-protomer contacts in F-actin, specific single cysteine actin mutants were probed using fluorescence spectroscopy. As mentioned before, the D-loop is a highly dynamic structural element of actin that is involved in inter-protomer contacts in the longitudinal interface. Crystal structures of ADP-G-actin and ATP-G-actin along with metadynamic simulations propose an allosteric relationship between the D-loop conformation (ordered or disordered) and the nucleotide state of actin **(24, 25, 26)**. Cryo-EM 3-D reconstruction docks CrnΔCC next to the D-loop **(12)** and both Crn1 and CrnΔCC's affinity to F-actin have been linked to the nucleotide state of actin **(8, 10)**. In this work, three mutants were chosen along the D-loop, Q41C/C374S (C41), V45C/C374S (C45) and K50C/C374S (C50) to study the effect of CrnΔCC on the loop region. These mutants were labeled with the small fluorescent probe acrylodan, and the changes in the emission properties of acrylodan-actin upon CrnΔCC binding were followed. Coronin induced small changes in the emission spectra of acrylodan attached to these mutants (Figure 4.15). C41 showed a 5 nm red shift with a corresponding slight decrease in acrylodan fluorescence intensity, suggesting an exposure of the label upon coronin binding (Figure 4.15A, B and C). Acrylodan at residues C45 and C50 showed both a blue shift (3 nm and 7 nm, respectively) and an increase in the acrylodan fluorescence intensities, suggesting a burial of the label upon coronin binding (Figure 4.15A and B). Results of the C50 residue are in agreement with the cryo-EM model predictions **(12)**. The reactivity of these D-loop cysteines toward acrylodan was determined under pseudo-first-order reaction conditions (a representative plot for C45 modification by acrylodan is shown in Figure 4.16B). Interestingly, coronin had no effect on the reactivity of the cysteine introduced at residue 50, as

seen by a lack of change in label uptake upon its binding (Figure 4.16A); it however caused an increase in acrylodan label uptake for both C41 and C45 (Figure 4.16A). Although changes are overall small, our results show a structural effect of coronin on the D-loop region.

Using M1C/C374S yeast actin mutant (C1), we also probed the N-terminal region of actin located in its SD1. C1 conjugated acrylodan showed 10 nm blue shift with a corresponding increase of ~30% in its fluorescence intensity, suggesting the label is more buried upon coronin binding (Figure 4.15A and B). CrnΔCC was already shown to have an effect on the C-terminus of actin, as it also induced a blue shift along with a small increase in the fluorescence intensity (~15%). Although the C-and N-terminus are both located in SD1, they reside on opposite faces of this subdomain. According to the cryo-EM reconstruction data analysis, the N-terminus of actin is not located at the actin binding interface with coronin. Our results therefore show that coronin binding induces structural changes in this region of the actin molecule.

Another structural element, the H-loop, was also probed by looking at the effect of CrnΔCC on S265C/C374S yeast actin mutant (C265). Coronin binding causes no significant change in fluorescence emission (Figure 4.15A and B). Also, it does not have any effect on the reactivity of the cysteine introduced at this position, as it does not cause a change in the rate of acrylodan label uptake (Figure 4.16A).

W-loop residue 167's reactivity in the presence of coronin was also assessed using A167C/C374S yeast actin mutant. There is no change in acrylodan label uptake upon CrnΔCC binding (Figure 4.16A), suggesting that coronin does not have an effect on this important structural element of the actin filament.

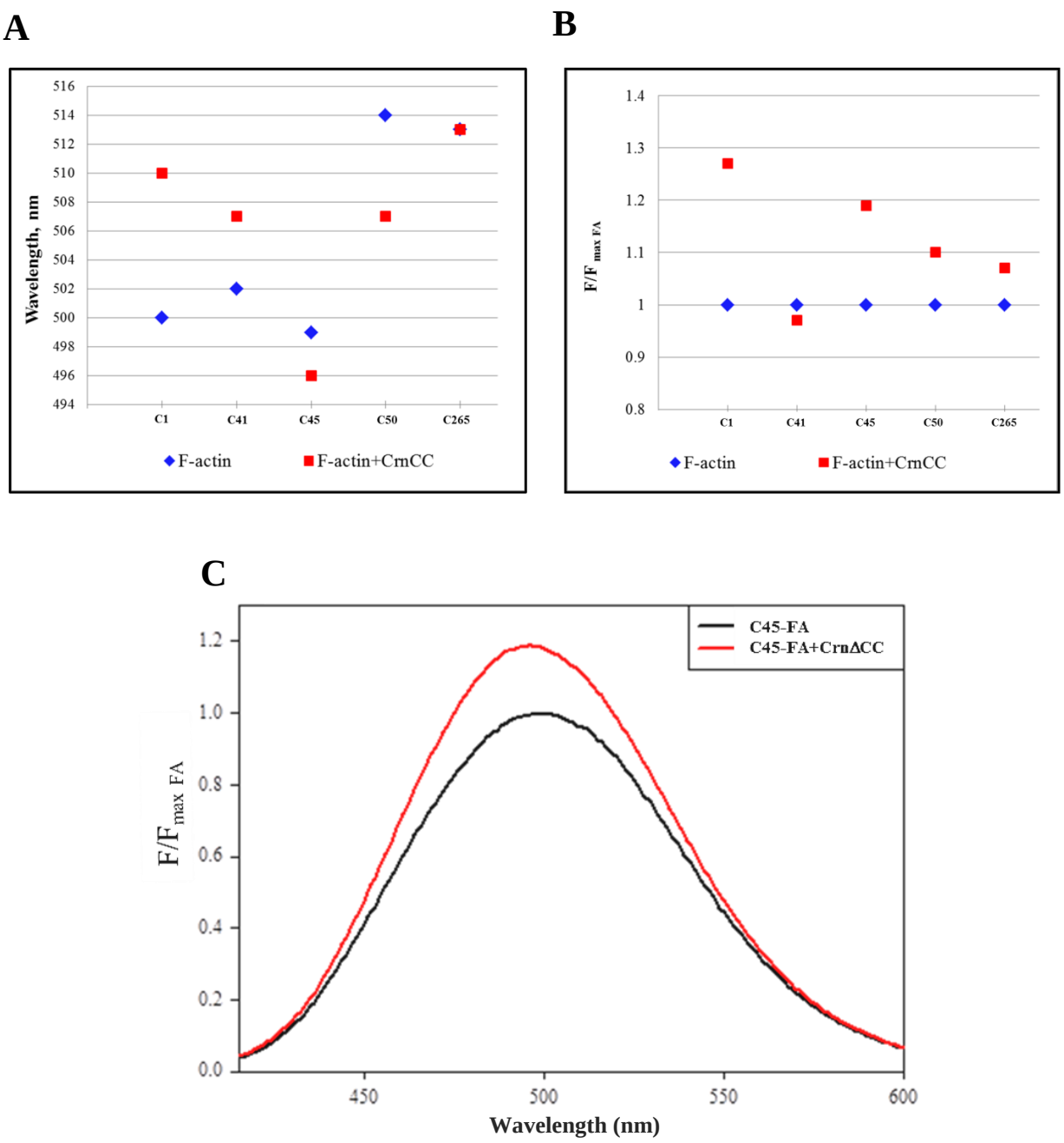

Figure 4.15- Cysteine scanning of yeast actin mutants with acrylodan.
A, λ_{max} of the fluorescence emission of acrylodan conjugated to cysteine mutants in F-actin alone (♦) or in the presence of CrnΔCC (■) versus mutant cysteine sequence position. **B**, Fluorescence emission at λ_{max} of acrylodan conjugated to cysteine mutants in F-actin alone (♦) or in the presence of CrnΔCC (■) versus mutant cysteine sequence position. Fluorescence intensities (F) are reported relative to that of actin mutant alone ($F_{max\ FA}$). **C,** Representative acrylodan emission spectra of Q45C/C374S yeast F-actin mutant alone (black trace), in the presence of CrnΔCC (red trace) are shown.

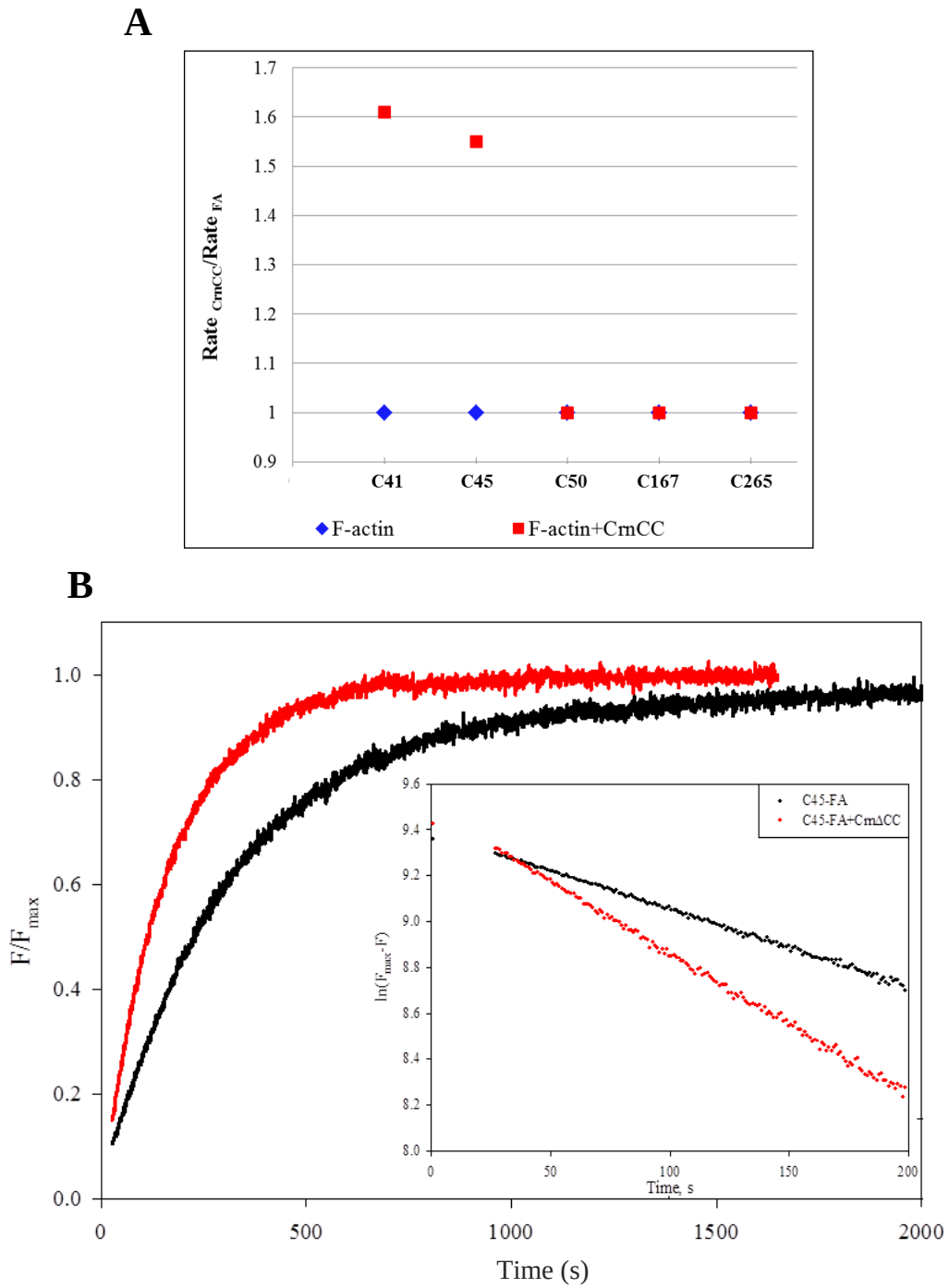

Figure 4.16- Acrylodan labeling of single cysteine yeast actin mutants.

A, acrylodan-labeling rates of single cysteine mutants alone (♦) and with CrnΔCC (■) as a function of sequence position. Modifications by acrylodan were monitored via fluorescence increase at 462 nm. The resulting rate constants were normalized to the rate constant of F-actin, under pseudo-first-order conditions. **B**, Representative acrylodan labeling plot of V45C/C374S actin is shown. The rate of V45C/C374S F-actin labeling in the presence of CrnΔCC (red trace) increased approximately 1.8-fold over that of F-actin alone (black trace).

CrnΔCC restores the polymerization of TMR-actin.

Modification of Cys374 on rabbit skeletal actin with tetramethylrhodamine-maleimide (TMR) blocks actin polymerization into filaments **(24, 25, 27).** It is assumed that the probe occupies a hydrophobic pocket in the cleft between SD1 and SD3, the same position where other depolymerizing factors, such as gelsolin segment 1 and vitamin D-binding protein bind, blocking the interactions of subdomain 2 with that site **(28)**. Cofilin was shown to rescue the polymerization of TMR-actin **(29)**; it bridges between SD1-3 and SD2 of two adjacent protomers, establishing new inter-protomer contacts that substitute for the disrupted longitudinal interface. We used it here for comparison with the effect of coronin on TMR-actin polymerization (Figure 4.17A and B). Similarly to cofilin, CrnΔCC also restores the polymerization of TMR-modified actin as indicated by the observed increase in light scattering (Figure 4.17A and B). This rescue is effective both when coronin is added to TMR-actin after it failed to polymerize for ~12 minutes on its own (with $MgCl_2$ and KCl) and when it is premixed with TMR-G-actin before the addition of $MgCl_2$ and KCl. Electron microscopy (EM) images do not show any filaments of TMR-actin alone, however filaments can be observed when coronin is added to the sample (Figure 4.17C and D). The observed increase in light scattering is indeed due to at least partial filament formation and not protein aggregation. Notably, the rescue of filament formation from TMR-actin by coronin and cofilin appears equally efficient.

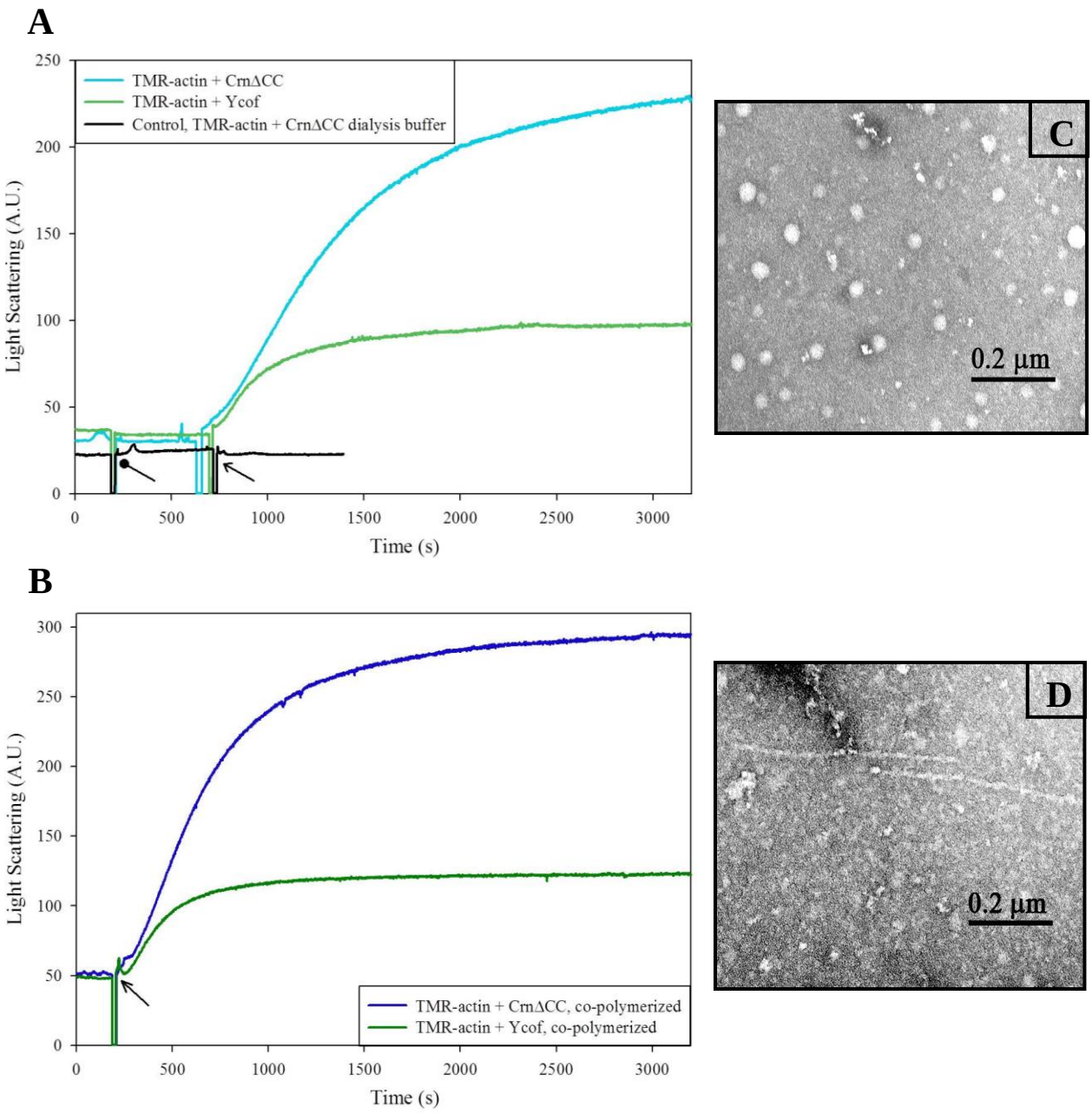

Figure 4.17-CrnΔCC rescues the polymerization of TMR labeled actin.
These experiments were carried out with different TMR-yeast actin preparations yielding similar results. Representative plots are shown. **A**, (*black trace*) neither addition of polymerizing salts (3.0 mM $MgCl_2$ & 50 mM KCl, (● *arrow*) nor addition of CrnΔCC dialysis buffer (*arrow*) changed the light-scattering from 10 µM ATP-G-TMR-actin. Alternative addition of 10 µM CrnΔCC (*light blue trace*) or 10 µM cofilin (*light green trace*) were made after the same initial incubation time (*indicated by the same arrow*) and caused fast polymerization of TMR-G-actin. **B**, 10 µM Mg-TMR-actin was polymerized at 25 °C with 3 mM $MgCl_2$ and 50 mM KCl in the presence of 10 µM CrnΔCC (*dark blue trace*), or 10 µM Ycof (*dark green trace*). At the time points indicated by (*arrow*), polymerizing salts (3.0 mM $MgCl_2$+ 50 mM KCl) were added. *A.U.*, arbitrary units. EM images of TMR-actin alone **(C)** and in the presence of CrnΔCC **(D)** are shown**.**

CrnΔCC increases the melting temperature of ADP-F-actin.

Equimolar amounts of CrnΔCC increase the melting temperature (Tm) of ADP-F-actin by 1.3°C +/- 0.1°C in DSC assays (Figure 4.18), which is consistent with F-actin stabilization. CrnΔCC does not change the Tm of BeFx-ADP-F-actin, which is already higher than that of ADP-F-actin. Thus, there is no further stabilization of BeFx-ADP-F-actin by the addition of coronin. The effect of coronin on the melting temperature of F-actin is reproducible but small. This can be attributed to the fact that CrnΔCC itself undergoes a thermal unfolding with a Tm at 48°C, i.e. 15°C below that of F-actin (Figure 4.18). Considering the fact that there is no overlap between the CrnΔCC and F-actin melting peaks, and the relatively high temperature, it is possible that only a fraction of coronin remains bound to the filaments and is protected from melting under the conditions of our DSC experiments. The stabilizing effect of coronin is therefore most likely underestimated in this assay.

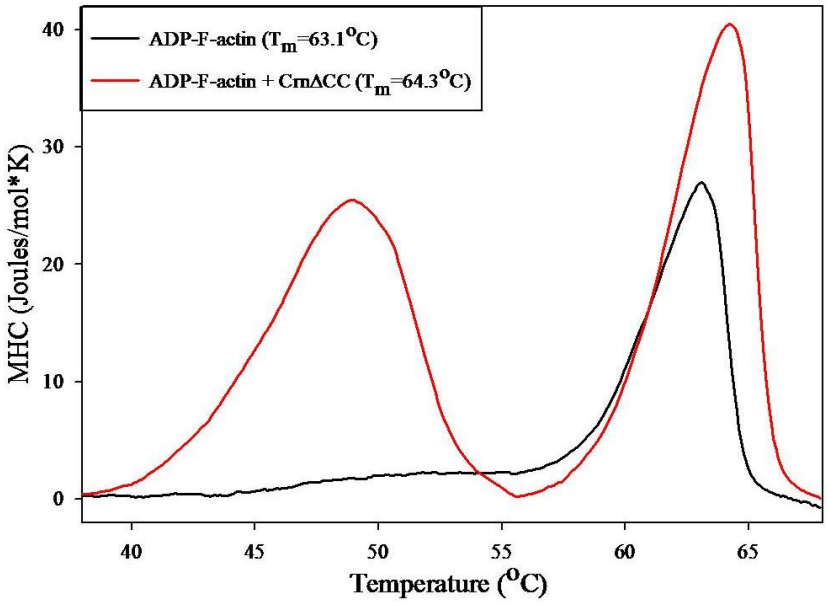

Figure 4.18- CrnΔCC increases the stability of yeast F-actin.
DSC scans showing molar heat capacity (MHC) of 15 μM yeast F-actin alone (black trace) and in the presence of 15 μM CrnΔCC (red trace). Similar results were reproduced in two independent experiments. Representative plots are shown.

DISCUSSION

In this chapter, CrnΔCC's effects on the structure and dynamics of actin filaments were examined using a combination of methods, including site-directed mutagenesis, solution biochemistry assays, fluorescence measurements, chemical cross-linkings, and electron and TIRF microscopy.

Crn1 enhances cofilin's severing activity of ADP-F-actin but is also suspected to sever actin filaments independently of other factors **(10)**. Moreover, EM and atomic force microscopy (AFM) images (Reisler lab, unpublished data) observations implied a severing activity of F-actin by CrnΔCC on its own. Earlier seeded polymerization assays had also pointed towards a severing role of CrnΔCC; an increase in the assembly rate of actin was observed when CrnΔCC was incubated with the pre-formed F-actin before the pyrene-labeled monomeric actin was added. The increase in cofilin severing of actin filaments could be due to an additive effect of the two proteins. To test the possibility of independent severing of actins filaments by CrnΔCC we used real-time TIRF microscopy. In these experiments no breaks occurred in F-actin over 15 minutes incubation time under different pH conditions.

The above conclusion was confirmed in seeded polymerization assays modified such that F-actin would be handled more "gently" to minimize any potential shearing caused by mixing or pipetting. Our results showed that CrnΔCC does not increase the assembly rate of actin (Figure 4.2A and B). In addition, the average filament length was measured to be the same with or without coronin when actin filaments were immobilized on poly-Lysine slips and imaged by TIRF microscopy (Figure 4.3). It appears that prior indications of filament severing by coronin might be due to its effect on their mechanical properties. Coronin may decrease the mechanical stability of filaments and increase their shearing when subjected to mechanical stress. *In vitro*,

this could be induced by “harsh” handling procedures such as vortexing and pipetting while *in vivo*, this could be caused by cellular functions and the presence of other structural elements and/or proteins. This possibility requires further scrutiny.

The role of coronin in the plasticity of the actin cytoskeleton is undeniably important in the immune system cells, cancer cell proliferation and neurite outgrowth. Many studies that have been conducted in which “coronin-mediated mechanisms” have been tampered with show defects in these various cellular processes. Most strikingly, coronin 1 deficiencies give rise to immune deficiencies in mice and humans that are characterized by severe T lymphocytopenia, whereas complete absence of coronin-1A—the hematopoietic-specific member of the Coronin family— is associated with severe combined immunodeficiency in humans **(30)**. Recent reports identified Coronin-1A as a mediator of the critical role of F-actin deconstruction in cytotoxic function and immunological secretion. Using super-resolution nanoscopy, mammalian Coronin-1A was demonstrated to promote the deconstruction of F-actin density that facilitates effective delivery of lytic granules to the immunological synapse **(31)**. In vitro studies also suggested Coronin-1A to have a suppressive effect on neurite outgrowth by inhibiting the polymerization of actin filaments **(32)**. Also, new findings suggest that the post-transcriptional silencing of Coronin-1C by a microRNA, miR-206, reduces tumor cell migration and affects the actin skeleton and cell morphology in triple-negative breast cancer (TNBC) cells **(33)**.

CrnΔCC rescues the polymerization of TMR-labeled yeast and skeletal actin as observed by light scattering and EM. This result is in agreement with the increase in longitudinal disulfide cross-linking of Q41C yeast actin mutant by CrnΔCC and the EM evidence of coronin’s contacts with two actin protomers in the filament. The acceleration of disulfide formation by CrnΔCC suggests a decrease in the time average mean distance between Cys-374 and the DNase I binding

loop on adjacent actin protomers in F-actin. This could lead to tighter contacts between the two regions, providing increased stability to the actin filament. Because of dynamic motions within the filaments, certain unfavorable states are allowed to occur, albeit infrequently. Our results suggest that coronin increases the frequency of the filament-preferred states and reduces the amplitude of the destabilizing states by reducing their occurrence frequency.

The nucleotide binding cleft is a major structural element of actin. Coronin related changes in the nucleotide and phosphate site on actin were assessed by looking at the effect of a quencher (nitromethane) on the etheno-nucleotide bound to F-actin. CrnΔCC's recognition of the nucleotide binding cleft is indicated by an increase in the fluorescence emission and a decrease in the accessibility of etheno-ADP to collisional quenchers (nitromethane) in the presence of CrnΔCC. This decrease in accessibility could be due to a tighter conformation of the nucleotide cleft in the presence of coronin, or to a steric hindrance imposed by coronin binding to the actin filament. We tested for the nucleotide binding cleft "closing" in the presence of coronin using two double cysteine yeast actin mutants, Q59C/D211C and S60C/D211C, and homo-bifunctional, thiol specific reagents, methanothiosulfonates (MTS). CrnΔCC decreased the cross-linking rates between residues S60C and D211C with all three MTS reagents and this indicates a decrease in the average distance between the two residues. Although CrnΔCC had a different effect on the cross-linking of Q59C and D211C with each of the MTS reagents, the overall effect was also a decrease in the mean distance between the two residues. One possible interpretation of our results is that CrnΔCC tightens the nucleotide binding cleft by stabilizing it in a particular semi-open conformation, reducing its flexibility to open and close. These results are in agreement with the collisional quenching experiments, since rendering the cleft less flexible would decrease the accessibility of the bound nucleotide to collisional quenchers.

Some of the inter-protomer actin cross-linkings explored in this work occur because of dynamic motions within the filaments, which involve also "visiting" infrequently populated states that destabilize actins filaments structure (C50-C265 and C50-C167 cross-linkings are shown in figures 4.8 and 4.10, respectively). These cross-linkings were enhanced by cofilin yet inhibited by coronin. This finding attests to the opposite effects these two proteins have on the actin filament dynamics. Cofilin binding increases the occurrence of these low frequency states, as it enhances filament dynamics. Cofilin may even stabilize the formation of such states by providing additional contacts that block filament disruption. In contrast, coronin is limiting some of the filament dynamics and decreasing the probability of transient occurrence of unstable conformations. Coronin's ability to bind to two or three actin protomers in the filament appears sufficient, however, to allow for its ability to rescue the polymerization of actin dimers trapped by cross-linking in conformations which do not favor their filament formation. These results point yet again to decreased dynamics of coronin-actin filaments and/ or increased rigidity.

In contrast to the acceleration of Q41C cross-linking, CrnΔCC inhibited the lateral disulfide cross-linking of S265C yeast actin mutant (Figure 4.7). The inhibition of disulfide formation suggests that coronin binding causes an increase in the mean distance between Cys-374 and the hydrophobic loop, either by shifting the H-loop away or by inhibiting its close approach to the C-terminus of the adjacent protomer in F-actin. The H-loop is one of actin's structural elements and its mobility is necessary for filament stability; when the loop is locked by intra-molecular disulfide bond formation to the surface of the G-actin monomer, filaments are not formed **(34)**. Cofilin also inhibits the cross-linking of Cys374 to Cys265 **(23)**, whereas phalloidin accelerates the cross-linking by stabilizing the extension of the H-loop to the opposite strand **(35)**. Phalloidin is a cyclic-peptide toxin which stabilizes actin filaments by promoting

inter-strand contacts on the lateral interface **(21, 34, 36)**, whereas cofilin destabilizes actin filaments by weakening the lateral contacts of the actin filament **(23, 37)** and their binding to actin filaments is mutually exclusive **(15, 38)**. The inhibition of the S265C cross-linking is the only effect shared by both coronin and cofilin. Independently, the two proteins induce opposite effects on all the other cross-linkings, but when added together the effect of cofilin is the dominating one. Because of their similar effect with the S265C cross-linking, it was interesting to look at coronin's effect on the release of phalloidin, which would shed further light on its effect on the lateral filament contacts. This was done by using rhodamine phalloidin as a fluorescent probe. Although coronin on its own did not cause the release of rhodamine-phalloidin, it highly accelerated the release induced by cofilin. This effect could be due to coronin causing an increased destabilization of the lateral interface, potentially allowing a faster binding of cofilin and intensifying its effect on the release of phalloidin.

To test for that, we looked at the effect of CrnΔCC on the binding of yeast cofilin to BeFx-F-actin. Beryllium fluoride (BeFx)—an inorganic phosphate (Pi) analog—belongs to the group of F-actin stabilizing factors, along with aluminum fluoride (AlF_4) and phalloidin. These small molecules are antagonistic to ADF/cofilin binding and stabilize F-actin by reducing the critical concentration for polymerization and introducing conformational changes in the filament structure. BeFx stabilizes in particular the structure of subdomain 2, as indicated by strong and cooperative inhibition of its cleavage by subtilisin (in the DNase I binding-loop (D-loop)) and trypsin (in the 60–69 loop) **(39)**, and by electron microscopy studies **(40)**. The complexes of beryllium and aluminum with fluoride were found to be good structural analogs of Pi **(41)** and are widely used in studying the activity of various nucleotide binding proteins. Yeast cofilin binds to BeFx-F-actin, albeit at a much slower rate and lower affinity than to F-actin **(42)**. This

yields a system that allows for easier detection of any improvement in its binding to F-actin. Although Pi alone also inhibits the binding of yeast cofilin to F-actin **(43)**, BeFx binds to F-actin with orders of magnitude higher affinity ($K_d = 2\ \mu M$) than Pi ($K_d = 1.5$ mM) **(44)**. BeFx competes with Pi for binding to the nucleotide-binding cleft of ADP-F-actin protomers at the place of the γ-phosphate of ATP **(45)** without altering the ionic strength of the solution; this makes it a more suitable choice for our experimental purposes. Our results show that CrnΔCC indeed increases the binding of yeast cofilin to yeast BeFx-F-actin, as measured by co-sedimentation assays (Figure 4.19). A conversation with members of the Goode lab during a poster presentation at the 2013 American Society of Cell Biology meeting further validated our interesting results. Multi-color TIRF microscopy was used in real-time for spatial and temporal assays of effects of coronin on cofilin-mediated actin severing to show coronin accelerated cofilin decoration of filaments and enhanced severing by 6-10 fold. However, the time interval from appearance of cofilin decoration to severing was not altered (unpublished results, Goode lab).

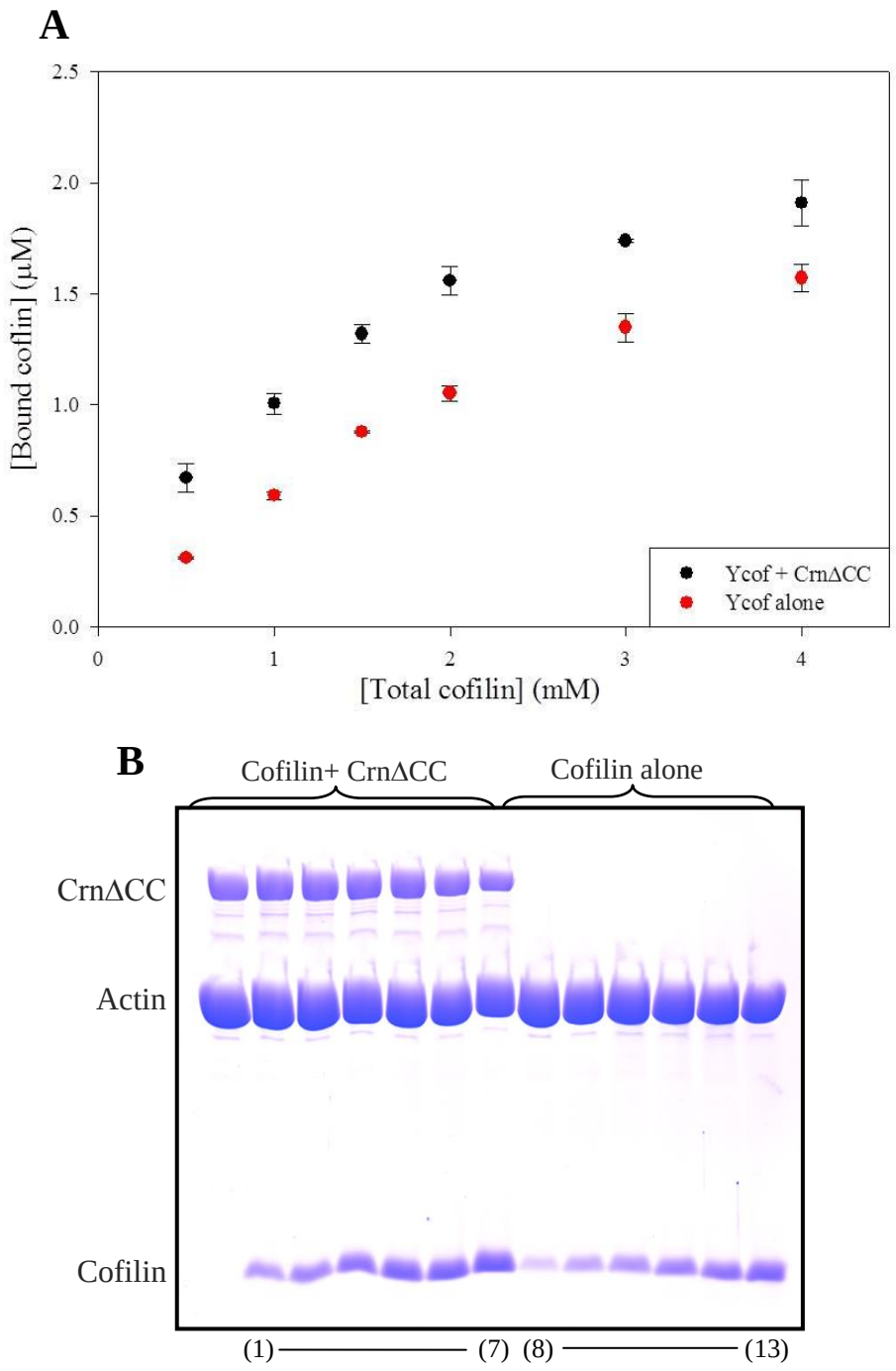

Figure 4.19- The effect of CrnΔCC on the binding of cofilin to BeFx-F-actin.

A, plots of amount of cofilin bound to BeFx-F-actin as measured by high speed co-sedimentation assays and quantified from SDS-PAGE patterns in the absence of CrnΔCC (●) and in its presence (●). ***B***, SDS-PAGE patterns of 4 µM BeFx-F-actin pelleted with varying amounts of cofilin (0.5, 1, 1.5, 2, 3, and 4 µM) in the presence (*lanes 1-7*) and absence (*lanes 8-13*) of 2 µM CrnΔCC; the pellets were concentrated 5X by re-suspending them in a smaller volume.

Taken together, our results provide a plausible two-fold mechanism for the synergistic effect CrnΔCC has on the severing activity of cofilin. Coronin increases the binding of cofilin to the actin filament and causes also slight structural changes that promote severing by cofilin. Cofilin binding lowers both the persistence length of actin filaments and the filament flexural rigidity by approximately 5-fold **(46).** The increased flexibility of cofilin-decorated filaments results from reorganization of actin subdomain 2 **(18, 47, 48, 49)** and as a consequence promotes severing due to a mechanical asymmetry **(50, 51)**. Coronin-induced changes in filament dynamics and/or rigidity further promotes this mechanical asymmetry as it generates a bigger change in stiffness between coronin bound regions and those where cofilin is bound and causes the increase in cofilin's severing of actin filaments.

Overall, our results shed light on the structural changes that coronin induces in actin filaments, and provide a plausible mechanism by which coronin mediates cofilin-induced disassembly of actin filaments.

REFERENCES

1. Humphries C.L., Balcer H.I., D'Agostino J.L., Winsor B., Drubin D.G., Barnes G., Andrews B.J., Goode B.L. (2002). Direct regulation of Arp2/3 complex activity and function by the actin binding protein coronin. *J. Cell Biol.* **159,** 993-1004.
2. Bharathi V., Pallavi S.K., Bajpai R., Emerald B.S., Shashidhara L.S. (2004). Genetic characterization of the Drosophila homologue of coronin. *J. Cell Sci*. **117**, 1911-22.
3. Yan M., Di Ciano-Oliveira C., Grinstein S., Trimble W.S. (2007). Coronin function is required for chemotaxis and phagocytosis in human neutrophils. *J. Immunol. 178,* 5769-78.
4. Cai L., Marshall T.W., Uetrecht A.C., Schafer D.A., Bear J.E. (2007). Coronin 1B coordinates Arp2/3 complex and cofilin activities at the leading edge. *Cell*. **128**, 915–29.
5. Föger N., Rangell L., Danilenko D.M., Chan A.C. (2006). Requirement for coronin 1 in T lymphocyte trafficking and cellular homeostasis. *Science.* **313**, 839-42.
6. Liu S.L., Needham K.M., May J.R., Nolen B.J. (2011). Mechanism of a concentration-dependent switch between activation and inhibition of Arp2/3 complex by coronin. *J. Biol. Chem.* **286,** 17039-46.
7. Goode B.L., Wong J.J., Butty A.C., Peter M., McCormack A.L., Yates J.R., Drubin D.G., Barnes G. (1999). Coronin promotes the rapid assembly and cross-linking of actin filaments and may link the actin and microtubule cytoskeleton in yeast. *J. Cell. Biol.* **144**, 83-98.
8. Cai L., Makhov A.M., Bear J.E. (2007). F-actin binding is essential for coronin 1B function in vivo. *J. Cell Sci*. **120**, 1779–90.
9. Brieher W.M., Kueh H.Y., Ballif B.A., Mitchison T.J. (2006). Rapid actin monomer-insensitive depolymerization of Listeria actin comet tails by cofilin, coronin and Aip1. *J. Cell Biol.* **175**, 315–24.
10. Gandhi M., Achard V., Blanchoin L., Goode B.L. (2009). Coronin switches roles in actin disassembly depending on the nucleotide state of actin. *Mol. Cell*. **34**, 364-374.
11. Ono S. (2003). Regulation of actin filament dynamics by actin depolymerizing factor/cofilin and actin-interacting protein 1: new blades for twisted filaments. *Biochemistry*. **42**, 13363-70.
12. Ge P., Durer Z.A., Kudryashov D., Zhou Z.H., Reisler E. (2014). Cryo-EM reveals different coronin binding modes for ADP- and ADP-BeFx actin filaments. *Nat. Struct. Mol. Biol*. **21**, 949-54.

13. Spudich J.A. and Watt S. (1971). The regulation of rabbit skeletal muscle contraction. I. Biochemical studies of the interaction of the tropomysion-troponin complex with actin and the proteolytic fragments of myosin. *J. Biol. Chem*. **246**, 4866-71.
14. Grintsevich E.E., Galkin V.E., Orlova A., Ytterberg A.J., Mikati M.M., Kudryashov D.S., Loo J.A., Egelman E.H., Reisler E. (2010). Mapping of drebrin binding site on F-actin. *J. Mol. Biol*. **398,** 542-54.
15. McGough A., Pope B., Chiu W., Weeds A. (1997). Cofilin changes the twist of F-actin: implications for actin filament dynamics and cellular function. *J Cell Biol.* **138**, 771–81.
16. Pavlov D., Muhlrad A., Cooper J., Wear M., Reisler E. (2007). Actin filament severing by cofilin. *J. Mol. Biol*. **365**, 1350-58.
17. Andrianantoandro E. and Pollard T.D. (2006). Mechanism of actin filament turnover by severing and nucleation at different concentrations of ADF/cofilin. *Mol. Cell*. **24**, 13-23.
18. Bobkov A.A., Muhlrad A., Kokabi K., Vorobiev S., Almo S.C., Reisler E. (2002). Structural effects of cofilin on longitudinal contacts in F-actin. *J. Mol. Biol.* **323**, 739-50.
19. Oztug Durer Z.A., Diraviyam K., Sept D, Kudryashov D.S., Reisler E. (2010). F-actin structure destabilization and DNase I binding loop: fluctuations mutational cross-linking and electron microscopy analysis of loop states and effects on F-actin. *J. Mol. Biol*. **395**, 544-57.
20. Lorenz M., Popp D., Holmes K.C. (1993). Refinement of the F-actin model against X-ray fiber diffraction data by the use of a directed mutation algorithm. *J. Mol. Biol.* **234**, 826-36.
21. Steinmetz, M., Stoffler, D., Muller, S., Jahn, W., Wolpensinger, B., Goldie, N. (1998). Evaluating atomic models of F-actin with an undecagold-tagged phalloidin derivative. *J. Mol. Biol*. **276**, 1−6.
22. Faulstich H., Schäfer A.J., Weckauf M. (1977). The dissociation of the phalloidin-actin complex. *Hoppe Seylers Z. Physiol. Chem*. **358**, 181-84.
23. Bobkov A.A., Muhlrad A., Shvetsov A., Benchaar S., Scoville D., Almo S.C., Reisler E. (2004). Cofilin (ADF) affects lateral contacts in F-actin. *J Mol Biol*. **337**, 93-104.
24. Otterbein L.R., Graceffa P., Dominguez R. (2001). The Crystal Structure of Uncomplexed Actin in the ADP State. *Science.* **293**, 708-11.
25. Graceffa P., Dominguez R. (2003). Crystal structure of monomeric actin in the ATP state. Structural basis of nucleotide-dependent actin dynamics. *J. Biol. Chem*. **36**, 34172-80.

26. Pfaendtner J., Lyman E., Pollard T.D., Voth G.A. (2010). Structure and dynamics of the actin filament. *J. Mol. Biol*. **396**, 252-63.
27. Kudryashov D.S., Phillips M., Reisler E. (2004) Formation and destabilization of actin filaments with tetramethylrhodamine-modified actin. *Biophys. J*. **87,** 1136-45.
28. Dominguez R. (2004). Actin-binding proteins—a unifying hypothesis. *Trends Biochem Sci.* **29**, 572-78.
29. Kudryashov D.S., Galkin V.E., Orlova A., Phan M., Egelman E.H., Reisler E. (2006) Cofilin cross-bridges adjacent actin protomers and replaces part of the longitudinal F-actin interface. *J Mol Biol*. **358,** 785-97.
30. Moshous D., de Villartay J.P. (2014). The Expanding Spectrum of Human coronin 1A deficiency. *Curr. Allergy Asthma Rep*. **12**, 481.
31. Mace E.M., Orange J.S. (2014). Lytic immune synapse function requires filamentous actin deconstruction by Coronin 1A. *Proc. Natl. Acad. Sci. U.S.A.* **18**, 6708-13.
32. Terzi Y.K., Kocaefe Y.C., Ayter S. (2014). Coronin 1A inhibits neurite outgrowth in PC12 cells. *Neurosci. Lett*. **582**, 38-42.
33. Wang J., Tsouko E., Jonsson P., Bergh J., Hartman J., Aydogdu E., Williams C. (2014). MiR-206 inhibits cell migration through direct targeting of the actin-binding protein Coronin 1C in triple-negative breast cancer. *Mol. Oncol*. **14**, 161-66.
34. Shvetsov, A., Musib, R., Phillips, M., Rubenstein, P. A., and Reisler, E. (2002). Locking the Hydrophobic Loop 262−274 to G-Actin Surface by a Disulfide Bridge Prevents Filament Formation. *Biochemistry*. **41**, 10787−93.
35. Scoville D., Stamm J.D., Toledo-Warshaviak D., Altenbach C., Phillips M., Shvetsov A., Rubenstein P.A., Hubbell W.L., Reisler E. (2006). Hydrophobic loop dynamics and actin filament stability. *Biochemistry*. **45**, 13576-84.
36. Dancker, P., Low, I., Hasselbach, W., and Wieland, T. (1975). Interaction of Actin with Phalloidin: Polymerization and Stabilization of F-actin. *Biochim. Biophys. Acta.* **400**, 407−14.
37. McGough A, Chiu W. (1999). ADF/cofilin weakens lateral contacts in the actin filament. *J Mol Biol.* **291**, 513-19.
38. Hayden S.M., Miller P.S., Brauweiler A., Bamburg J.R. *(*1993). Analysis of the interactions of actin depolymerizing factor with G- and F-actin. *Biochemistry.* **32,** 9994–10004.

39. Muhlrad A., Cheung P., Phan B.C., Miller C., Reisler E. (1994). Dynamic properties of actin. Structural changes induced by beryllium fluoride. *J. Biol. Chem*. **269**, 11852-58.
40. Orlova A., Egelman E.H. (1992). Structural basis for the destabilization of F-actin by phosphate release following ATP hydrolysis. *J. Mol. Biol*. **227**, 1043-53.
41. Chabre M. (1990). Aluminofluoride and beryllofluoride complexes: a new phosphate analogs in enzymology. *Trends Biochem. Sci*. **15**, 6-10.
42. Muhlrad A., Ringel I., Pavlov D., Peyser Y.M., Reisler E. (2006). Antagonistic effects of cofilin, beryllium fluoride complex, and phalloidin on subdomain 2 and nucleotide-binding cleft in F-actin. *Biophys. J*. **91**, 4490-99.
43. Muhlrad A., Pavlov D., Peyser Y.M., Reisler E. (2006). Inorganic phosphate regulates the binding of cofilin to actin filaments. *FEBS J*. **273**, 1488-96.
44. Carlier M.F., Pantaloni D. (1988). Binding of phosphate to F-ADP-actin and role of F-ADP-Pi-actin in ATP-actin polymerization. *J. Biol. Chem*. **263**, 817-25.
45. Combeau C., Carlier M.F. (1988). Probing the mechanism of ATP hydrolysis on F-actin using vanadate and the structural analogs of phosphate BeF-3 and A1F-4. *J. Biol. Chem*. **263**, 17429-36.
46. McCullough B.R., Blanchoin L., Martiel J.L., De la Cruz E.M. (2008). Cofilin increases the bending flexibility of actin filaments: implications for severing and cell mechanics. *J. Mol. Biol*. **38**, 550-58.
47. Galkin V.E., Orlova A., Kudryashov D.S., Solodukhin A., Reisler E., Schröder G.F., Egelman E.H. (2011). Remodeling of actin filaments by ADF/cofilin proteins. *Proc. Natl. Acad. Sci. U S A*. **108**, 20568-72.
48. Paavilainen V.O., Oksanen E., Goldman A., Lappalainen P. (2008). Structure of the actin-depolymerizing factor homology domain in complex with actin. *J. Cell Biol*. **182**, 51-9.
49. Muhlrad A., Kudryashov D., Michael Peyser Y., Bobkov A.A., Almo S.C., Reisler E. (2004). Cofilin induced conformational changes in F-actin expose subdomain 2 to proteolysis. *J. Mol. Biol*. **342**, 1559-67.
50. Bobkov A.A., Muhlrad A., Pavlov D.A., Kokabi K., Yilmaz A., Reisler E. (2006). Cooperative effects of cofilin (ADF) on actin structure suggest allosteric mechanism of cofilin function. *J. Mol. Biol*. **356**, 325-34.

51. Suarez C., Roland J., Boujemaa-Paterski R., Kang H., McCullough B.R, Reymann A.C., Guérin C., Martiel J.L., De la Cruz E.M., Blanchoin L. (2011). Cofilin tunes the nucleotide state of actin filaments and severs at bare and decorated segment boundaries. *Curr. Biol.* **10**, 862-68.

CHAPTER 5
Conclusion

Actin is a highly conserved cytoskeletal protein and the most abundant in virtually all eukaryotic cells. Rapid remodeling of the actin cytoskeleton is essential for many cellular processes including cell growth, differentiation, division and motility. However, without "accessory" proteins, actin-based processes will not proceed fast enough in response to stimuli in the cell. These actin-associated proteins are numerous and important in the reconfiguration of actin networks *in vivo*. Each protein has its own role, timing and location of action, but they all act in concert to control and regulate the processes and mechanisms by which the actin cytoskeleton is remodeled. Understanding the biochemical and cellular aspects of the interactions of these proteins with actin is crucial as it leads to a better understanding of the structure and dynamics of the actin cytoskeleton. This dissertation focuses on characterizing the mechanisms of drebrin, coronin and cofilin interactions with actin and studying their independent and inter-dependent roles in actin structure and dynamics.

We first mapped the DrABD binding interface on actin filaments. Our results reveal polymorphism of DrABD binding to F-actin and suggest the existence of two binding sites. Despite a difference in affinities (K_d~7.5 μM for DrABD and ~0.17 μM for Drb1-300), the same modes of F-actin binding and binding polymorphism are observed for both DrABD and Drb1-300 constructs. DrABD binding is centered on actin subdomain 2 and bridges two adjacent actin protomers. This DrABD binding site overlaps with the cofilin binding site on F-actin, which would explain the competition between these two proteins **(1)**. Our results also explain the observed displacement of α–actinin from dendritic spines by drebrin overexpression. The binding site of both proteins are found to involve the C-terminus of actin and an overlapping region in SD1, namely actin residues 86-117 for α–actinin and actin residues 99-107 for DrABD. This study was therefore important as it provided structural insight into the reciprocal

relationship between drebrin and other ABPs that are also involved in the regulation of the actin cytoskeleton in neuronal cell.

Next, using depolymerization assays, differential scanning calorimetry (DSC), and polymerization deficient actins as tools, we demonstrate that F-actin is stabilized by drebrin binding. Also, in different cases of longitudinal and lateral inter-protomer contact perturbations that impair actin polymerization, we observe the rescue of filament formation by three drebrin constructs, Drb1-300, Drb2-252 and Drb-FL. Despite being the strongest binding module within the drebrin molecule, DrbABD alone does not rescue the polymerization of these actins. Furthermore, our combined results provide a structural analysis of the drebrin-induced actin filament stabilization. Although drebrin inhibits F-actin depolymerization from both B- and P-ends, we show that drebrin protects the P-end of actin to a lesser degree than the B-end. These results, obtained with both the Drb-FL and Drb 1–300 constructs, suggest that the intrinsically disordered C-terminal part of the drebrin molecule is responsible for the stronger inhibition of B-end depolymerization. Structural information available on F-actin-ADF/cofilin interactions **(2, 3, 4)**, together with our previously mentioned drebrin-actin interface mapping results, suggest that the unstructured C-terminal part of drebrin may be oriented toward the B-end of the filament. This means that the N-terminal part of drebrin, in which the actin binding "core" is localized, is oriented toward the P-end of the filament. The dissociation of actin monomers will therefore weaken the drebrin-F-actin complex more drastically at the P-end than at the B-end, explaining why drebrin protects the filament from depolymerizing better at the B-end than at the P-end.

Overall, this study points to the likely role and mode of action of drebrin in preserving the integrity of F-actin structures in dendritic spines.

In this thesis, we also examine another actin binding protein, coronin, and study the effects of its shorter construct, CrnΔCC, on actin filaments. Class-average images of actin filament segments decorated with either full-length coronin or CrnΔCC were indistinguishable by two-dimensional classification-averaging analysis **(5)**. CrnΔCC was also shown previously to function similarly to the full-length protein, and to synergize with cofilin both in the *in vitro* and *in vivo* assays **(6)**. Interestingly, the addition of Aip1 in a mixture of full length coronin, cofilin and F-actin increased the severing activity of cofilin the same way that CrnΔCC did (personal communication, unpublished results, Goode et al.). We can speculate that Aip1 blocks the inhibitory effect of Crn1's coiled-coil domain (perhaps by binding to it) and activates its synergistic role in the cofilin-mediated severing. Taken together, these results strengthen the significance of observations on the mechanism of CrnΔCC action on actin filaments.

Using a combination of site-directed mutagenesis, solution biochemistry methods, electron and TIRF microscopy, we examine the effects of CrnΔCC on the structure of actin filaments by studying its effect on inter-protomer contacts in F-actin. We compare coronin's effects on F-actin to the changes in filaments induced by cofilin. We also study how the two proteins act when they are present together, to shed light on the mechanism(s) by which coronin modulates cofilin's effects on actin filaments. We find that coronin causes slight structural changes that decrease the flexibility or dynamic motions of some structural elements of F-actin and/or increases the rigidity of actin filaments. CrnΔCC also increases the binding of cofilin to the actin filament. Our results provide a plausible mechanism for the synergistic effect CrnΔCC has on the severing activity of cofilin. Coronin-induced filament rigidity generates a bigger change in stiffness between cofilin free regions and those where cofilin is bound. This added mechanical asymmetry causes the increase in cofilin's severing of actin filaments.

Overall, our results shed light on the structural changes that coronin induces in actin filaments, and provide a plausible mechanism by which coronin mediates cofilin-induced disassembly of actin filaments.

The work in this thesis emphasizes the importance of understanding the functions of the different actin binding protein, to explain the cross-talk that occurs between them and to elucidate the mechanism by which they modulate the structure and dynamics of the actin cytoskeleton.

REFERENCES

1) Zhao L., Ma Q.L., Calon F., Harris-White M.E., Yang F., Lim G.P., Morihara T., Ubeda O.J., Ambegaokar S., Hansen J.E., Weisbart R.H., Teter B., Frautschy S.A., Cole G.M. (2006). Role of p21-activated kinase pathway defects in the cognitive deficits of Alzheimer disease. *Nat Neurosci.* **9**, 234-42.

2) Paavilainen V.O., Oksanen E., Goldman A., Lappalainen P. (2008). Structure of the actin-depolymerizing factor homology domain in complex with actin. *J Cell Biol.* **182**, 51-59.

3) Grintsevich E.E., Benchaar S.A., Warshaviak D., Boontheung P., Halgand F., Whitelegge J.P., Faull K.F., Loo R.R., Sept D., Loo J.A., Reisler E. (2008). Mapping the cofilin binding site on yeast G-actin by chemical cross-linking. *J. Mol. Biol.* **377**, 395-409.

4) Galkin V.E., Orlova A., Kudryashov D.S., Solodukhin A., Reisler E., Schröder G.F., Egelman E.H. (2011). Remodeling of actin filaments by ADF/cofilin proteins. *Proc. Natl. Acad. Sci. U S A.* 108, 20568-72.

5) Ge P., Durer Z.A., Kudryashov D., Zhou Z.H., Reisler E. (2014). Cryo-EM reveals different coronin binding modes for ADP- and ADP-BeFx actin filaments. *Nat. Struct. Mol. Biol*. **21**, [Epub ahead of print].

6) Gandhi M., Achard V., Blanchoin L., Goode B.L. (2009). Coronin switches roles in actin disassembly depending on the nucleotide state of actin. *Mol Cell*. **34**, 364-374.